



Romana Schmiedt, BSc, BSc

**Evaluation and modification of surface characteristics,  
mechanical properties and in vitro biological response of  
chitosan based functional inorganic-organic hybrid materials**

**MASTER'S THESIS**

to achieve the university degree of

Diplom-Ingenieurin

Master's degree programme: Advanced Materials Science

submitted to

**Graz University of Technology**

Supervisor

Mag.rer.nat. Dr.rer.nat. Stefan Spirk

Institute for Chemistry and Technology of Materials

Univ.-Prof. Dipl.-Ing. Dr.techn. Franz Stelzer

Institute for Chemistry and Technology of Materials



## **AFFIDAVIT**

I declare that I have authored this thesis independently, that I have not used other than the declared sources/resources, and that I have explicitly indicated all material which has been quoted either literally or by content from the sources used. The text document uploaded to TUGRAZonline is identical to the present master's thesis.

---

Date

---

Signature



## *Abstract*

### **Evaluation and modification of surface characteristics, mechanical properties and in vitro biological response of chitosan based functional inorganic-organic hybrid materials**

by Romana Schmiedt

Chitosan is the deacetylated derivative of chitin, which is abundant in nature building the exoskeleton of shrimps and other crustaceans. It shows unique biological properties, related to its polycationic structure, for instance high biocompatibility, biodegradability, non-toxicity and antimicrobial activity. Its use for biomedical and pharmaceutical applications, e.g. as wound dressing, scaffold for tissue engineering or drug delivery vehicle, has therefore received great attention in recent years.

In this thesis, the design of different nanometric chitosan-based hybrid materials is presented. The aim of our studies was to improve and modulate the mechanical and biological characteristics of chitosan. Hybrid materials were prepared by mixing different chitosan solutions with sol-gel solutions of prehydrolysed/-condensed alkoxysilanes. Thin films with nanometre thickness on various substrates were created by spin coating, whereas foils with micron thickness were obtained by a simple casting procedure. The prepared materials are characterised by a wide range of different techniques with special emphasis on the material's surface characteristics.

Atomic force microscopy (AFM) images of surfaces were acquired and wetting properties were assessed with contact angle measurements. For the determination of mechanical properties dynamic mechanical analysis (DMA) measurements at different relative humidities and uniaxial tensile tests were performed. We found that sol-gel products incorporated into the chitosan matrix define wettability, while also increasing mechanical strength. Protein adsorption and cell adhesion are key aspects in the biological performance of a material. The interaction between hybrid materials and the proteins bovine serum albumin and fibrinogen was studied by employing multi-parameter surface plasmon resonance spectroscopy (MP-SPR). Real-time analysis of protein adsorption revealed that the choice of alkoxysilane can be used to tune protein affinity. We achieved to demonstrate that prepared hybrid films are highly cytocompatible and present suitable substrates for the adhesion and proliferation of osteoblasts and fibroblasts as determined by crystal violet and MTT assays.

## *Kurzfassung*

### **Bewertung und Modifikation der Oberflächeneigenschaften, mechanischen Eigenschaften und biologischen Wirkung von Chitosan-basierten funktionellen anorganisch-organischen Hybridmaterialien**

von Romana Schmiedt

Chitosan ist das deacetylierte Derivat von Chitin, welches dem Aufbau des Exoskeletts von Garnelen und anderen Krustentieren dient. Im Zusammenhang mit seinem polykationischen Charakter besitzt es einzigartige biologische Eigenschaften, zum Beispiel hohe Biokompatibilität, Bioabbaubarkeit, Ungiftigkeit und antimikrobielle Aktivität. Der Einsatz in biomedizinischen und pharmazeutischen Anwendungen, z.B. als Wundauflage, Gerüst für das Tissue Engineering oder Arzneistoffabgabesystem, hat daher in den letzten Jahren große Beachtung gefunden.

In der vorliegenden Arbeit wird die Entwicklung unterschiedlicher nanometrischer Hybridmaterialien auf der Basis von Chitosan vorgestellt. Zielsetzung unserer Untersuchungen war eine Verbesserung und Modulation der mechanischen und biologischen Eigenschaften von Chitosan. Hybridmaterialien wurden durch das Mischen unterschiedlicher Chitosan-Lösungen mit Sol-Gel-Lösungen von prähydrolysierten/-kondensierten Alkoxysilanen hergestellt. Nanometer dicke Dünnschichtfilme konnten auf verschiedenen Substraten durch Rotationsbeschichtung aufgebracht werden, während Mikrometer dicke Folien durch ein Gießverfahren erhalten wurden. Die hergestellten Materialien wurden durch eine Vielzahl unterschiedlicher Methoden untersucht, wobei das Hauptaugenmerk auf die Charakterisierung der Materialoberflächen gelegt wurde.

Rasterkraftmikroskopische Aufnahmen der Oberflächen wurden angefertigt und die Benetzungseigenschaften der Oberflächen in Kontaktwinkelmessungen ermittelt. Zur Bestimmung der mechanischen Eigenschaften wurden dynamisch-mechanische Analysen bei unterschiedlicher relativer Luftfeuchtigkeit und uniaxiale Zugversuche durchgeführt. Es konnte gezeigt werden, dass Sol-Gel Produkte in der Chitosan-Matrix die Benetzbarkeit definieren, während sie gleichzeitig die mechanische Festigkeit verbessern. Proteinadsorption und Zelladhäsion sind wichtige Faktoren im biologischen Verhalten eines Materials. Die Wechselwirkung der Hybridmaterialien mit den Proteinen Bovines Serumalbumin und Fibrinogen wurden mittels Multi-Parametrischer Oberflächenplasmonenresonanzspektroskopie untersucht. Echtzeitanalysen der Proteinadsorption zeigten, dass durch die Wahl der Alkoxysilane die Proteinaffinität eingestellt werden kann. Unter Einbeziehung von Kristallviolett und MTT Tests konnte des Weiteren nachgewiesen werden, dass Hybridmaterialien in hohem Maße zellkompatibel sind und ein geeignetes Trägermaterial für die Adhäsion und Vermehrung von Osteoblasten und Fibroblasten darstellen.

# *Acknowledgements*

The work presented in this thesis would not have been possible without contributions from various people. Therefore I want to acknowledge the works of Katrin Niegelhell related to the AFM and SPR measurements and Adriana Kovalcik related to the DMA measurements, at the Institute of Chemistry and Technology of Materials (ICTM). With respect to the cell tests I want to acknowledge the work of Uros Maver and Lidija Gradisnik from the University of Maribor. Furthermore I want to thank Uros Maver for making my stay at the University of Maribor possible and to allow me to work in his laboratory.

I am grateful to Stefan Spirk for the supervision and Franz Stelzer, head of the institute, for the co-supervision of my thesis. I want to thank Stefan Spirk for offering me this interesting and promising research topic, for his guidance from the first day and his advice. I would like to underline the constant encouragement received during my work and the manifold opportunities to increase my knowledge, including the possibility to attend and present our work at two conferences.

I want to thank all members and associates of the group of Stefan Spirk, in particular Katrin Niegelhell, David Rieshofer, Manuel Kaschowitz, Claudia Payerl, Katrin Jammerneegg, Wolfgang Binder and Armin Häusl, for their assistance and the great time we had. Furthermore I want to thank all other people from the Institute for Chemistry and Technology of Materials for providing a friendly and cooperative working environment.

I also would like to thank my friends from the students home, especially Katharina Regitnig, Matthias Zechner and Christoph Wiesmeier, as well as my friends from my master's classes, in particular Michaela Zagler, which were a true support throughout.

My highest gratitude goes to my family who supported and encouraged me in every respect through my educational journey.





# Contents

<b>Motivation</b>	<b>1</b>
<b>1 Introduction</b>	<b>3</b>
<b>2 Theoretical background</b>	<b>5</b>
2.1 Composite/Hybrid materials . . . . .	5
2.2 Biomaterials . . . . .	7
2.2.1 Introduction . . . . .	7
2.2.2 Protein Adsorption . . . . .	8
2.2.3 Fields of application: Wound dressings and orthopaedic implants . . . . .	9
2.3 Chitosan . . . . .	10
2.3.1 Introduction . . . . .	10
2.3.2 Moisture sorption behaviour . . . . .	12
2.3.3 Chitosan and its biological and physiological properties . . . . .	13
2.3.4 Applications . . . . .	14
2.4 Silanes and sol-gel processing . . . . .	15
2.5 Chitosan-Siloxane Hybrid Materials . . . . .	16
<b>3 Principles of applied tests and methods</b>	<b>17</b>
3.1 Spin coating . . . . .	17
3.2 Surface Plasmon Resonance Spectroscopy (SPR) . . . . .	18
3.3 Stylus profilometry . . . . .	18
3.4 Atomic Force Microscopy (AFM) . . . . .	19
3.5 Contact angle . . . . .	20
3.6 Cell culturing . . . . .	21
3.7 Tensile testing . . . . .	22
3.8 Dynamic mechanical analysis (DMA) . . . . .	24
<b>4 Experimental</b>	<b>25</b>
4.1 Materials . . . . .	25
4.1.1 For sample preparation . . . . .	25
Chemicals . . . . .	25
Materials . . . . .	25
Equipment . . . . .	26
4.1.2 For sample characterisation . . . . .	26
Solutions . . . . .	26
Materials . . . . .	26
Equipment . . . . .	26
4.1.3 For cell testing . . . . .	26
Chemicals . . . . .	26
Solutions . . . . .	27

Materials . . . . .	27
Equipment . . . . .	27
4.2 Material preparation . . . . .	28
4.2.1 Thin film preparation . . . . .	29
4.2.2 Specimen preparation for SPR measurements . . . . .	30
4.2.3 Foil preparation . . . . .	30
4.2.4 Specimen preparation for tensile testing and DMA . . . . .	32
4.3 Material characterisation . . . . .	33
4.3.1 Stylus profilometry . . . . .	33
4.3.2 Contact angle measurement . . . . .	33
4.3.3 Atomic force microscopy (AFM) . . . . .	34
4.3.4 Surface Plasmon Resonance Spectroscopy (SPR) . . . . .	35
4.3.5 Cell testing . . . . .	35
4.3.6 Tensile testing . . . . .	38
4.3.7 Dynamic mechanical analysis (DMA) . . . . .	38
<b>5 Results and Discussion</b>	<b>39</b>
5.1 Film thickness . . . . .	40
5.2 Contact angle . . . . .	42
5.3 Atomic Force Microscopy (AFM) . . . . .	46
5.4 Surface Plasmon Resonance Spectroscopy (SPR) . . . . .	47
5.5 Cell testing . . . . .	51
5.5.1 Cytotoxicity . . . . .	51
5.5.2 Cell attachment . . . . .	54
5.6 Tensile testing . . . . .	57
5.7 Dynamic mechanical analysis (DMA) . . . . .	61
<b>Summary and Conclusion</b>	<b>65</b>
<b>Bibliography</b>	<b>67</b>
<b>A Protocols</b>	<b>77</b>
<b>B Figures</b>	<b>79</b>
B.1 Atomic Force Microscopy Images . . . . .	79
B.2 Wafer size for cell attachment tests . . . . .	81
<b>C Tables</b>	<b>83</b>
C.1 Layer thickness . . . . .	83
C.2 Contact angle measurements . . . . .	85
C.3 Surface Plasmon Resonance Spectroscopy measurements . . . . .	87
C.4 Cytotoxicity tests . . . . .	89
C.5 Tensile tests . . . . .	90

# List of Figures

1.1	Schematic representation of the sol-gel process for different alkoxy-silanes. . . . .	3
1.2	Schematic representation of the hybrid material formation from acidic chitosan solutions and prehydrolysed/-condensed alkoxy-silanes. . . . .	4
2.1	Classification of composites based on reinforcement type. . . . .	6
2.2	Reactions occurring at the end stage of the blood coagulation cascade. . . . .	8
2.3	Promising fields of application for chitosan based materials: wound dressings (left) and orthopaedic implants (right). Figure reprinted from [32] and [33]. . . . .	9
2.4	Chemical structure of chitosan. . . . .	10
2.5	Chitosan's pH-dependent structure and solubility. . . . .	11
2.6	Moisture sorption isotherm typical for chitosan, displaying a sigmoidal shape and hysteresis. . . . .	12
2.7	Schematic representation of the sol-gel process and its products. . . . .	15
3.1	Stages of the spin coating process: 1.-2. Fluid deposition 3. Spinning 4. Solvent evaporation and layer formation. . . . .	17
3.2	Schematic representation of the surface plasmon resonance spectroscopy (SPR) detection principle. Light is passed through a prism, at the angle $\Theta$ , and is totally internally reflected at the surface-solution interface. Changes at the interface are monitored by changes in the angle of the reflection minimum. . . . .	18
3.3	Schematic representation of the atomic force microscope detection principle in contact mode. Deflection of the cantilever is measured by changes in the position of the reflected laser beam. . . . .	19
3.4	Illustration of the contact angle, $\Theta$ , at the three-phase boundary solid, liquid and vapour. Drop shape in equilibrium is the result of a balance of three forces. . . . .	20
3.5	Young's equation: $\Theta$ , contact angle; $\gamma_L$ , surface free energy of the liquid; $\gamma_S$ , surface free energy of the solid; $\gamma_{SL}$ , interfacial free energy of the liquid and solid. . . . .	20
3.6	Growth of cells in culture. After several subcultivations senescence and cell death in finite cell lines occurs. By transformation cells will establish a continuous cell line. . .	21
3.7	Detection principle of MTT assays. The yellow tetrazolium dye MTT is converted to the corresponding insoluble purple formazan by NAD(P)H-dependent cellular enzymes. . . . .	22
3.8	Example of a stress-strain curve typical for a ductile material. . . . .	23
3.9	In dynamic mechanical analysis a sinusoidal stress is applied and the resulting strain is measured. The phase angle, $\delta$ , describes the lag between applied stress and strain response. . . . .	24
4.1	Filtration of hot acetic acid solutions of chitosan through a pleated filter. . . . .	28
4.2	Preparation of chitosan and chitosan-based hybrid thin films on silicon substrates by spin coating. . . . .	30
4.3	Preparation of chitosan and chitosan-based hybrid foils by solution casting. . . . .	31

4.4	Washing of foils in 0.25 M NaOH solution in order to remove remaining acetic acid. Afterwards foils are fixed and dried at 60 °C for one or two days. . . . .	31
4.5	Stamping out of dumbbell specimens from chitosan foils using a cutting die and a screw press. . . . .	32
4.6	Determination of layer thickness by measuring height variations perpendicular to a scratch using a contact stylus profiler (EKTAK 150, Veeco). . . . .	33
4.7	Contact angle measurements of thin films at a Drop Shape Analyzer (DSA 100S, Krüss). . . . .	34
4.8	Atomic Force Microscope (Veeco Multimode, Bruker). . . . .	34
4.9	Surface plasmon resonance instrument (SPR Navi™ 200, BioNavis). . . . .	35
4.10	Tensile testing of dumbbell specimen stamped out of chitosan and chitosan hybrid foils at a electromechanical universal testing machine (AGS-X Series, Shimadzu). . . . .	38
4.11	Dynamic Mechanical Analysis instrument (Q800, TA Instruments). Figure is taken from the homepage of the Institute for Chemistry and Technology of Materials (ICTM) [96]. . . . .	38
5.1	Chitosan hybrid materials can be processed into different forms: thin films on silicon wafers (top right), titanium (bottom right) and gold (bottom center) prepared by spin coating; foils (top center) from solution casting. . . . .	39
5.2	Thickness of thin films on silicon wafers prepared from medium molecular weight chitosan CS <sub>M</sub> and different particles by spin coating. Layer thickness is determined from three height profiles of one coating measured on a Stylus Profiler. . . . .	41
5.3	Thickness of thin films on silicon wafers prepared from low molecular weight chitosan CS <sub>L</sub> and different particles by spin coating. Layer thickness is determined from three height profiles of one coating measured on a Stylus Profiler. . . . .	41
5.4	Static contact angles of water on films prepared from low molecular weight chitosan CS <sub>L</sub> and different particles. Six drops of 3 µL Milli-Q water are placed on two different thin films. Measurements are carried out roughly two months after spin coating. . . . .	43
5.5	Static contact angles of water on films prepared from medium molecular weight chitosan CS <sub>M</sub> and different particles. Six drops of 3 µL Milli-Q water are placed on two different thin films. Measurements are carried out roughly two months after spin coating. . . . .	43
5.6	Static contact angles of water on chitosan and selected hybrid thin films. Three drops of 3 µL Milli-Q water are placed on one thin film. Measurements are carried out five days after spin coating. . . . .	44
5.7	Static contact angles of water on neat chitosan films one day, one week and two months after preparation. 15 drops of 3 µL Milli-Q water are placed on five different thin films. . . . .	44
5.8	Static contact angles of water on thin films prepared from spin coating of mixtures with different ratios of chitosan solution and ethanol. Six drops of 3 µL Milli-Q water are placed on two different thin films. Measurements are carried out one day after spin coating. . . . .	45
5.9	2 x 2 µm <sup>2</sup> AFM images of chitosan and selected chitosan hybrid thin films on silicon with a z-scale of 20 nm. 10 x 10 µm <sup>2</sup> AFM images of the same materials are displayed in Figure B.1. . . . .	46
5.10	Typical shape of a SPR sensogram for the adsorption of proteins. . . . .	47

5.11	Crystal structure of bovine serum albumin (left) and human fibrinogen (right). Figures reprinted from [106] and [107]. . . . .	47
5.12	Overlay of SPR sensograms for the adsorption of bovine serum albumin onto chitosan and selected hybrid thin films. Protein ( $c = 1 \text{ mg/mL}$ in buffer) is injected at $t = 5 \text{ min}$ and surfaces are rinsed with buffer ( $\text{pH } 7.4, 10 \text{ mM PBS} + 100 \text{ mM NaCl}$ ) at $t = 35 \text{ min}$ . Flow rate is set to $20 \text{ }\mu\text{L/min}$ . . . . .	48
5.13	Bovine serum albumin mass adsorbed onto chitosan and selected hybrid thin films determined from three SPR measurements. . . . .	48
5.14	Overlay of SPR sensograms for the adsorption of fibrinogen onto chitosan and selected hybrid thin films. Protein ( $c = 1 \text{ mg/mL}$ in buffer) is injected at $t = 5 \text{ min}$ and surfaces are rinsed with buffer ( $\text{pH } 7.4, 10 \text{ mM PBS} + 100 \text{ mM NaCl}$ ) at $t = 35 \text{ min}$ . Flow rate is set to $20 \text{ }\mu\text{L/min}$ . . . . .	49
5.15	Fibrinogen mass adsorbed onto chitosan and selected hybrid thin films determined from three SPR measurements. . . . .	49
5.16	Fibroblast viability, compared to untreated cells, when exposed to sample solutions that were in contact with chitosan and selected hybrid thin films. Cell number is determined from four measurements using crystal violet staining. Different material incubation times (24 h, 1 week) and incubation media (with or without 5% FBS) are tested. . . . .	51
5.17	Osteoblast viability, compared to untreated cells, when exposed to sample solutions that were in contact with chitosan and selected hybrid thin films. Cell number is determined from four measurements using crystal violet staining. Different material incubation times (24 h, 1 week) and incubation media (with or without 5% FBS) are tested. . . . .	52
5.18	Osteoblast viability, compared to untreated cells, when exposed to sample solutions that were in contact with hybrid thin films containing TEOS derived silica particles. Cell number is determined from four measurements using crystal violet staining. Different material incubation times (24 h, 1 week) and incubation media (with or without 5% FBS) are tested. . . . .	52
5.19	Osteoblast viability, compared to untreated cells, when exposed to sample solutions that were in contact with hybrid thin films containing a broad range of particles. Cell number is determined from four measurements using crystal violet staining. Different material incubation times (24 h, 1 week) and incubation media (with or without 5% FBS) are tested. . . . .	53
5.20	Fluorescence images as an overlay of two images recorded at different excitation/emission wavelengths, of osteoblastic cells on chitosan thin films (left) and a glass control (right) using a combination of Live/Dead staining assay and confocal microscopy. . . . .	54
5.21	Fibroblast attachment and proliferation on surfaces of selected hybrid thin films in relation to neat chitosan thin films as determined by MTT assay. . . . .	55
5.22	Osteoblast attachment and proliferation on surfaces of selected hybrid thin films in relation to neat chitosan thin films as determined by MTT assay. . . . .	56
5.23	Representative stress-strain curves of chitosan foils prepared from mixtures of acetic acid/water and ethanol in a ratio of 9:1 (w/w) in comparison to neat chitosan foils. The loading speed is $0.5 \text{ mm/min}$ . . . . .	57

5.24	Representative stress-strain curves of chitosan foils reinforced with silica particles from sol-gel processing of TEOS in comparison to neat chitosan foils. Loading speed is 0.5 mm/min. . . . .	58
5.25	Representative stress-strain curves of chitosan foils reinforced with 7.3% ChNCs in comparison to neat chitosan foils. The loading speed is 0.5 mm/min. . . . .	59
5.26	Summary of mechanical properties of unreinforced chitosan foils and chitosan foils reinforced with TEOS derived silica-particles and chitin nanocrystals : Ultimate tensile strength (top left), yield strength (top right), elastic modulus (bottom left) and break strain (bottom right). (1) CS <sub>M</sub> , (2) CS <sub>M</sub> :EtOH 9:1, (3) CS <sub>M</sub> :T (2.9%), (4) CS <sub>M</sub> :T (5.9%), (5) CS <sub>M</sub> :T (11.5%) and (6) CS <sub>M</sub> :ChNC (7.3%). . . . .	60
5.27	Storage modulus (G') at room temperature as a function of increasing relative humidity of neat chitosan foils. DMA measurements are performed by applying an oscillating strain of 0.0300% at a frequency of 1 Hz. . . . .	61
5.28	Storage modulus (G') at room temperature as a function of increasing relative humidity of chitosan foils reinforced with 5.8% silica particles from sol-gel processing of TEOS. DMA measurements are performed by applying an oscillating strain of 0.0300% at a frequency of 1 Hz. . . . .	62
5.29	Storage modulus (G') at room temperature as a function of increasing relative humidity of chitosan foils reinforced with 7.3% ChNCs. DMA measurements are performed by applying an oscillating strain of 0.0300% at a frequency of 1 Hz. . . . .	63
B.1	10 x 10 μm <sup>2</sup> AFM images of chitosan and selected hybrid thin films on silicon. 2 x 2 μm <sup>2</sup> AFM images of the same materials are displayed in Figure 5.9. . . . .	79
B.2	10 x 10 μm <sup>2</sup> and 2 x 2 μm <sup>2</sup> images of chitosan hybrid thin films containing particles from sol-gel processing of TEOS. . . . .	79
B.3	10 x 10 μm <sup>2</sup> and 2 x 2 μm <sup>2</sup> images of chitosan hybrid thin films containing particles from sol-gel processing of GLYMO as well as cellulose nanocrystals. . . . .	80
B.4	10 x 10 μm <sup>2</sup> and 2 x 2 μm <sup>2</sup> images of chitosan hybrid thin films containing silicon dioxide nanoparticles with an average BET diameter of 10 nm (SiO <sub>2</sub> *) and 15 nm (SiO <sub>2</sub> **). . . . .	80
B.5	Size of the coated wafers which have been used for fibroblast attachment tests as determined by surface integration using a MatLab script. Coloured areas correspond to different samples. . . . .	81
B.6	Size of the coated wafers which have been used for osteoblast attachment tests as determined by surface integration using a MatLab script. Coloured areas correspond to different samples. . . . .	81

# List of Tables

2.1	Selected reactions of the body in contact with a foreign body, i.e. a biomaterial [23, 25].	7
4.1	Particle solutions/suspensions employed in chitosan hybrid material preparation. . .	29
4.2	Composition of the 58 different types of chitosan and chitosan hybrid thin films on silicon. . . . .	29
4.3	Composition of the six different types of chitosan and chitosan hybrid foils. . . . .	30
4.4	Stylus Profilometer settings used for thin film thickness measurements. . . . .	33
4.5	Chitosan hybrid thin films on silicon studied by means of atomic force microscopy. . .	34
4.6	Chitosan hybrid thin films on gold studied by means of surface plasmon resonance spectroscopy. . . . .	35
4.7	Chitosan hybrid thin films on silicon for which cytotoxicity and cell attachment is assessed. Tested materials are indicated with a $x$ . . . . .	36
5.1	Summary of the MTT test results from the growth of fibroblasts on chitosan and different hybrid thin films with silicon wafers as substrates. The size factor accounts for deviations from the normal sample size. Attachment of cells on hybrid materials is expressed in relation to neat chitosan thin films (=1.00). . . . .	55
5.2	Summary of the MTT test results from the growth of osteoblasts on chitosan and different hybrid thin films with silicon wafers as substrates. The size factor accounts for deviations from the normal sample size. Attachment of cells on hybrid materials is expressed in relation to neat chitosan thin films (=1.00). . . . .	56
5.3	Mechanical parameters obtained from uniaxial tensile tests of chitosan foils prepared from mixtures of chitosan dissolved in acetic acid/water diluted with ethanol in a ratio of 9:1 (w/w) in comparison to neat chitosan foils. Results are mean values of five measurements. . . . .	57
5.4	Mechanical parameters obtained from uniaxial tensile tests of chitosan foils reinforced with silica particles from the sol-gel process of TEOS in comparison to neat chitosan foils. The loading speed is 0.5 mm/min. . . . .	58
5.5	Mechanical parameters obtained from uniaxial tensile tests of foils reinforced with 7.3% ChNCs in comparison to neat chitosan foils. Results are mean values of five measurements. . . . .	59
C.1	Layer thickness of thin films from neat chitosan. . . . .	83
C.2	Layer thickness of chitosan hybrid thin films containing particles from TEOS sol-gel processing. . . . .	83
C.3	Layer thickness of chitosan hybrid thin films containing particles from APTES sol-gel processing. . . . .	83
C.4	Layer thickness of chitosan hybrid thin films containing particles from GLYMO sol-gel processing. . . . .	83
C.5	Layer thickness of chitosan hybrid thin films containing silicon dioxide nanoparticles with an average BET diameter of 10 nm ( $S^*$ ). . . . .	84

C.6	Layer thickness of chitosan hybrid thin films containing silicon dioxide nanoparticles with an average BET diameter of 15 nm (S**).	84
C.7	Layer thickness of chitosan hybrid thin films containing cellulose nanocrystals (CNCs).	84
C.8	Static water contact angles on thin films from neat chitosan.	85
C.9	Static water contact angles on chitosan hybrid thin films containing particles from TEOS sol-gel processing.	85
C.10	Static water contact angles on chitosan hybrid thin films containing particles from APTES sol-gel processing.	85
C.11	Static water contact angles on chitosan hybrid thin films containing particles from GLYMO sol-gel processing.	85
C.12	Static water contact angles on chitosan hybrid thin films containing silicon dioxide nanoparticles with an average BET diameter of 10 nm (S*).	86
C.13	Static water contact angles on chitosan hybrid thin films containing silicon dioxide nanoparticles with an average BET diameter of 15 nm (S**).	86
C.14	Static water contact angles on chitosan hybrid thin films containing cellulose nanocrystals (CNCs).	86
C.15	Static water contact angles on selected chitosan hybrid thin films five days after preparation.	86
C.16	Static water contact angles on chitosan hybrid thin films prepared from different dilutions with ethanol.	87
C.17	SPR angular shifts and corresponding protein masses for the adsorption onto neat chitosan surfaces after rinsing with buffer.	87
C.18	SPR angular shifts and corresponding protein masses for the adsorption onto surfaces with the composition CS <sub>M</sub> :TEOS 9:1 after rinsing with buffer.	87
C.19	SPR angular shifts and corresponding protein masses for the adsorption onto surfaces with the composition CS <sub>M</sub> :TEOS 2:1 after rinsing with buffer.	88
C.20	SPR angular shifts and corresponding protein masses for the adsorption onto surfaces with the composition CS <sub>M</sub> :APTES 9:1 after rinsing with buffer.	88
C.21	SPR angular shifts and corresponding protein masses for the adsorption onto surfaces with the composition CS <sub>M</sub> :APTES 2:1 after rinsing with buffer.	88
C.22	Fibroblast viability, compared to untreated cells, when exposed to sample solutions that were in contact with chitosan and selected hybrid thin films as determined by crystal violet staining.	89
C.23	Osteoblast viability, compared to untreated cells, when exposed to sample solutions that were in contact with chitosan and selected hybrid thin films as determined by crystal violet staining.	89
C.24	Osteoblast viability, compared to untreated cells, when exposed to sample solutions that were in contact with hybrid thin films containing TEOS derived silica particles as determined by crystal violet staining.	89
C.25	Osteoblast viability, compared to untreated cells, when exposed to sample solutions that were in contact with hybrid thin films containing a wide range of different particles as determined by crystal violet staining.	90
C.26	Mechanical parameters obtained from uniaxial tensile tests of neat chitosan foils.	90



C.27 Mechanical parameters obtained from uniaxial tensile tests of chitosan foils containing ethanol in a ratio of CS <sub>M</sub> :EtOH 9:1. . . . .	90
C.28 Mechanical parameters obtained from uniaxial tensile tests of chitosan foils containing 2.9% silica particles from sol-gel processing of TEOS. . . . .	91
C.29 Mechanical parameters obtained from uniaxial tensile tests of chitosan foils containing 5.8% silica particles from sol-gel processing of TEOS. . . . .	91
C.30 Mechanical parameters obtained from uniaxial tensile tests of chitosan foils containing 11.5% silica particles from sol-gel processing of TEOS. . . . .	91
C.31 Mechanical parameters obtained from uniaxial tensile tests of chitosan foils containing 7.3% chitin nanocrystals (ChNCs). . . . .	91



# List of Abbreviations

<b>CS<sub>M</sub></b>	Chitosan with medium molecular weight
<b>CS<sub>L</sub></b>	Chitosan with low molecular weight
<b>PMC</b>	Polymer matrix composites
<b>DD</b>	Degree of deacetylation
<b>TEOS</b>	Tetraethyl orthosilicate
<b>APTES</b>	3-Aminopropyl triethoxysilane
<b>GLYMO</b>	3-Glycidoxypropyl trimethoxysilane
<b>SiO<sub>2</sub>*</b>	Silicon dioxide nanoparticles (average BET diameter of 10 nm)
<b>SiO<sub>2</sub>**</b>	Silicon dioxide nanoparticles (average BET diameter of 15 nm)
<b>CNC</b>	Cellulose nanocrystals
<b>ChNC</b>	Chitin nanocrystals
<b>AFM</b>	Atomic Force Microscopy
<b>MP-SPR</b>	Multi-Parameter Surface Plasmon Resonance
<b>DMA</b>	Dynamic Mechanical Analysis
<b>BSA</b>	Bovine Serum Albumin
<b>ATCC</b>	American Type Culture Collection
<b>MTT</b>	(3-(4,5-Dimethylthiazol-2-yl)-2,5-diphenyltetrazolium bromide)
<b>DMEM</b>	Dulbecco's Modified Eagle Medium
<b>FBS</b>	Fetal bovine serum
<b>PBS</b>	Phosphate-buffered saline



# Motivation

A commonly described problem in the use of polymers for advanced medical materials is that mechanical demands necessary for their successful application are not fully met. Chitosan, a polycationic polysaccharide derived from natural resources, is a promising candidate for various medical purposes. Several works exploring the use of chitosan in fields such as tissue engineering, wound dressings or coatings of orthopaedic devices have reported the need for chitosan with better mechanical properties [1, 2, 3, 4]. For this reason large efforts have been made to improve the mechanical properties of chitosan, by developing different types of chitosan-based composite biomaterials. However any type of reinforcement agent will not only change the mechanical behaviour but might also influence the biological performance, e.g. the biocompatibility, biodegradability or bioactivity of a device. In the best case the contribution from the reinforcing compound is beneficial, improving the biological performance of the composite.

To evaluate how the structure, chemical composition and content of a reinforcing agent affect the biological properties of a composite, a generic approach should be used. In the case of chitosan, for instance, changes in antimicrobial properties, cell adhesion or protein adsorption should be carefully examined. An ideal system for such investigations should be readily producible, form homogeneous composite structures and allow an easy modification of the reinforcing agent. Furthermore it should be possible to use a wide set of chemical and biological methods to characterise the prepared materials.

In previous studies it was found that mixing of chitosan and different alkoxy silanes, subjected to a sol-gel process, will produce nanometric composite films with variable thickness in a fast and reproducible way [5]. Sol-gel processing is a collective term used for methods where small precursor molecules are polymerized, thereby creating networks and subsequently solid materials. Organofunctional alkoxy silanes can be used for the formation of a wide range of different functional particles. An advantage of this method is that the properties of the formed material can be easily changed by variations in parameters such as temperature, pH, solvent or type of functional group. In addition, it has been reported that such chitosan-siloxane hybrid materials can enhance cell growth and support nerve regeneration [6, 7]. This suggests a promising system for the improvement of chitosan materials, also allowing a straightforward modification of the reinforcing agent and possible changes in the biological properties.



# Chapter 1

## Introduction

Chitosan is a polysaccharide produced by deacetylation of chitin, which is abundant in nature in the exoskeleton of shrimps and other crustaceans. It possesses remarkable biological properties, which make it an attractive material for medical applications. For instance, chitosan is known to be biocompatible, biodegradable and non-toxic [8]. Moreover, it has antibacterial and antifungal activity as well as haemostatic properties [9, 10]. It can form films, sponges, gels, membranes, beads and scaffolds. Chitosan-based materials could be useful in the development of novel wound dressings, scaffolds for tissue engineering and for the delivery of genes and drugs.

Materials made from neat chitosan often lack mechanical stability related to chitosan's hydrophilic nature and water sorption characteristics. These limitations in the use of chitosan can be overcome by combining chitosan with a second component which enhances its mechanical stability, for example an inorganic particle or fibre, thus forming a composite. An interesting class of composites are hybrid materials, where both components are mixed at a microscopic (i.e. nanometric) scale. Hybrid material synthesis is closely related to sol-gel chemistry, which can be engaged in the material preparation. In sol-gel processes small precursor molecules are polymerised, thereby forming structures and networks.

An example for such a sol-gel process is the hydrolysis and condensation of alkoxy silanes or organofunctional silanes as small precursor molecules with an acid or a base as a catalyst. For instance, polymerisation of tetraethyl orthosilicate (TEOS) will provide silica particles in a process that allows an easy modification of the product's properties through changes in the preparation conditions. In the same way the polymerisation of organofunctional silanes can be used to create organofunctional particles (Figure 1.1).

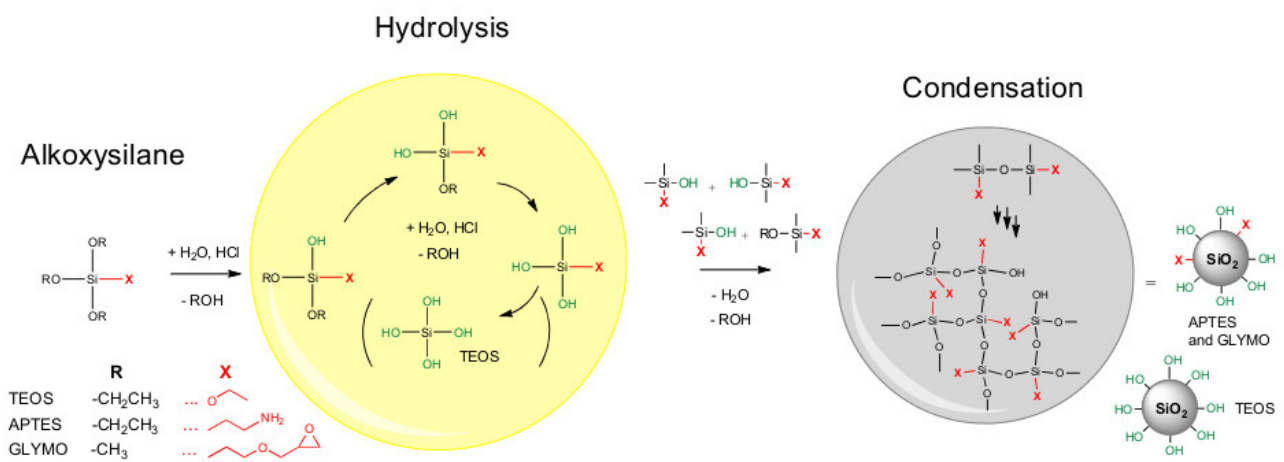


FIGURE 1.1: Schematic representation of the sol-gel process for different alkoxy silanes.

Upon mixing of the synthesised particles with acidic chitosan solutions, crosslinking of hydroxyl rich silanes with the primary amino or hydroxyl groups of chitosan will occur (Figure 1.2). After the solvent is removed, bulk materials are formed. Chitosan-based hybrid materials can be processed into different bulk materials, e.g. into films with micron thickness (i.e. foils) by a simple casting procedure or into thin films with nanometre thickness by spin-coating. The good film forming capability of this system has been previously described by our group [5].

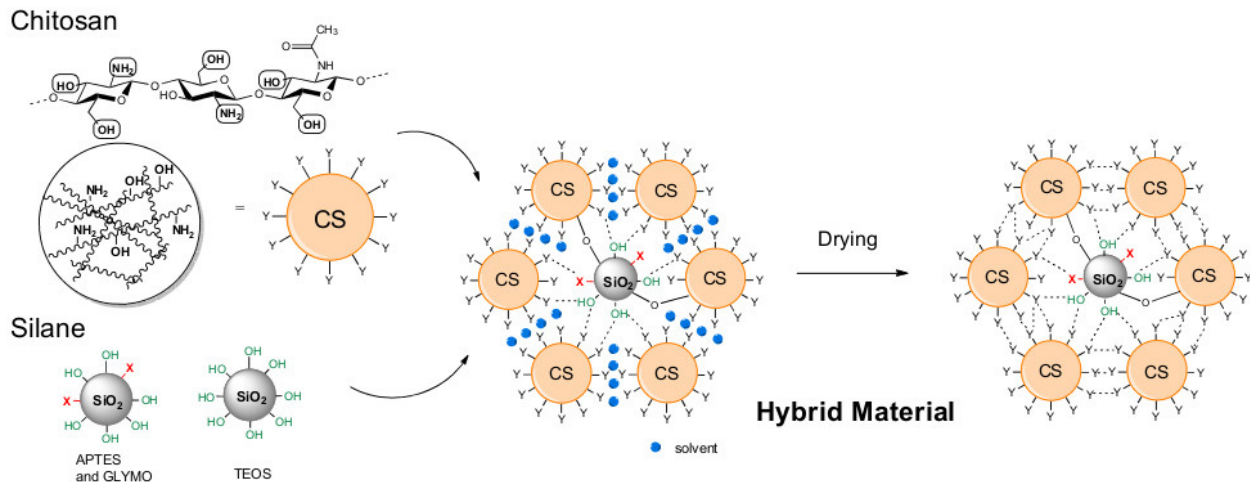


FIGURE 1.2: Schematic representation of the hybrid material formation from acidic chitosan solutions and prehydrolysed/-condensed alkoxy silanes.

The interaction of a biomaterial's surface and biological matter is a crucial aspect in the design of biomaterials and a critical factor for its performance. Protein adsorption is important, as the initial protein layer will mediate cell colonisation and direct the overall biocompatibility. A first examination of a biomaterial's surface will include both a determination of general surface properties, e.g. chemical composition, roughness, wettability as well as studying its interaction with proteins and cells.

In this work, the use of various alkoxy silanes for hybrid material preparation is explored. Three different alkoxy silanes (TEOS, APTES, GLYMO) are subjected to a sol-gel process and combined with chitosan to form inorganic-organic hybrid materials. For comparison purposes, chitosan composites containing silicon dioxide nanoparticles and nanocrystals derived from cellulose (CNCs) and chitin (ChNCs) are prepared. On one hand, it should be examined to which extent the mechanical properties of neat chitosan can be improved. The most convenient way to do this is to reinforce foils prepared from solution casting and to subject them to classical stress-strain experiments. In addition, properties of foils at different relative humidities are examined using dynamic mechanical analysis (DMA). On the other hand we strive to evaluate the biological properties of hybrid materials. Films prepared from spin-coating are more suitable for such purposes, due to a higher film homogeneity compared to foils. Initially, surfaces of thin films are characterised with atomic force microscopy and the wettability of the surfaces are determined in contact angle measurements. Adsorption of the proteins bovine serum albumin (BSA) and fibrinogen is assessed via surface plasmon resonance (SPR) spectroscopy. Cytocompatibility and cell attachment of fibroblasts and osteoblasts is determined with crystal violet and MTT assays.



# Chapter 2

## Theoretical background

### 2.1 Composite/Hybrid materials

Composites are materials consisting of one or more components, which have different chemical and physical properties [11]. In composites, new and unique properties distinct from the parent materials can be achieved. As opposed to alloys and copolymers, each component maintains its chemical and physical identity thereby creating multiphase materials. Constituent materials are classified into reinforcing agent and matrix material (host). The reinforcing agent is embedded in the matrix and can be of different size and shape for example in the form of whiskers or fibres. Composites are typically produced by simple mixing of the components.

Hybrid materials are a special type of composite, where mixing of the components occurs on the microscopic scale, i.e. on a nanometre or molecular level. The thus produced materials are more homogeneous and can have improved properties compared to traditional composites (e.g. transparency). Usually one of the constituent in the hybrid is organic and the other one is inorganic. The interaction between them can solely be based on van der Waals forces and electrostatic interactions (Class I hybrids) or could also contain covalent bonding (Class II hybrids). Preparation of hybrid materials often incorporate sol-gel synthetic approaches which are described in more detail in Chapter 2.4. [12]

The difference between hybrid materials and nanocomposites is not that clear. Sometimes these terms are synonymously used. Nanocomposite frequently describes materials where discrete particles (e.g.  $\text{Al}_2\text{O}_3$ ,  $\text{ZnO}$ ) in the nanoregime, nanoclays, nanorods or carbon nanotubes (CNTs) are homogeneously dispersed in a matrix [13, 14], whereas in hybrid materials the inorganic constituents are often formed *in situ* (i.e. sol-gel processing) [12].

Constituent materials are combined in such a way that beneficial properties are highlighted whereas disadvantageous sites are suppressed. As an example the incorporation of solid particles interacting with the polymer strands of the matrix will limit polymer chain movement and will therefore add rigidity and mechanical strength to the formed material. Very often composites have been developed for applications where both high mechanical strength and low weight is required (good strength-to-weight ratio) for example for aircraft constructions. Composites can provide high corrosion resistance, hardness and can offer great design flexibility. They are not only developed to improve mechanical properties but also to find materials with exceptional electrical and optical properties. [11, 15]

One very familiar example of a composite is concrete which consists of construction aggregate (loose stones) as reinforcing agent and cement as matrix material. Compared to cement, concrete has improved compression strength. Though concrete shows high compression strength it lacks resistance towards tensile load. For that reason, steel reinforcing bars or steel fibres can be incorporated into the

matrix material. Composites can also be found in nature [16]. Chitin with proteins, most importantly sclerotin, and calcium carbonate forms composites, constituting the shells of crustaceans. Bird beaks are made out of calcium phosphate and keratin. Bone is a composite of hydroxyapatite and the protein collagen.

Synergistic effects resulting from a certain material's combination are greatly affected by the chemistry of the material, the geometry of the components, size effects in general and the interaction between the components. The reinforcing agent represents only a small mass fraction of the whole material. Most properties of the composite are hence directed by the matrix, for instance cohesion, toughness or thermal expansion. As a consequence composites are often classified according to their matrix: polymer-matrix composites (PMC), metal-matrix composites (MMC) and ceramic-matrix composites (CMC). PMC have found wide application since they are easily processable. Furthermore composites can be classified according to the type of reinforcement which can be particulate- or fibre-reinforced as well as structural reinforcements in the form of laminates and panels (Figure 2.1).

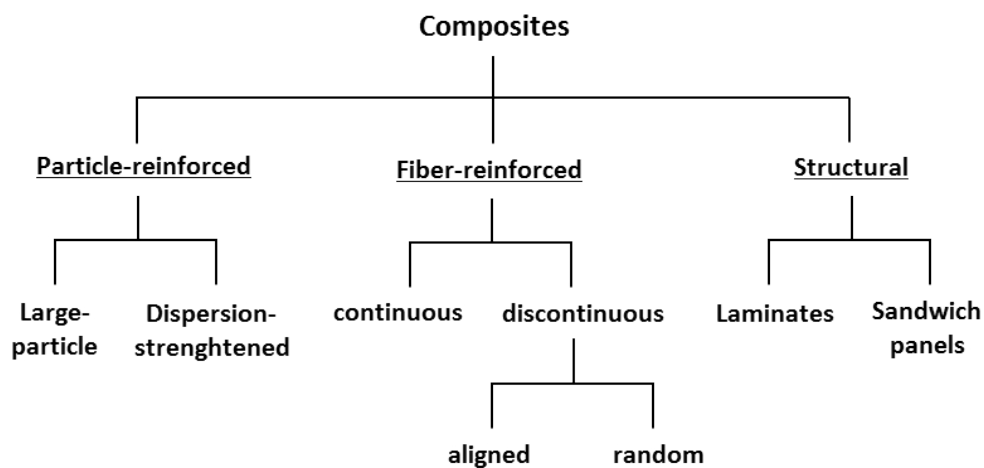


FIGURE 2.1: Classification of composites based on reinforcement type.

Among the fibre reinforced composites, mostly aramid, glass and carbon fibres are employed. An interesting class of composites are natural fibre reinforced polymer-matrix composites, in particular the use of fibres from cellulosic sources (i.e. lignocellulose) [17]. These abundant and often cheap fibres from renewable resources are embedded into a polymer matrix in order to improve strength and toughness of the material. Embedding these fibres into a natural and biodegradable matrix, for example polylactic acid can be used to create more environmentally friendly materials.

Several applications of polymer composites in the design of biomaterials and implants are highlighted in the review of *Ramakrishna et al.* [18]. Major concerns for the use of polymers in medical applications are long term durability and mechanical stability which are for example important for orthopaedic devices. PMCs can be superior also in this respect. For example polymers on the basis of acrylates reinforced with glass particles are used as dental filler materials [19]. Composites might offer new solutions in the search for materials that meet both the mechanical and biological demands of medical materials. Furthermore, appropriate material combinations allow adjustment of implants properties to the large spectrum of mechanical properties present in biological tissues. [18, 20]

## 2.2 Biomaterials

### 2.2.1 Introduction

Biomaterial is defined as a material that is in contact and/or interacts with a living system. The American National Institute of Health describes a biomaterial as *any substance or combination of substances, other than drugs, synthetic or natural in origin, which can be used for any period of time, which augments or replaces partially or totally any tissue, organ or function of the body, in order to maintain or improve the quality of life of the individual* [21]. In the IUPAC Recommendations of 2012 biomaterial is defined as a *material exploited in contact with living tissues, organisms, or microorganisms* [22]. However, a biomaterial can also be understood as a material derived from a bio-based source (e.g. cellulose, polylactic acid).

Biomaterials cover all classes of materials: metals, ceramics, polymers and composites [23]. Prominent examples for metallic biomaterials are titanium, stainless steel and different steel alloys which are for example used in femoral stems, heart valves or stents. Ceramics are often employed for orthopaedic applications, for example artificial bone. Polymers such as PEEK, PMMA or PE can be found for instance in intraocular lenses or as coating material. The field of biomaterials science does not only deal with the development of mechanical implants for permanent replacement (artificial hips, artificial hearts) but also includes removable materials (catheters, wound dressings) and biodegradable materials (surgical sutures). Biomaterials are in everyday use in dentistry, surgery, ophthalmology, wound care and drug delivery. They can be bioinert, avoiding any chemical or biological interaction, or bioactive, guiding the host response [23]. Furthermore design of new biomaterials plays an essential role in tissue engineering and regenerative medicine. In tissue engineering polymeric scaffolds are used for the growth of cells in order to obtain newly generated tissues [24].

A basic consideration in the development of biomaterials is to avoid any toxic or harmful reactions of the cells, tissues or the entire body towards the material, which is the subject of biocompatibility studies. A mutual and innocuous interaction between a material and the host is a complex process involving protein layer formation, immunogenic and inflammatory reactions, repair and regeneration processes for instance. Table 2.1 lists several important reactions of body and tissues when brought into contact with a foreign object. [23, 25]

TABLE 2.1: Selected reactions of the body in contact with a foreign body, i.e. a biomaterial [23, 25].

Reaction	Description
Adsorption of plasma proteins	Protein adsorption to the biomaterial surface and formation of a provisional matrix.
Macrophage activation and foreign body giant cell formation	Macrophages fuse due to the presence of a large foreign object (i.e. biomaterial).
Thrombosis (=blood clotting)	Activation of the coagulation cascade leading to blood clot formation.
Tissue specific cell responses	For example bone ingrowth thereby enhancing mechanical fixation.

In the development of biomaterials both a fundamental understanding of the material's engineering aspects, its preparation, structure and mechanical properties and its biological characteristics are necessary.

## 2.2.2 Protein Adsorption

In the first stage after implantation the material is exposed to blood and proteins immediately adsorb onto the surface [26, 27, 28]. This initial protein layer formation also explains why metals, ceramic and polymers can induce a similar *in vivo* response though exhibiting completely different surface characteristics [26]. Cells and other body components interact rather with the protein layer than with the material surface itself [27]. Notably, the composition of the protein layer is not static and under constant reconstruction (e.g. Vroman effect) [29]. The formed protein layer will define the subsequent biological response, for example the attachment of cells in particular macrophages and platelets. Therefore protein adsorption will modulate possible foreign body reactions as well as inflammatory and immunogenic responses in general.

Protein adsorption represents the first stage in the formation of a fibrous capsule around the material [26, 27, 28]. Fibrinogen plays a key role in this process. It can bind to platelets, thereby mediating their surface adhesion and aggregation. Other proteins that are supposed to influence platelet adhesion are vitronectin, von Willebrand factor and unfolded albumin [29]. At the end stage of the coagulation cascade fibrinogen is converted into fibrin by thrombin (Figure 2.2). Fibrin as opposed to fibrinogen is insoluble and will form a blood clot (=thrombus) by crosslinking with factor XIII.

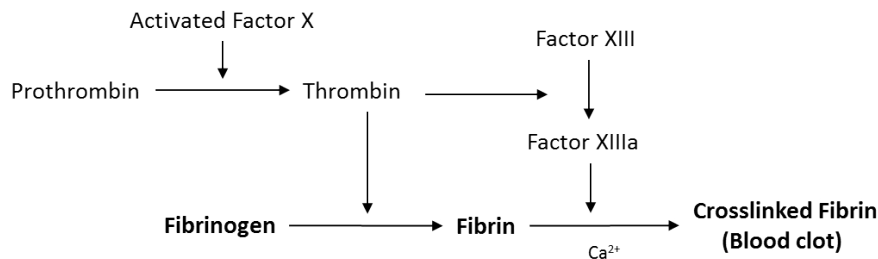


FIGURE 2.2: Reactions occurring at the end stage of the blood coagulation cascade.

Blood clot formation goes with the risk of stroke, heart attack and pulmonary embolism, which often make anticoagulant medication a necessity after implantation of an artificial device. Therefore several studies have focused on ways to reduce unspecific protein adsorption [26]. One approach is to graft polymers onto the surface of the device [30]. The creation of a bioinert coating on a material is a way to improve the bioactivity of the whole device. *Whiteside et al.* found that protein resistant surfaces frequently possess several common features: the presence of polar functional groups, the presence of hydrogen acceptor molecules, the absence of hydrogen acceptor molecules and the absence of a net charge [26, 29]. The rationale behind these rules is to produce a hydration layer around the material, which induces a high activation barrier for protein adsorption.

Methods to study the interaction between a material's surface and proteins are for example surface plasmon resonance spectroscopy (SPR), quartz crystal microbalance (QCM) or various *ex situ* methods [29]. Surface chemistry, especially the control over protein adsorption, is an important aspect in the design of new biomaterials, greatly influencing the overall bioactivity of a device [27].

### 2.2.3 Fields of application: Wound dressings and orthopaedic implants

A wound is a type of injury where the normal structure and function of a tissue is disrupted. Wounds can be created due to physical or thermal forces (burning) or as a result of a disease. Wound healing is a multistage process which happens quickly after the injury. In the first phase, haemostasis occurs by the activation of the clotting cascade (Chapter 2.2.2) in order to stop bleeding and the consequent blood loss. Inflammatory reactions occur early in the wound healing process which include cellular and vascular responses. After a few days, fibroblasts and epithelial cells migrate to the wound and proliferate, replacing the damaged tissue. Fibroblasts produce collagen thus providing strength to the newly formed tissue. [31]

Wound dressings (Figure 2.3) should promote wound healing. Furthermore dressings should provide and maintain a moist environment, allow exchange of air, prevent infection by acting as a barrier to microorganism and/or having antimicrobial properties, remove blood and excess exudates and show low adherence. Since a wide variety of wounds exist one wound dressing might not be suitable for another type and stage of wound. Modern wound dressings are often made from synthetic polymers or natural polymers (e.g. alginate, collagen, chitosan and hyaluronic acid) processed into the form of fibres, hydrogels, membranes, scaffolds and sponges. Recent developments in wound care have also focused on developing systems for controlled delivery of drugs from the dressing to the wound. [1, 31]



FIGURE 2.3: Promising fields of application for chitosan based materials: wound dressings (left) and orthopaedic implants (right). Figure reprinted from [32] and [33].

As some of us might already have experienced, bone is able to repair fractures. This is possible due to reconstruction and reorganisation processes within cortical bone in a concerted interplay between two types of cells: osteoblasts and osteoclasts. Osteoblasts, derived from mesenchymal stem cells, are responsible for the formation of new bone, secreting collagen and hydroxyapatite. The osteoblasts are trapped inside the matrix they have created, where they do not divide anymore and are now referred to as osteocytes. On the other hand, osteoclasts degrade and remove bone. In the design of bone grafts and orthopaedic implants (Figure 2.3) the impact on these two cell types is critical for its integration. Orthopaedic implants (plates, nails, joints, femoral stems etc.) are currently made from metals or metal alloys such as stainless steel, cobalt-chromium nickel alloys or nickel-titanium alloys [34]. Common issues in the use of orthopaedic devices are infections and loosening, which can eventually cause implant failure. Therefore the focus lies on the prevention of bacterial colonisation and the promotion of the ingrowth of bone cells (osseointegration). Respective coatings for orthopaedic implants can be especially useful to address these issues and are intensively studied [35, 36].

## 2.3 Chitosan

### 2.3.1 Introduction

Chitosan is a linear, semi-crystalline, polysaccharide consisting of  $\beta$ -(1-4)-linked D-glucosamines and N-acetyl-D-glucosamines (Figure 2.4). It is obtained by the deacetylation of chitin. Chitin (poly-N-acetyl-D-glucosamine) is the second most abundant polysaccharide after cellulose. In fact, the structure of chitosan and cellulose are highly similar. The only difference between them is the functional group on C2 of each monomer unit. In chitin the hydroxyl group of cellulose is replaced by an acetylamino group. Chitin consists not entirely of N-acetyl-D-glucosamines but rather, like chitosan, possesses D-glucosamine constituents. Therefore the boundary between chitin and chitosan is kind of blurred. Chitin with a degree of deacetylation of 50 % or above is frequently referred to as chitosan and below as chitin [37]. Another differentiation criterion is the solubility of the substance with chitin being insoluble and chitosan being soluble in acidic aqueous medium. Chitosan is produced from chitin by alkaline treatment or by enzymatic hydrolysis with chitin deacetylase. Partial deacetylation can for example be achieved with sodium hydroxide (40-50 wt%) treatment at 90–120 °C for 4–5 hours [2]. Depending on the processing conditions, chitosan with different molecular weight and different degree of deacetylation is received [38].

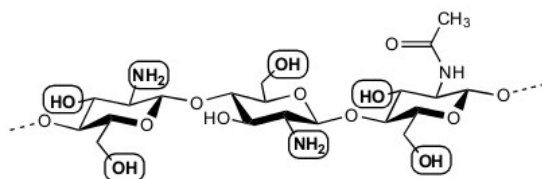


FIGURE 2.4: Chemical structure of chitosan.

The word chitin dates back to the ancient Greek term chiton which means covering. Indeed chitin is a molecule with structuring effects and in combination with proteins (e.g. sclerotin) and calcium carbonate forms a composite material which builds up the chitinous exoskeleton of insects. It not only naturally occurs in the exoskeletons of various arthropods (e.g. crabs, shrimps, lobsters or insects) but also exists in the cell walls of fungi, the radula of molluscs, in annelids and in cephalopods. Estimations of the annual natural production are in the range of  $10^{10}$  to  $10^{11}$  tons [39]. Commercially available chitin is obtained from the shells of shrimps and crabs as a byproduct of the seafood industry. During processing shells are demineralised with hydrochloric acid and the dried decalcified shrimp shells are deproteinised with sodium hydroxide [40, 41]. Due to its high number of inter- and intramolecular hydrogen bonds, chitin shows high crystallinity and in turn high strength and low solubility [41]. Chitin forms sheets with three known allomorphs,  $\alpha$ -chitin,  $\beta$ -chitin and  $\gamma$ -chitin. The last one is also considered as a special form of  $\alpha$ -chitin.  $\alpha$ -Chitin is found in shrimp shells, whereas  $\beta$ -chitin can for example be found in squids. Chitin is highly hydrophobic and is insoluble in water, as well as most organic and inorganic solvents. This highly impacts its processability and applicability. Only a limited number of solvents are known for chitin. For instance DMAc/LiCl mixture, hexafluoroisopropyl alcohol and ionic liquids have been used for such purposes. [42]

The most prominent derivative of chitin is chitosan. As already mentioned chitosan, in contrast to chitin, is soluble in acidic aqueous media. The solubility is related to the protonation of the amino group in acidic medium, leading to an overall positive charge of the polysaccharide. Therefore chitosan exists as a polycation in acidic medium. At pH value of 6 to 6.5 or higher [2] chitosan becomes deprotonated again, the polysaccharide becomes insoluble and precipitates (Figure 2.5).

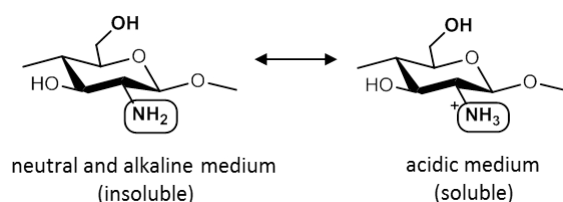


FIGURE 2.5: Chitosan's pH-dependent structure and solubility.

The degree of deacetylation (DD) is defined as the fraction of D-glucosamine units in the polysaccharide. Analytical tools for its determination ranges from spectroscopic methods such as IR-spectroscopy, UV spectrophotometry, <sup>1</sup>H liquid NMR and <sup>13</sup>C solid state NMR, to chromatographic methods like pyrolysis gas chromatography, GPC, HPLC and different titration methods [43, 44]. Properties of chitosan largely depend on the molecular weight and the degree of deacetylation. Moreover the arrangement of deacetylated sites can determine several properties of the polysaccharides [2]. For instance, degree of deacetylation and molecular weight impacts solubility, swelling behaviour, biodegradability, biocompatibility, its antimicrobial and haemostatic properties [2, 40].

Chitosan can be processed into different forms such as microspheres, films, nanoparticles and nanofibres, beads, scaffolds, membranes and gels to mention just a few. Material formation is governed by the formation of hydrogen bonds between the polymer chains [45]. Chitosan can bind metal cations and anions like palladium, copper, silver or iodine through complex formation via the free amino groups. For example, the chitosan sorption capacity for various heavy and toxic metals is in the range of 1 mmol/g [46, 47].

The reactive amino group and the carboxyl group of chitosan are ideal target sites for derivatisation, for example O-/N-carboxyalkylation, acylation, thiolation or phosphorylation [41, 44]. Sulfation of the amino group gives rise to a polyanionic chitosan-derivative. Another way to process chitosan is to graft molecules onto the chitosan backbone. For instance, poly(acrylonitrile), poly(methyl methacrylate), poly(N-isopropylacrylamide), poly(ethylene glycol), poly(styrene) or poly(dimethylsiloxane) have been grafted onto chitosan [37, 41]. Graft copolymers with cyclodextrins or small molecules like EDTA have been reported as well [37].

Chitosan with low molecular weight or oligosaccharides are preferred for some applications. Therefore, different techniques for the degradation of chitosan have been developed using chemical (e.g. HNO<sub>2</sub>, HCl), physical (e.g. radiation, thermal) or enzymatic (e.g. chitinases, chitosanases, glucanases) routes [40]. Crosslinking of chitosan can produce more stable networks, with improved mechanical properties. Commonly employed linker molecules are glutaraldehyde, sulfuric acid, genipin, epoxy compounds or quinones [48]. Furthermore, chitosan can be used as part of different blends and hybrid materials.

### 2.3.2 Moisture sorption behaviour

Understanding the way chitosan adsorbs and distributes water and how this affects the molecular ordering of the chitosan chains is important for the description of macroscopic properties as well as for several applications (e.g. food packaging). Chitosan can adopt different structures (polymorphism), depending on the state of hydration. Water distribution and diffusion rates can be assessed using nuclear magnetic resonance (NMR) spectroscopy [49, 50]. NMR studies have been useful to elucidate the structuring role of the acetate anions in chitosan films produced from solution casting. Acetate anions have plasticising effects on casted films, increasing film flexibility [49]. It was found that at higher moisture contents removal of acetic acid from the material spontaneously occurs. This removal of acetate counterions, which electrostatically interact with the polymeric network, causes reorganisation of the material structure [50].

Monitoring water content values at a constant temperature and different relative water pressures, displayed as moisture sorption isotherms, is another way to study polymer-water interactions. Moisture sorption isotherms of chitosan films have a sigmoidal shape and display a hysteresis for adsorption and desorption (Figure 2.6). Water content during desorption is higher than during adsorption at a given humidity. Maximum moisture contents for chitosan are typically around 0.30 (g of water/g of polymer) [51, 52, 53]. *Agrawal et al.* [53] describes that water sorption is related to the binding of water molecules by the hydroxyl group rather than the amino groups, which do not contribute to the binding of water at low partial pressures. Therefore water sorption isotherms depend only slightly on the degree of deacetylation. [53, 54]

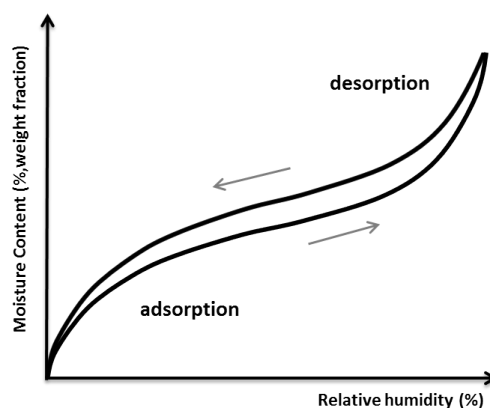


FIGURE 2.6: Moisture sorption isotherm typical for chitosan, displaying a sigmoidal shape and hysteresis.

Water can act as a plasticiser or as an antiplasticiser depending on the amount of water and the temperature [53]. Plasticising effects are related to increased chain flexibility due to the disruption of polymer strand interactions. Water content in chitosan has an influence on the glass transition temperature, secondary relaxation phenomena and mechanical properties [49]. For example, the glass transition temperature ( $T_g$ ) can vary between 18–62 °C depending on the water content as determined from dielectric relaxation studies [55]. Literature reports using DSC and DMTA reported  $T_g$  values ranging from 30 °C to 222 °C, or no glass transition at all [49, 55].



### 2.3.3 Chitosan and its biological and physiological properties

Chitosan shows antimicrobial activity against a broad range of organisms, including different types of bacterial strains, yeast and fungi [9, 56, 57]. Fungi are more susceptible towards chitosan compared to bacteria [9]. Activity against both gram positive and gram negative bacteria is widely reported. Though in literature it is somewhat controversial whether chitosan's impact on gram positive or gram negative bacteria is higher [9]. Chitosan's antimicrobial activity has been attributed to bacteriostatic mechanism (stopping bacterial reproduction) as well as bactericidal mechanism (killing bacteria), although a clear distinction between them is often missing [56]. Yet, its mode of action is also still not fully understood and different models have been proposed [9, 56, 57]. In the most widely applied model, the antimicrobial activity of chitosan is linked to the interactions of the polycationic polysaccharide and the negatively charged membrane surface of the bacterium. These interactions cause an increase in cell membrane permeability and disruption of the osmotic barrier. In the end, a loss of proteins and other cellular components of the bacterium can occur. The second proposed mechanism involves the binding of chitosan to bacterial DNA, the inhibition of mRNA synthesis and subsequently inhibition of the protein biosynthesis by intracellular chitosan molecules. The third mechanism is related to the chelating of metals and the binding of nutrients that are essential for bacterial growth.

Although chitosan inhibits the growth of several microorganisms, it is regarded as non-toxic and biocompatible as well as being FDA approved for the use in wound dressings [8, 10]. From the current state of knowledge, a low toxicity in the  $\mu\text{g}/\text{ml}$  range can be assumed. However, *in vitro* and *in vivo* toxicity can vary with type of derivatisation, formulation, salt form, degree of deacetylation and molecular weight. Chemical and biological purity needs to be ensured, with the latter being a critical issue due to the natural origin of chitosan. [8]

Furthermore chitosan promotes differentiation of mesenchymal stem cells into osteoblasts and increases osteoblast viability. At the same time, the number of osteoclasts is reduced by the action of chitosan. Eventually chitosan enhances osseointegration and assists bone fracture healing. It has been found that chitosan displays anticancer properties. For example, it can act against secondary breast and prostate tumour formation in bone. [58]

The foreign body reaction towards chitosan is small, with no or minor encapsulation observed [59]. Chitosan exhibits mucoadhesive properties. The interaction between chitosan and negatively charged mucin involves electrostatic interactions, hydrogen bonding, and hydrophobic interactions [60]. It shows permeation enhancing effects, opening epithelial tight junctions [62]. Furthermore, chitosan is well known to be haemostatic. The haemostatic mechanism of chitosan is often attributed to the agglutination of red blood cells [10, 61].

Knowledge about the biodistribution of chitosan is of great interest, particularly with regard to applications in drug delivery. Circulation times and stability can be adapted by changes in molecular weight. Notably molecular weight of chitosan should be low enough to allow renal clearance or otherwise be degraded by enzymes. For instance, chitosan is degraded by lysozymes and bacterial enzymes in the colon. [8]

### 2.3.4 Applications

Chitosan has been intensively studied for potential medical applications. This is related to some of its characteristics, namely high biocompatibility, antimicrobial and haemostatic properties, which are described in Chapter 2.3.3 in more detail. Often, these favourable properties are a result of its polycationic character, which is a distinctive feature to other polysaccharides. Besides medical applications, chitosan is used in agriculture, personal care, foods, pharmaceuticals, as well as water and waste treatment [42].

Its application in agriculture ranges from the protection of plants against pathogenic viruses, bacteria, fungi, insects and pest, towards the use as a seed coating and as soil amendment for the controlled release of nutrients and fertilisers. In plants, it can induce defense responses and enhance host resistance. [63, 64]

Hair or skin care products and toothpastes containing chitosan have already found commercial distribution. It has been demonstrated that chitosan shows good skin compatibility and is suitable for skin care. It can maintain skin moisture due to its moisture-retention ability. Hair is negatively charged and by electrostatic interaction chitosan can form a clear elastic film on it, thereby making it softer and increasing its mechanical strength. [65]

The interest in chitosan for application in the food industry is closely related to its natural activity against a broad range of bacteria, yeasts and fungi as well as its good film forming capability e.g. as edible coatings for fruits. It can improve the shelf life of food and can act as a thickener and stabiliser [66]. It is not digestible (dietary fibre) and has been assumed to reduce fat absorption in the body, though *in vivo* no effect has been found [67, 68]. Chitosan's high metal ion sorption capacity can be used for the recovery of metallic compounds in industrial processes or removal from waste water [46, 47]. Furthermore, it is investigated as a flocculant and clarifier in water treatment [69]. It can improve filtration processes by binding particles which can then be more easily removed.

Chitosan in the form of porous interconnected structures can be used as scaffold for tissue engineering [59]. In this regard chitosan's biodegradability, non-toxicity and capability to facilitate cell attachment and proliferation are advantageous characteristics [3]. The most explored applications of chitosan in tissue engineering are the regeneration of cartilage, intervertebral discs, skin, liver, blood vessels, nerves and bone [3, 4]. It is a promising material for wound and burn dressings or other wound management dedicated materials, due to its antimicrobial and haemostatic properties as well as its high moisture retention properties and oxygen permeability [1, 70]. Chitosan-based wound dressings effectively promote wound closure and restoration and have already found commercial use. Chitosan is a promising candidate for future applications as bone substitute or coating of orthopaedic devices, often in combination with hydroxyapatite or other calcium-based materials [71].

Chitosan's ability to bind to negatively charged molecules (e.g. DNA) via electrostatic interactions can be utilised for gene delivery. Furthermore, chitosan can be used for the delivery of drugs in different types of formulations, for instance as hydrogel, drug conjugate (e.g. drug-loaded nanoparticles), biodegradable release system or polyelectrolyte complex. Such systems can be used for the administration of a broad range of therapeutics including various proteins and peptides, growth factors, anti-cancer and anti-inflammatory agents and antibiotics. The incorporation of imaging agents (e.g. quantum dots) in chitosan opens up possible uses in the area of bioimaging. [2, 72]

## 2.4 Silanes and sol-gel processing

Silanes are, in analogy to alkanes, a class of chemical compounds consisting of one or multiple silicon atoms with the general formula  $\text{Si}_n\text{H}_{2n+2}$ . The silicon atom represents the center of a tetrahedron, forming four single bonds. An early development in sol-gel processing was the observation that the hydrolysis of tetraethyl orthosilicate in acidic solutions leads to the formation of  $\text{SiO}_2$  particles [73]. This process can be catalysed both from acids and bases. Organosilanes contain at least one carbon atom. Several organosilanes with the general formula  $(\text{RO})_3\text{Si-X}$ , where RO is a hydrolysable group (e.g. methoxy or ethoxy group) and X an organofunctional group, have received particular attention. These types of silanes can act as coupling agents and can be used to functionalise surfaces [74]. The three Si-OR bonds can easily hydrolyse in water forming silanol groups, which can create stable covalent bonds with surfaces. A prominent example is the formation of self assembled monolayers of 3-aminopropyl triethoxysilane (APTES) [75]. The free amino group of APTES can be used for subsequent reactions.

The sol-gel process describes a technique for the preparation of different kinds of materials from small precursor molecules (Figure 2.7). First, precursor molecules, typically metal or semi-metal alkoxides, undergo hydrolysis and condensation, thereby forming colloidal particles (sol). These colloidal particles can create interconnected three-dimensional networks (gel). The solid phase shows different forms somewhere between a dispersion of discrete particles to a continuous network, depending on factors such as time and solvent concentration. Advantages of sol-gel processing are the mild reaction conditions, in particular the ambient reaction temperature and the easy manipulation of the material properties by variation of the processing conditions (e.g. temperature and pH) [76]. Evaporation of the solvent under ambient pressures will lead to significant shrinkage and the formation of a dense xerogel. Under supercritical conditions a highly porous aerogel with low density is formed. The prepared structures can additionally be processed by heat treatment causing further polycondensation, sintering and transformation into a crystalline material i.e. a dense ceramic. Sol-gel processes are commonly used for the preparation of coatings, fibres and nanoparticles with frequent applications in optical devices. [77]

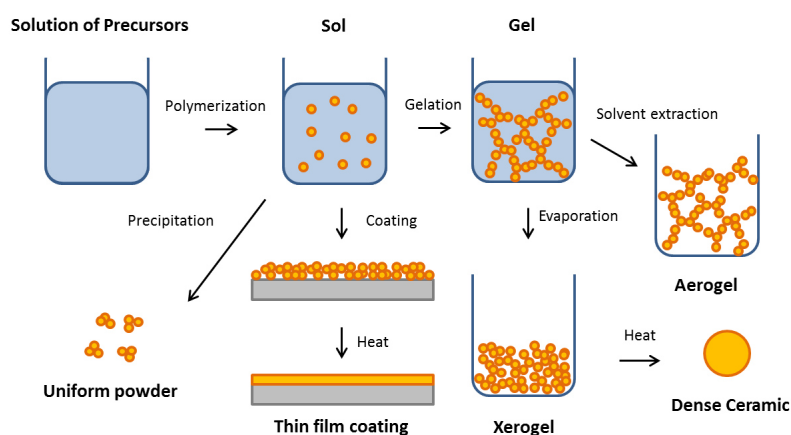


FIGURE 2.7: Schematic representation of the sol-gel process and its products.

## 2.5 Chitosan-Siloxane Hybrid Materials

As previously described sol-gel processing of different alkoxy silanes can be deployed to create inorganic-organic hybrid materials. Hybrids have been prepared from a wide range of different sol-gel products and polysaccharides such as cellulose, chitin, alginate or carrageenan [78].

Chitosan contains three types of reactive functional groups: one primary and one secondary hydroxyl group as well as one amino group. These functional groups are available for modification and crosslinking. For example the amino functional group has been coupled to the poly(siloxane) network through an urea bridge using 3-isocyanatopropyl triethoxysilane (ICPTES) [79]. The amino group has also been reported to crosslink with 3-glycidoxypropyl trimethoxysilane (GLYMO, GPTMS) through an acid-catalysed addition of the amino group to the epoxy functionality [80]. Hybrids with different ratios of chitosan and GLYMO were prepared in the work of *Shirosaki et al.* [6]. In this work it has been demonstrated that adhesion and proliferation of MG63 osteoblast cells on hybrid materials is higher compared to neat chitosan, thus making it an attractive material for orthopaedic applications.

The hydroxyl group of the silane and the hydroxyl group of chitosan can react thereby forming a covalent bond. In addition hydrogen bonds between chitosan and the poly(siloxane) network from different precursors will add to the stabilisation of prepared hybrids [5]. Structured nanocomposites could be obtained from the combination of chitosan with sol-gel processed 3-aminopropyl triethoxysilane (APTES) in molar ratios of 0.6:1 [81]. Adding lithium perchlorate affected the morphology and crystalline structure of the films, by interfering the molecular interactions between chitosan and poly(aminosiloxane) domains. This is in good agreement with results from other experiments employing FT-IR, XRD, scanning SEM and EDX, where they found that strong interactions are established in hybrid materials using APTES as crosslinking agent [82].

Chitosan-siloxane hybrid materials are stable in different forms and at different environmental conditions. Several studies report the fabrication of chitosan based hybrid materials in the form of films and membranes. As microspheres chitosan or its derivatives are interesting candidates for drug delivery applications [83] and potential uses as catalyst [84]. Chitosan hybrids containing hydrophobic silica showed improved thermal degradation, lower water affinity, better acid stability and ability to retard a model drug [85]. Stable thin films on silicon substrates prepared from chitosan and different alkoxy silane precursors, subjected to a sol-gel process, have been reported by our group [5]. Tetraethyl orthosilicate, tri-*tert*-butoxysilanol, trimethyl ethoxysilane, *p*-trifluoromethyltetra-fluorophenyl triethoxysilane, trivinyl methoxysilane, (methoxymethyl)trimethyl-silane, and hexamethoxydisilane were used as precursor molecules.

In several of the above mentioned works a reduction in swelling of the prepared hybrid materials compared to chitosan was reported [6, 80, 82]. In addition good biocompatibility and promising results in terms of osseointegration [6] and nerve regeneration [7] have been found.

# Chapter 3

## Principles of applied tests and methods

### 3.1 Spin coating

Spin coating is a technique used to deposit uniform thin films on flat substrates. Silicon wafers are commonly employed substrates. One of the main advantages of spin coating is that films can be quickly prepared with minimal efforts. It is an example for chemical solution deposition and often used for the processing of polymers. Films with a thickness in the range of a few nanometres up to several microns can be formed. Other techniques of thin film deposition are for example chemical and physical vapour deposition, sputtering or Langmuir-Blodgett deposition.

The coating material is dissolved and drops of the solution are placed on the substrate, usually at the centre (Figure 3.1). The substrate is spun at high speed spreading the solution over the substrate by centrifugal forces. Excess material is thereby thrown off. In order to obtain a solid layer, the solvent has to be removed. Solvent already evaporates during the coating process. In addition, residual solvent can be removed in a separate drying step which can also involve heat treatment. Evaporation of solvent is facilitated by the use of volatile solvents.

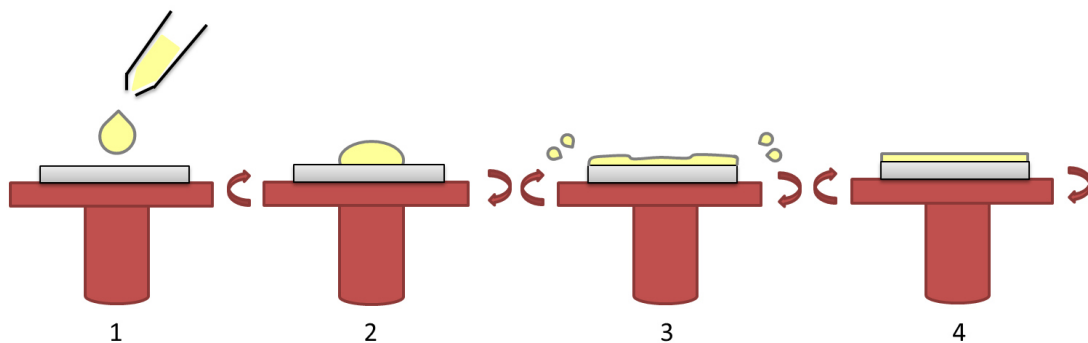


FIGURE 3.1: Stages of the spin coating process: 1.-2. Fluid deposition 3. Spinning 4. Solvent evaporation and layer formation.

Rotation speed, acceleration speed and coating time are the parameters defined for every coating process. Film thickness eventually depends on various factors, in particular the fluid material (e.g. molecular weight of the polymer, concentration and viscosity of the solution), the spinning parameters and the type of substrate. Lower spin speeds and shorter spin times create thicker films. For example, if a polymer is deposited, the layer thickness increases with higher molecular weight and also higher concentration of the polymer in the solution. In addition, higher film thickness can be created by consecutive layer deposition. Spin coating is of great technological importance for example for the deposition of photoresists for photolithography [86].

### 3.2 Surface Plasmon Resonance Spectroscopy (SPR)

Surface plasmon resonance is a surface characterisation method that is especially useful in the elucidation of adsorption processes. SPR takes advantage of a change in intensity of p-polarized light in total internal reflection at the surface-solution interface, due to optical excitation of surface plasmons in thin metal films (e.g. Au). Resonance can be achieved at a given wavelength and angle, when the resonance condition of the surface plasmon waves are fulfilled, and it is a characteristic for the interface. Therefore slight changes at the interface e.g. occurring during adsorption of molecules or a change in layer thickness can be monitored as a change of the SPR signal. Usually the change in the angle of the reflection minimum is determined. In a typical setup (Figure 3.2), p-polarized laser light is generated, passed through a glass prism and detected with a photodetector. At the face of the prism where total reflection takes place, a sensor slide comprising of a glass support and a metal thin film (e.g. gold) is placed. The metal film can be coated with a material of interest, which can possess binding sites for adsorbents. Alternatively, receptor molecules can be directly immobilized on the metal surface. A flow cell is placed on top of the functional material allowing a precise stream of potential adsorbents. [87]

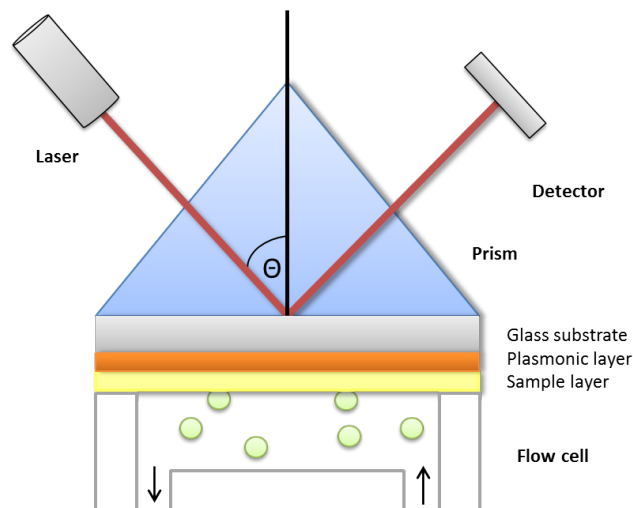


FIGURE 3.2: Schematic representation of the surface plasmon resonance spectroscopy (SPR) detection principle. Light is passed through a prism, at the angle  $\Theta$ , and is totally internally reflected at the surface-solution interface. Changes at the interface are monitored by changes in the angle of the reflection minimum.

### 3.3 Stylus profilometry

A profilometer is an instrument used to display the profile of a surface, by determining vertical changes during lateral movement of a probe. In a contact profilometer a diamond stylus is vertically aligned, thus establishing a contact between the surface and the stylus tip. The stylus is gently moved along the substrate and lateral changes are detected. From the measured surface profile, surface roughness, peak-to-valley height and various other topographical parameters can be derived. [88]

### 3.4 Atomic Force Microscopy (AFM)

Atomic Force Microscopy allows measurement of atomic forces on a nanometre scale, creating three dimensional images of the surface topography. The resolution of common AFM instruments is typically below 0.2 nm vertically and 3 nm laterally. The principle of this method is similar to other types of surface probes microscopy (SPM) techniques: A cantilever with a tip is moved by piezo elements in all three dimensions (x, y and z axis). Movement along the z axis allows control over the applied force between tip and sample. A laser is focused on the end of the cantilever and any displacement of the deflected beam is monitored via a Position Sensitive Detector (PSD) (Figure 3.3). In contact mode, height variations cause bending of the cantilever which is monitored by the vertical PSD elements as a signal deflection. The z-piezo changes the position of the cantilever so that the original signal is restored, which in turn means that a constant force between sample and tip is maintained. The z-position at all points along the x, y area creates the height image. Height variations are represented by different colours related to a specific height defined in a scale bar. Therefore this method also allows to determine surface roughness at the measured area. At the same time, the material contrast of a specimen can be recorded. During scanning, the lever is subjected to torsion due to lateral friction forces, caused by changes in elasticity, hardness, roughness, adhesion or chemical interactions, but also contributions from height variations. At the PSD this is detected as horizontal changes of the deflected beam. This adds information on material properties and their distribution (e.g. amorphous or crystalline). [89]

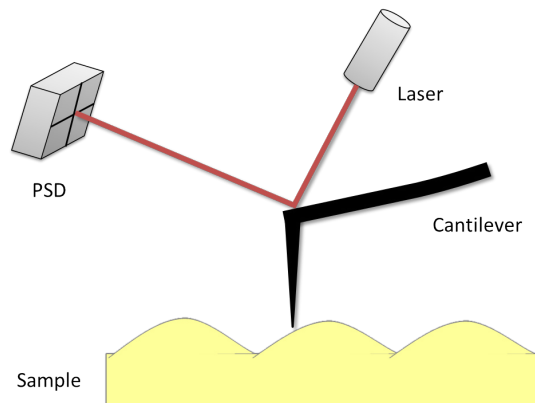


FIGURE 3.3: Schematic representation of the atomic force microscope detection principle in contact mode. Deflection of the cantilever is measured by changes in the position of the reflected laser beam.

For AFM there are different modes of operation and numerous special techniques such as Liquid AFM and Conductive AFM have been established. Moreover, AFM can be used as a tool for the manipulation of atoms and molecules. Modes of operation can be classified into three categories: Contact mode, tapping mode and non-contact mode. In contact mode a contact is established between tip and substrate. In tapping mode, the cantilever oscillates at or close to its resonant frequency. The tip touches the surface only at the minimum point of the oscillation curve. Changes in the resonance frequency of the system are used to determine distances and lateral changes. In non-contact mode the tip oscillates a few angstroms away from the surface. [90]

### 3.5 Contact angle

Measuring the contact angle between a liquid drop and the surface of a solid is a way to determine the solids wettability. The contact angle is defined as the angle created by a liquid drop at the boundary of the three phases solid, liquid and vapour (Figure 3.4). The shape of the drop depends on the competing adhesive forces between the liquid and the surface on one hand and the cohesive forces within the drop on the other hand. Low contact angles involve higher interactions causing a wider spreading of the liquid, while higher contact angles correspond to low liquid/solid interactions and hence small spreading of the drop. Surfaces displaying contact angles above  $90^\circ$  are classified as low-wetting or non-wetting. In the case of water as the liquid, wettable surfaces are termed hydrophilic and non-wetting surfaces hydrophobic.

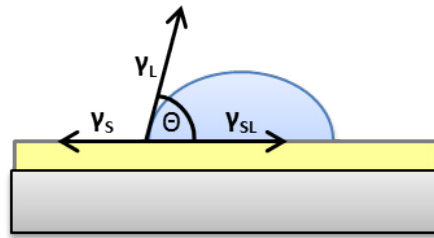


FIGURE 3.4: Illustration of the contact angle,  $\Theta$ , at the three-phase boundary solid, liquid and vapour. Drop shape in equilibrium is the result of a balance of three forces.

Young's equation describes the relationship between the contact angle  $\Theta$ , the surface free energy of the liquid  $\gamma_L$ , the surface free energy of the solid  $\gamma_S$  and the interfacial free energy of the liquid and solid  $\gamma_{SL}$  (Figure 3.5).

$$\gamma_S = \gamma_L \cdot \cos\theta + \gamma_{SL}$$

FIGURE 3.5: Young's equation:  $\Theta$ , contact angle;  $\gamma_L$ , surface free energy of the liquid;  $\gamma_S$ , surface free energy of the solid;  $\gamma_{SL}$ , interfacial free energy of the liquid and solid.

Through contact angle measurements with several liquids, surface energies can be calculated. In most cases such measurements are carried out with water and diiodomethane. A common method to calculate free surface energies from contact angle measurements is the one by Owens-Wendt-Rabel-Kaelble (OWRK).

Contact angles can be classified as static contact angles and dynamic contact angles. In the static (sessile) drop method, drops are placed on the surface and the respective contact angles are measured. In the dynamic contact angle method, the advancing and receding angle is measured by changing the volume of the drop. The volume of the liquid drop is continuously increased (wetting) to cause higher contact angles. This way the advancing (maximum) contact angle can be determined. For the receding (minimum) contact angle, the volume of the drop is continuously decreased (dewetting). From the difference of the advancing and receding contact angle, the contact angle hysteresis can be calculated.



### 3.6 Cell culturing

Cell culturing is the growth of cells in an artificial environment. It usually refers to the growth of eukaryotic mostly animal derived cells, as opposed to cultures of plant, fungi or bacteria. Though there are many advantageous aspects of cell culture, such as precise control over pH, temperature and gaseous environment, adjusted hormone and nutrition supply, uniformity of cells derived from a characterised cell line, and avoidance of animal experiments, the applicability of cell culturing is limited. Most importantly, results from cell culture experiments might not be adaptable to the full organism. Cells growing in an artificial environment, after several subcultivations, often display different phenotypical or genetical properties and loss of tissue-specific functionality compared to their *in vivo* counterparts.

Cells are removed from the donor which can be either in an adult, embryo or egg state. After acquiring the selected tissue, fatty and necrotic cells are removed. Fine dissection and mechanical or enzymatic disaggregation of the tissue as well as explant growth are ways to obtain primary cell cultures. As soon as primary cells are passaged, one speaks of a cell strain. A passage includes harvesting, dilution and reseeding of cells. For the harvesting of the cells, medium is removed, the cell monolayer is washed, trypsin is added and removed again leaving back a residual film. After incubation at 37 °C for 10 minutes cells round up and can be resuspended in medium. After that, cells can be used for testing purposes or after dilution can be reseeded starting a new passage. [91]

One reason for the passaging of cells is that after forming a confluent monolayer, strictly adherent cells cannot grow anymore which can lead to a reduced proliferation rate and finally to the death of the whole cell culture. Passage of cells furthermore provides an easy way to change the medium and to control the cell number. After several serial passages cells show senescence and death unless the cells are transformed in order to form an immortalised cell line (Figure 3.6). [91]

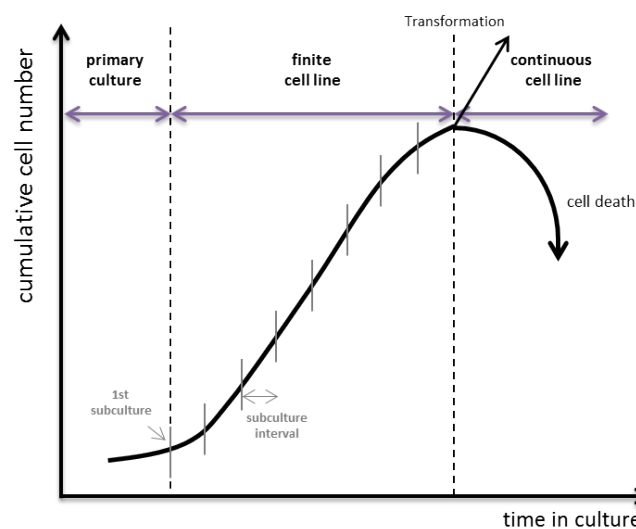


FIGURE 3.6: Growth of cells in culture. After several subcultivations senescence and cell death in finite cell lines occurs. By transformation cells will establish a continuous cell line.

For testing purposes cells derived from primary culture or cells from an established cell line can be used. Primary cells are directly derived from an isolated tissue and display properties similar to the cells in the *in vivo* state. However their use is limited since, as already mentioned, after confluency has been reached cells have to be subcultivated. On the other hand, cells from an established cell line which can for example be received from ATCC (American Type Culture Collection) are well characterised and allow comparability of tests performed with the same line.

Cytotoxicity is the ability of a particular chemical or biological substrate to be toxic to cells. Various methods do exist to assess toxicity, which can be either *in vitro* or *in vivo* methods. One routine to assess *in vitro* toxicity is to expose cells to the substance under examination. Afterwards, cell viability can be determined using different assays, for instance crystal violet, neutral red or MTT assay [92]. Assays are typically performed in microtiter plates, an approach enabling automatisation. Crystal violet, a dye, is incorporated into the DNA of cells and used to determine absolute cell numbers. In MTT assays, the reduction of the water soluble, yellow dye 3-(4,5-dimethylthiazol-2-yl)-2,5-diphenyltetrazolium bromide (MTT) to the corresponding insoluble, purple formazan 5-(4,5-dimethylthiazol-2-yl)-1,3-diphenylformazan is detected (Figure 3.7). Dimethyl sulfoxide or SDS in acid solution is added to the dye in order to solubilise the formed formazan. Reduction of the dye occurs within the cell and requires the presence of reduction equivalents. Studies showed that reduction of the tetrazolium salt is carried out by the succinate dehydrogenase located in the inner mitochondrial membrane as well as by enzymes located on the endoplasmatic reticulum, on cost of the reduction equivalents NADH and NADPH [93]. Overall MTT reduction is a parameter for metabolic activity of a cell rather than for cell respiration as had been previously assumed. Dead or non-proliferating cells show no or very little metabolic activity and are therefore not detected.

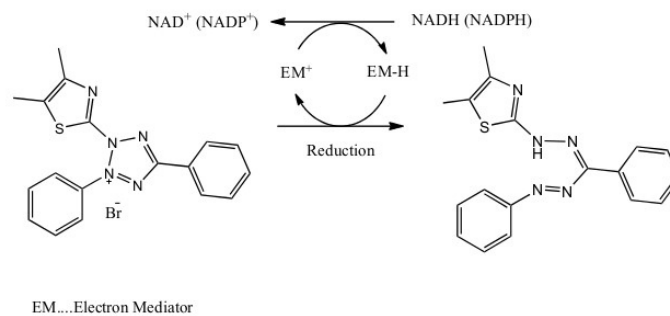


FIGURE 3.7: Detection principle of MTT assays. The yellow tetrazolium dye MTT is converted to the corresponding insoluble purple formazan by NAD(P)H-dependent cellular enzymes.

### 3.7 Tensile testing

Tensile tests are one of the most fundamental techniques in material science. They provide information about a material's mechanical properties by applying controlled tension on a sample until failure. A typical tensile specimen consists of two shoulders and a gauge section with specific dimensions. Tensile tests are typically carried out with universal testing machines which can also measure a material's response towards compression, bending or torsion. In order to perform tensile tests, specimen are

clamped between two heads with grips. The lower head is coupled to a stationary base and the upper head is connected to a moveable crosshead. Tension is applied by lifting the crosshead. From tensile tests stress-strain curves are drawn (Figure 3.8). It has to be noted that speaking of stress, this can mean true stress/strain or engineering stress/strain. True stress is the applied load divided by the actual cross-sectional area at any given point, while engineering stress describes the load divided by the instant cross-area.

Tensile tests are used to measure a material's ultimate tensile strength, yield strength, young's modulus (elastic modulus), toughness and other material parameters. Ultimate tensile strength is the maximum stress a material can withstand until it breaks. Yield strength is a measure of the stress at which a material changes from being elastically deformed to being plastically deformed. This value is of practical importance since plastic deformation is not reversible, therefore limiting the forces that can be applied on a specimen. There are different definitions of yield. In case of a not well-defined yield point it is common to use the offset yield point at 0.2% plastic strain. Young's modulus or elastic modulus describes the linear elastic behaviour of a material in small deformations (Hooke's law applies) and is defined as the ratio of the stress to the strain. Stiff materials exhibit high elastic moduli, whereas soft materials have low elastic moduli. The area under the stress-strain curve, the toughness of a material, describes the ability of a material to resist fracture. It also gives the amount of energy per unit volume that can be absorbed by the material.

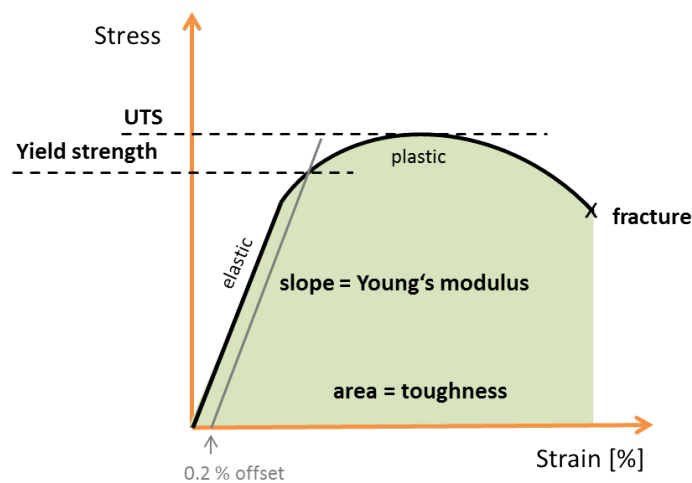


FIGURE 3.8: Example of a stress-strain curve typical for a ductile material.

Brittle materials are characterised by their low deformability when tensile forces are applied. On the other hand, ductile materials are deformed during tensile testing and can display necking in the area of fracture. Notably, a polymers stress-strain behaviour is influenced by the ambient temperature with respect to the glass transition temperature. A dramatical change of the mechanical properties at the glass transition temperature is observed, with polymers showing more brittle behaviour below their glass transition temperature and ductile behaviour above their glass transition temperature [94].

### 3.8 Dynamic mechanical analysis (DMA)

Dynamic mechanical analysis (DMA) is a method to measure frequency dependent mechanical properties of a sample under a periodic deformation and can be used to determine a material's viscoelastic behaviour. During the measurements, the temperature or the frequency and amplitude of the stress can be varied. As a prerequisite, applied stress does not have to exceed the elastic limit. In most cases, one of the two main different test modes is used, which are temperature sweep or frequency sweep mode. In temperature sweep mode, tests are carried out at a fixed frequency and the temperature is varied. In contrast in frequency sweep modes, a scanning of the periodic stress frequencies is conducted at a fixed temperature. Furthermore, in special set ups it is possible to perform measurements at varying relative humidity. DMA is a very sensitive technique for the observation of glass transition and other transition processes.

In dynamic mechanical analysis, a sinusoidal tensile force is applied and the resulting sinusoidal strain is measured (Figure 3.9). A purely elastic material has a phase difference between the stress and strain curves (= phase lag) of  $0^\circ$  which means they are in phase. On the other hand, a purely viscous material displays phase differences of  $90^\circ$ . Since most polymers are viscoelastic, they display phase differences between those two values. The amplitude of the stress-strain curves together with the observed phase lag provides information about a material's storage modulus, loss modulus or damping coefficient ( $\tan \delta$ ). These parameters can be plotted against varying temperatures, frequencies, or strain values. [95]

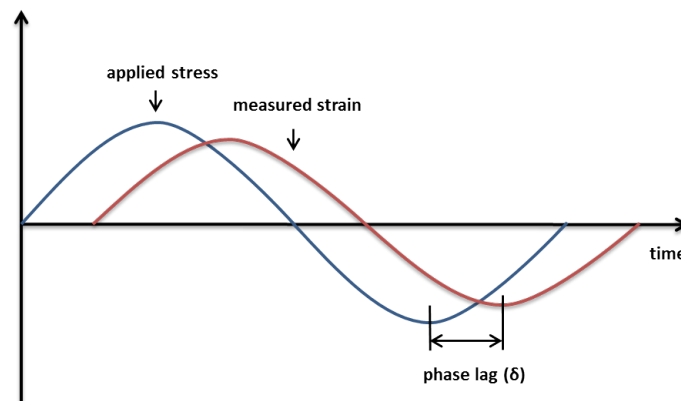


FIGURE 3.9: In dynamic mechanical analysis a sinusoidal stress is applied and the resulting strain is measured. The phase angle,  $\delta$ , describes the lag between applied stress and strain response.

The storage modulus ( $G'$ ) is a measure of the elastic response of a material and can be calculated by multiplying the fraction of stress to strain with the cosine of the phase lag. As its counterpart loss modulus ( $G''$ ) is a measure of the viscous response of a material and can be calculated by multiplying the fraction of stress to strain with the sinus of the phase lag. The third parameter,  $\tan \delta$ , is defined as the ratio of  $G''$  to  $G$  and is a measure of the energy dissipation in a material, i.e. damping. [95]

# Chapter 4

## Experimental

### 4.1 Materials

#### 4.1.1 For sample preparation

##### Chemicals

- **Medium molecular weight chitosan (CS<sub>M</sub>):** Sigma-Aldrich, Lot # MKBF 1336 V, CAS 9012-76-4
- **Low molecular weight chitosan (CS<sub>L</sub>):** Sigma-Aldrich, Lot # MKBH 1108V, CAS 2012-76-4
- **Acetic acid:** ≥ 99.7%, ACS reagent, Lot # STBD2538V, CAS 64-19-7
- **Tetraethyl orthosilicate purum (TEOS):** ≥ 98.0% (GC), Fluka, Sigma-Aldrich, Lot and Filling Code: 1122865 12305276, CAS 78-10-4
- **3-Aminopropyl triethoxysilane purum (APTES):** ≥ 98.0% (GC), Fluka, Sigma-Aldrich, Lot and Filling Code: 1171117 23605253, CAS 919-30-2
- **3-Glycidoxypropyl trimethoxysilane (GLYMO):** 98%, Chemical Company, Aldrich, LOT # 10830LU, CAS 2530-83-8
- **Silicon dioxide nanopowder 10 nm (BET):** 99.5%, spherical porous, particle size: 5-15 nm (BET), Sigma-Aldrich, CAS 7631-86-9
- **Silicon dioxide nanopowder 15 nm (BET):** 99.5%, spherical porous, particle size: 10-20 nm (BET), Sigma-Aldrich, CAS 7631-86-9
- **Chitin nanocrystals:** from HCl hydrolysis
- **Cellulose nanocrystals:** from H<sub>2</sub>SO<sub>4</sub> hydrolysis
- **Ethanol:** 96%, CAS 64-17-5
- **Hydrochloric acid:** 37%, AnalaR Normapur, VWR Chemicals, CAS 7647-01-0
- **Hydrogen peroxide:** 30 wt% in H<sub>2</sub>O, ACS reagent, Sigma-Aldrich, CAS 7722-84-1
- **Sulfuric acid:** 95%, AnalaR Normapur, VWR Chemicals, CAS 7664-93-9
- **Sodium hydroxide:** reagent grade 97%, Sigma-Aldrich, Lot # MKBG7454V 15-391-0036-0, CAS 1310-73-2

##### Materials

- **Silicon wafer:** Polished, MEMC Korea Company (Cheonan-Si, Korea)
- **Sensor slides for MP-SPR:** Gold, BioNavis (Ylöjärvi, Finland)
- **Plastic vessels:** with screw caps, volume roughly 300 mL
- **Plastic jars:** with screw caps, polystyrene, volume 40 mL
- **Petri dishes:** polystyrene, diameter 8.5 cm
- **Plastic syringes:** 10 mL (12 mL), Norm-Ject®, Henke-Sass Wolf (Tuttlingen, Germany)
- **Pleated and round filter**
- **Glass beaker, vessels and funnels**
- **Cutting die**

- **Wooden boards**
- **Clothespins**

### Equipment

- **Spin coater:** Polos SPIN150i, SPS-Europe (Putten, Netherlands)
- **Oven:** WTB-Binder, Binder GmbH (Tuttlingen, Germany)
- **Screw press:** hydraulic, PW 20H, P/O/WEBER (Remshalden, Germany)

### 4.1.2 For sample characterisation

#### Solutions

- **Buffer solution:** pH 7.4, 10 mM PBS + 100 mM NaCl
- **Bovine serum albumin** in buffer: 1 mg/mL
- **Fibrinogen** in buffer: 1 mg/mL

#### Materials

- **Razor blades**
- **AFM cantilever:** Silicon, NCH-VS1-W, resonance frequency 320 kHz, force constant 42 N/m, NanoWorld AG (Neuchatel, Switzerland)
- **Construction paper**
- **Cyanoacrylate superglue:** UHU Sekundenkleber blitzschnell PIPETTE

#### Equipment

- **Stylus profiler:** EKTAK 150 Stylus Profiler, Veeco (Anchorage, USA)
- **Drop Shape Analyzer:** Drop Shape Analysis System DSA100 with a T1E CCD video camera, Krüss GmbH (Hamburg, Germany)
- **Atomic force microscope:** Veeco Multimode Quadrax MM AFM, Bruker (Billerica, USA)
- **Surface plasmon resonance spectrometer:** SPR Navi™ 200, BioNavis (Ylöjärvi, Finland)
- **Thickness gauge:** Mitutoyo 543-551-1 Absolute Digimatic Indicator, Mitutoyo Corporation (Sadako, Japan)
- **Electromechanical universal testing machine:** AGS-X Series, Shimadzu (Kyoto, Japan)
- **Dynamic mechanical analyser:** Q800, TA Instruments (New Castle, USA)

### 4.1.3 For cell testing

#### Chemicals

- **DMEM advanced media:** Gibco, Cat. No 12491-015, Thermo Fisher Scientific (Waltham, USA)
- **FBS** (heat inactivated): Life Technologies (Carlsbad, USA)
- **Penicillin:** Powder, Sigma-Aldrich
- **Streptomycin:** Powder, Sigma-Aldrich
- **L-Glutamine:** Powder, Sigma-Aldrich
- **Trypan-blue:** Powder, Sigma-Aldrich

- **Crystal Violet 0.1%**
- **Trypsin:** Powder, Sigma-Aldrich
- **EDTA**

### Solutions

- **Trypan-blue 0.1%:** 100 mg trypan-blue dye in 100 mL of 1 x PBS.
- **Full cell media:** DMEM with 5% FBS containing penicillin (100 IE/mL), streptomycin (1 mg/mL) and L-glutamine (2 mM).
- **10 x PBS:** 80 g NaCl, 2 g KCl, 14.4 g Na<sub>2</sub>HPO<sub>4</sub>, 2.4 g KH<sub>2</sub>PO<sub>4</sub> in MilliQ water with final volume of 1 L. pH should be around 6.8. Sterilization of the solution by autoclaving. Final 1 x PBS contains 137 mM NaCl, 2.7 mM KCl, 10 mM Na<sub>2</sub>HPO<sub>4</sub> and 2 mM KH<sub>2</sub>PO<sub>4</sub>.
- **Trypsin-EDTA solution:** 8 g NaCl, 0.4 g KCl, 0.1 g Na<sub>2</sub>HPO<sub>4</sub>, 1.0 g D-glucose, 3 g TRIS dissolved in 800 mL MilliQ water; pH set with HCl to 7.7. Add 2.5 g Trypsin, 100 U/mL penicillin, 1 mg/mL streptomycin and 0.17 g EDTA. Add MilliQ water to final volume of 1 L.
- **Cellstain double staining kit:** 04511, Sigma-Aldrich

### Materials

- **Malassez Hemocytometer**
- **Cell Culture Flasks:** growth area 25 cm<sup>2</sup>
- **96 Well and 12 Well Tissue Culture Testplates:** crystal-grade polystyrene, gamma sterilised, non-pyrogenic, disposable, SPL Life Sciences (Pocheon, South Korea)
- **Pipette tips**

### Equipment

- **Centrifuge:** eppendorf centrifuge 5804R, Eppendorf Company (Hamburg, Germany)
- **Incubator:** Panasonic MCO-19A/CUVH-PE, Panasonic (Kadoma, Japan)
- **Laminar flow:** Hera Safe KSP, Thermo Fisher Scientific (Waltham, USA)
- **Light Microscope:** Axiovert 40 CFL with ZEN 2012 software, Zeiss (Graz, Austria)
- **UV spectrometer:** Multimode Microplate Reader, Varioskan™ LUX, Thermo Scientific (Waltham, USA)
- **Pipettes:** eppendorf and thermo scientific
- **Water Bath:** WB-30
- **Confocal Microscope:** Leica TCS SP5 II Confocal, Leica (Wetzlar, Germany)

## 4.2 Material preparation

Chitosan with low molecular weight ( $M_w \sim 50$  kDa, DD: 85 %), denoted by  $CS_L$ , and chitosan with medium molecular weight ( $M_w \sim 600$  kDa, DD: 86 %), denoted by  $CS_M$ , are purchased as chitosan flakes from Sigma-Aldrich (Steinheim, Germany). In previous studies molecular weight has been determined by viscometry and degree of deacetylation by titration. Chitosan flakes (1 g) are dissolved in 7 M acetic acid (99 g) at 60 °C and stirred at this temperature overnight. The solution is filtered hot through a pleated filter (Figure 4.1).



FIGURE 4.1: Filtration of hot acetic acid solutions of chitosan through a pleated filter.


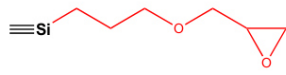
Alkoxysilanes, namely tetraethyl orthosilicate (TEOS), 3-aminopropyl triethoxysilane (APTES) and 3-glycidopropyl trimethoxysilane (GLYMO) are subjected to a sol-gel process by acidic hydrolysis with ethanol as solvent. 98.50 g ethanol and 1.00 g alkoxysilanes are placed into a plastic vessel with a screw cap. 0.50 g acidic water (pH 1.5, adjusted with HCl) is added as a catalyst. Under such conditions complete hydrolysis of alkoxysilanes is assumed, yielding a solution of 0.29% TEOS derived silica particles, 0.50% APTES derived particles and 0.71% GLYMO derived particles in ethanol. In addition, analogous silica particle solutions from TEOS in less amount of solvent are prepared. To that end, 1.00 g TEOS and 0.50 g acidic water are added to 48.50 g ethanol (0.58% particle concentration) and 23.50 g ethanol (1.15% particle concentration). All solutions are stirred for two days. After one month of storage they are discarded and new sol-gel mixtures are prepared.

Nanosized particles used for the preparation of hybrid materials include silicon dioxide nanoparticles with an average BET diameter of 5-15 nm, silicon dioxide nanoparticles with an average BET diameter of 10-20 nm, cellulose nanocrystals (CNC) and chitin nanocrystals (ChNC). Silicon dioxide nanoparticles (0.29 g) are suspended in ethanol (99.71 g) and the suspension is stirred for one day. Likewise cellulose nanocrystals (0.10 g) are suspended in ethanol (99.90 g) and the suspension is stirred for one day. Chitin nanocrystal suspension with a concentration of 0.73% in ethanol, have been prepared elsewhere, and are used as received. There is no time limit for the use of nanoparticle and nanocrystal suspensions.



All particles, including abbreviations and pictorial representations, and their respective concentrations in ethanol are listed in Table 4.1.

TABLE 4.1: Particle solutions/suspensions employed in chitosan hybrid material preparation.

Particle/Precursor molecule	Abbreviation	Concentration (w/w) in EtOH	Pictorial representation
Tetraethyl orthosilicate	TEOS, T	0.29, 0.58, 1.15%	
3-Aminopropyl triethoxysilane	APTES, A	0.50%	
3-Glycidoxypropyl trimethoxysilane	GLYMO, G	0.71%	
Silicon dioxide nanoparticles 10 nm (BET)	SiO <sub>2</sub> <sup>*</sup> , S <sup>*</sup>	0.29%	
Silicon dioxide nanoparticles 15 nm (BET)	SiO <sub>2</sub> <sup>**</sup> , S <sup>**</sup>	0.29%	
Cellulose nanocrystals	CNC	0.10%	
Chitin nanocrystals	ChNC	0.73%	

#### 4.2.1 Thin film preparation

Thin films of chitosan hybrid materials on silicon wafers are prepared by spin coating. Different particles are used, namely prehydrolysed/-condensed TEOS, APTES and GLYMO sol-gel particles, silicon dioxide nanoparticles with average BET diameters of 10 nm and 15 nm as well as cellulose nanocrystals. Both medium weight chitosan CS<sub>M</sub> and low molecular weight chitosan CS<sub>L</sub> are deployed and the ratio of the chitosan solution and the particle solution/suspension is varied between 9:1, 6:1, 4:1 and 2:1. Table 4.2 lists the composition of all 58 types of prepared thin films.

TABLE 4.2: Composition of the 58 different types of chitosan and chitosan hybrid thin films on silicon.

Type	Chitosan (CS)	Particle conc. in EtOH	CS solution : Particle solution (w/w)
1-8	CS <sub>M</sub> and CS <sub>L</sub>	0.29% TEOS	9:1, 6:1, 4:1 and 2:1
8-16		0.50% APTES	
17-24		0.71% GLYMO	
25-32		0.29% SiO <sub>2</sub> <sup>*</sup>	
33-40		0.29% SiO <sub>2</sub> <sup>**</sup>	
40-48		0.10% CNC	
49-56	CS <sub>M</sub> and CS <sub>L</sub> solutions with EtOH in a ratio of 9:1, 6:1, 4:1 and 2:1 (w/w) as reference		
57-58	CS <sub>M</sub> and CS <sub>L</sub> as reference		

Plates with a size of 1.5 cm x 1.5 cm are cut out of silicon wafers and are used as substrates for thin film deposition. Wafers are cleaned in Piranha solution, a mixture of sulphuric acid and hydrogen peroxide (ratio 2:1), for 10 minutes. Afterwards wafers are washed with distilled water and stored in water in a separate beaker. Before spin coating, every wafer is stored in distilled water for at least one hour in order to allow equilibration of the silicon/water interface. Chitosan and particle solutions/suspensions in their respective ratios (Table 4.2) and in appropriate amounts are placed into 40 mL plastic jars with a screw cap and mixed vigorously by hand for 1 minute. 100 µL of the

chitosan mixture are deposited onto cleaned silicon wafers. Wafers are spun on a spin coater at a speed of 4000 rpm for 60 sec with an acceleration speed of 2500 rpm/sec (Figure 4.2).

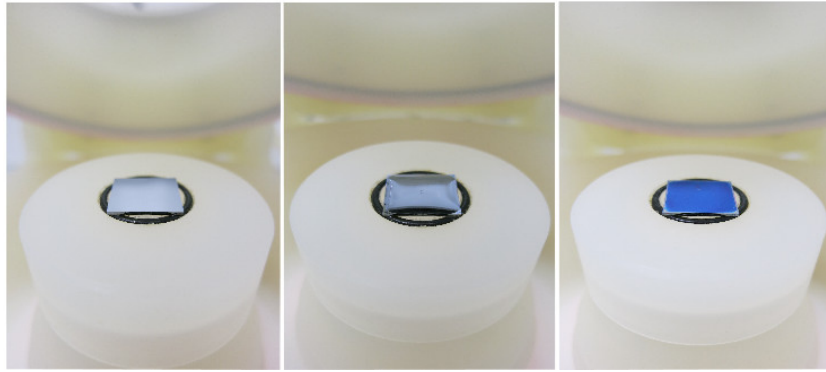


FIGURE 4.2: Preparation of chitosan and chitosan-based hybrid thin films on silicon substrates by spin coating.

Any remaining acetic acid in the films is removed by heating the sample in an oven at 40 °C for four hours. Thin films produced this way are used for stylus profilometry, contact angle measurements, AFM measurements and cell tests. The prepared collection of thin films is comprised of five samples for each type of hybrid thin film, which corresponds to a total number of 290 coated wafers. For the detailed study of selected hybrid thin films, additional samples are prepared, e.g. when thin films are studied in cell culture tests.

#### 4.2.2 Specimen preparation for SPR measurements

Gold sensor slides with a size of 2 cm x 1 cm are cleaned in Piranha solution for ten minutes. Afterwards slides are washed with distilled water and finally stored in MilliQ water. Thin films are deposited onto gold slides by spin coating of 120  $\mu$ L chitosan mixtures at a speed of 4000 rpm for 60 sec with an acceleration speed of 2500 rpm/sec.

#### 4.2.3 Foil preparation

Chitosan hybrid foils containing different amounts of particles from TEOS sol-gel processing and chitin nanocrystals are prepared by a simple casting procedure. Medium molecular weight chitosan  $CS_M$  is selected for foil preparation. The ratio of chitosan solution and particle solution is kept constant at 9:1 (w/w). Chitosan foils from neat chitosan and foils from chitosan solutions containing ethanol act as reference materials. Table 4.3 lists the composition of all 6 types of prepared foils.

TABLE 4.3: Composition of the six different types of chitosan and chitosan hybrid foils.

Type	Chitosan (CS)	Particle conc. in EtOH	$CS_M$ solution : Particle solution (w/w)	Particle conc. in the hybrid material
1	$CS_M$	0.29% TEOS	9:1	2.9%
2		0.58% TEOS		5.8%
3		1.15% TEOS		11.5%
4		0.73% ChNC		7.3%
5	$CS_M$ solution with EtOH in a ratio of 9:1 (w/w) as reference			
6	$CS_M$ as reference			

20.00 g chitosan solution and 0.22 g particle solution/suspension are placed into 40 mL plastic jars with a screw cap and mixed vigorously by hand for 1 minute. 20 mL of the mixture are drawn up with a plastic syringe and poured into a petri dish with a diameter of 8.5 cm (Figure 4.3). Foil formation occurs upon evaporation of the acetic acid/water/ethanol solvent mixture at ambient temperature and pressure after one or two days.

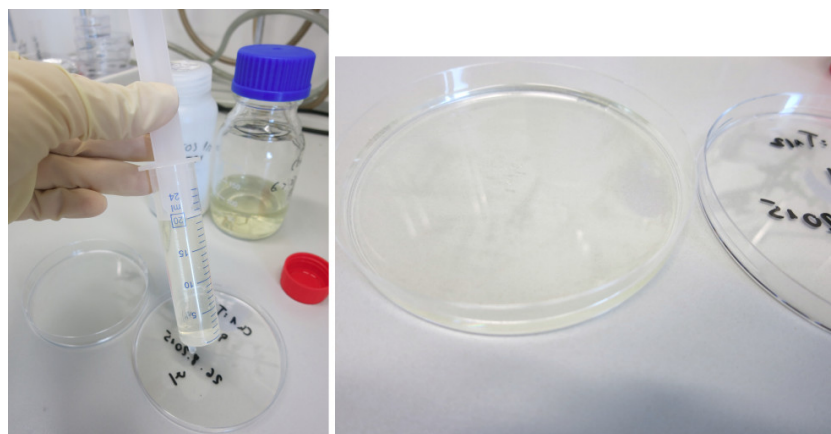


FIGURE 4.3: Preparation of chitosan and chitosan-based hybrid foils by solution casting.

In order to remove the remaining acetic acid, foils are washed with 0.25 M NaOH solution for one minute (Figure 4.4). This method is also employed by *Shirosaki et al.* [6] and *Amado et al.* [7]. Afterwards foils are washed three times with distilled water. Wet foils are placed between two plates of plastic with a piece of filter paper on top of the foil. It is important to ensure that foils, when placed between the plates, remain smooth and planar and do not for example form wrinkles. The two plates of plastic are fixed with four clothespins. Foils are placed in an oven at 60 °C for one day, or if the foils are still wet after one day, drying is extended for another day.

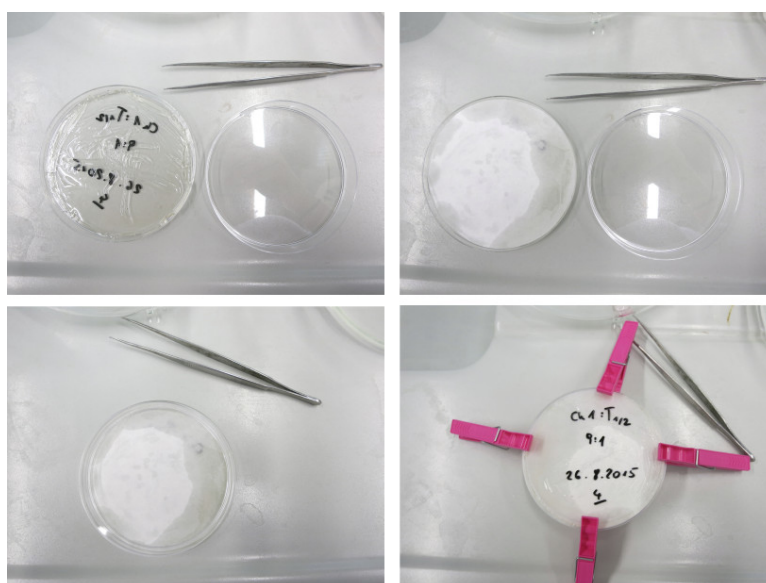


FIGURE 4.4: Washing of foils in 0.25 M NaOH solution in order to remove remaining acetic acid. Afterwards foils are fixed and dried at 60 °C for one or two days.

As a side note, significant variations in thickness within one foil as well as between different foils is observed. This might be attributed to small inclinations of the work bench or can be related to little variations in the amount of solvent in the filtrated chitosan solutions.

The prepared collection of foils is comprised of three samples for each type of hybrid foil, which corresponds to a total number of 18 foils.

#### 4.2.4 Specimen preparation for tensile testing and DMA

Dumbbell specimens are stamped out of the foils using a cutting die (Figure 4.5). The width of the narrow section of the dumbbell specimen is 4 mm and the distance between the shoulders is 25.5 mm. Foil and die punch are placed between two wooden boards which are pressed together with a screw press, thereby applying a force of 7 N.

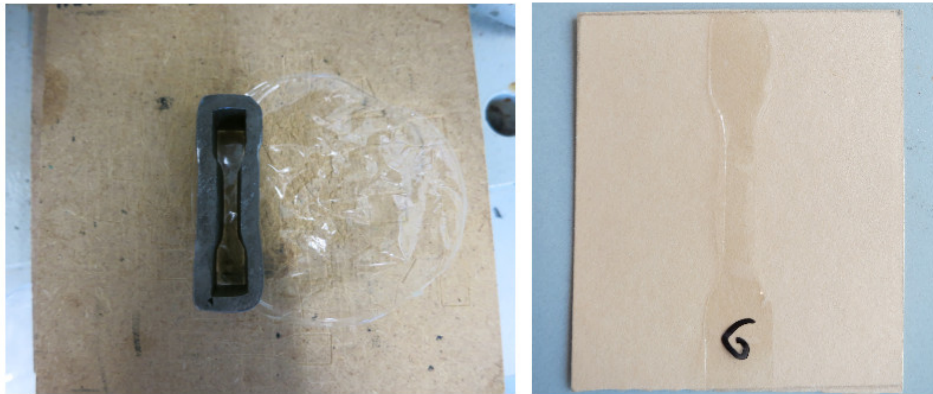


FIGURE 4.5: Stamping out of dumbbell specimens from chitosan foils using a cutting die and a screw press.

Usually five to six dumbbell specimens can be obtained from one foil. Thickness of dumbbell specimens along the gauge length at three adjacent positions is determined with a Mitutoyo Absolute Digimatic Indicator thickness gauge. A variation of 3  $\mu\text{m}$  in thickness within one specimen is tolerated and the mean average is calculated.

DMA specimen are stamped out just like tensile testing specimen, followed by the removal of the shoulders. The narrow section of the specimen is used for the measurements. Again, the thickness of the foils is determined prior to analysis.

### 4.3 Material characterisation

#### 4.3.1 Stylus profilometry

Height profiles are measured at a Veeco EKTAK 150 Stylus Profiler. Thin film is removed from the surface of the silicon wafer along a straight line with a razor blade. The height profile of the surface perpendicular to the direction of the scratch is measured at both ends and around the midpoint of the line (Figure 4.6). Table 4.4 lists the settings for profilometer measurements. From the depth of the scratch the layer thickness can be derived. The mean average of all three height values is calculated. The layer thickness of all 58 types of thin films is determined.



FIGURE 4.6: Determination of layer thickness by measuring height variations perpendicular to a scratch using a contact stylus profiler (EKTAK 150, Veeco).

TABLE 4.4: Stylus Profilometer settings used for thin film thickness measurements.

<b>Scan Type:</b> Hills and Valleys	<b>Length:</b> 1000 $\mu\text{m}$	<b>Duration:</b> 10 sec
<b>Radius:</b> 12.5 $\mu\text{m}$	<b>Stylus Force:</b> 3 mg	<b>Resolution:</b> 0.333 /pt

#### 4.3.2 Contact angle measurement

Static contact angles with water are recorded at a Kruss DSA 100S Drop Shape Analyzer. Drops of 3  $\mu\text{L}$  Milli-Q water are squeezed out of a syringe and placed on the surface of the thin films, using the sessile drop method (Figure 4.7). An image of the sessile drop is recorded with an integrated T1E CCD video camera. The shape of the drop is analysed and contact angles are determined via drop shape analysis software (DSA1 v 1.90). On every coated wafer three drops are placed at adjacent sites along one of the edges. Contact angles on two samples and therefore a total number of 6 values for each type of thin film are determined. These are measured for all 58 types of thin films.

The wettability of thin films from neat chitosan is investigated in more detail. In particular the change of contact angle with time is examined, since in the course of our studies it became apparent that as time between material preparation and contact angle measurements elapses, contact angles change. For this purpose, contact angles of pure chitosan thin films are measured one day, one week and two months after spin coating.

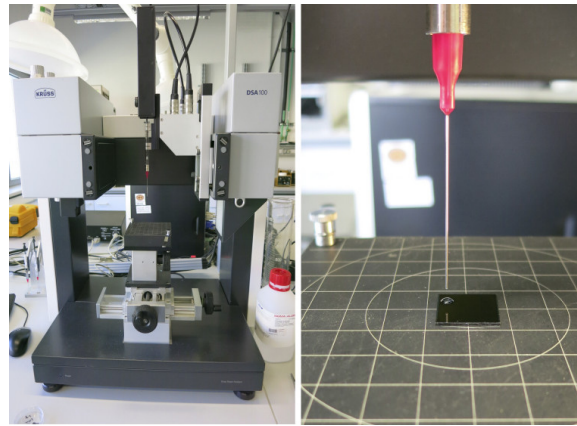


FIGURE 4.7: Contact angle measurements of thin films at a Drop Shape Analyzer (DSA 100S, Kruess).

### 4.3.3 Atomic force microscopy (AFM)

AFM images are recorded at a Bruker Veeco Multimode Atomic Force Microscope (Figure 4.8). Measurements are performed in tapping mode using a silicon cantilever at a resonance frequency of 320 kHz and a force constant of 42 N/m. A  $10 \times 10 \mu\text{m}^2$  surface area and a  $2 \times 2 \mu\text{m}^2$  detail of each sample are scanned. AFM images are processed, analysed and the root mean square roughness is calculated using nanoscope software (V7.30r1sr3; Veeco). Only selected chitosan hybrid thin films, which are listed in Table 4.5, are studied by means of AFM.

TABLE 4.5: Chitosan hybrid thin films on silicon studied by means of atomic force microscopy.

Material	CS solution : Particle solution (w/w)
CS <sub>M</sub>	-
CS <sub>L</sub>	-
CS <sub>M</sub> :TEOS	9:1, 6:1, 4:1, 2:1
CS <sub>L</sub> :TEOS	9:1
CS <sub>M</sub> :APTES	9:1, 2:1
CS <sub>M</sub> :GLYMO	2:1
CS <sub>M</sub> :SiO <sub>2</sub> *	9:1, 2:1
CS <sub>M</sub> :SiO <sub>2</sub> **	2:1
CS <sub>M</sub> :CNC	2:1



FIGURE 4.8: Atomic Force Microscope (Veeco Multimode, Bruker).

### 4.3.4 Surface Plasmon Resonance Spectroscopy (SPR)

SPR is employed to probe adsorption of bovine serum albumin and fibrinogen on selected chitosan hybrid materials (Table 4.6). Measurements are performed at a BioNavis SPR Navi™ 200 surface plasmon resonance spectrometer (Figure 4.9).

Coated gold sensor slides are placed into a sensor holder which is put into the instrument. For the controlled supply of proteins a flow chamber is placed on top of the thin film. Before measurements are started, surfaces are equilibrated with buffer (pH 7.4, 10 mM PBS + 100 mM NaCl). Flow rate is set to 20  $\mu\text{L}/\text{min}$ . Proteins ( $c = 1 \text{ mg}/\text{mL}$  in buffer) are injected and their interaction with the coating material is monitored. After 30 minutes, surfaces are rinsed with buffer in order to remove loosely attached proteins. For each material and protein combination three SPR measurements are conducted.

TABLE 4.6: Chitosan hybrid thin films on gold studied by means of surface plasmon resonance spectroscopy.

Material	CS <sub>M</sub> solution : Particle solution (w/w)
CS <sub>M</sub>	-
CS <sub>M</sub> :TEOS	9:1, 2:1
CS <sub>M</sub> :APTES	9:1, 2:1



FIGURE 4.9: Surface plasmon resonance instrument (SPR Navi™ 200, BioNavis).

### 4.3.5 Cell testing

Cytotoxicity and cell attachment tests are performed with fibroblasts from an ATCC cell line in the 7<sup>th</sup> passage and with osteoblasts from primary culture. The protocol for cell passaging by cell trypsinization and reseeding is provided in Appendix A. Cells, if not otherwise stated, are cultivated at cell culture conditions (5% CO<sub>2</sub>, 37 °C) in Dulbecco's Modified Eagle's Medium (DMEM) with 5% fetal bovine serum (FBS). Cells are counted in a hemocytometer using a light microscope. Dead cells are stained with the dye trypan blue. To that end, 100  $\mu\text{L}$  cell suspension is mixed with 900  $\mu\text{L}$  trypan blue (0.1%) solution. Only viable cells are counted and used for estimations of the present cell number in the suspensions.

Coated wafers are placed into 12 well-plates and sterilised with UV light for 30 minutes on both sides in a laminar flow hood. The first set of experiments evaluates if thin film materials display

cytotoxic effects. To that end, coated wafers are incubated in medium. Thereby possible release or degradation products from the layer can be collected and used for further studies (= sample solutions). Cell number after incubation with different sample solutions is quantified via crystal violet assay. In the next set of experiments, the ability of cells to attach and grow on selected thin films is examined. Cells are seeded onto the surfaces, where they are allowed to attach and proliferate. After removal of non-attached cells, by gently rinsing with PBS, the total cell number is determined using MTT assay. Table 4.7 summarises all types of thin films for which cytotoxicity and cell attachment is determined.

TABLE 4.7: Chitosan hybrid thin films on silicon for which cytotoxicity and cell attachment is assessed. Tested materials are indicated with a x.

Material	Fibroblasts		Osteoblasts	
	cytotoxicity	attachment	cytotoxicity	attachment
CS <sub>M</sub>	x	x	x	x
CS <sub>L</sub>	x		x	
CS <sub>M</sub> :TEOS 9:1	x	x	x	x
CS <sub>M</sub> :TEOS 6:1			x	
CS <sub>M</sub> :TEOS 4:1			x	
CS <sub>M</sub> :TEOS 2:1	x	x	x	x
CS <sub>L</sub> :TEOS 9:1			x	
CS <sub>L</sub> :TEOS 2:1			x	
CS <sub>M</sub> :APTES 9:1			x	
CS <sub>M</sub> :APTES 2:1	x	x	x	x
CS <sub>L</sub> :APTES 9:1			x	
CS <sub>L</sub> :APTES 2:1			x	
CS <sub>M</sub> :GLYMO 9:1			x	
CS <sub>M</sub> :GLYMO 2:1			x	
CS <sub>M</sub> :SiO <sub>2</sub> * 9:1			x	
CS <sub>M</sub> :SiO <sub>2</sub> * 2:1	x	x	x	x
CS <sub>L</sub> :SiO <sub>2</sub> * 9:1			x	
CS <sub>M</sub> :SiO <sub>2</sub> ** 9:1			x	
CS <sub>M</sub> :SiO <sub>2</sub> ** 2:1			x	
CS <sub>M</sub> :CNC 9:1			x	
CS <sub>M</sub> :CNC 2:1			x	

For the extraction of degradation products, one coated wafer of each studied thin film is incubated in 1 mL DMEM and another one in 1 mL DMEM with 5% FBS. The whole sample should be covered with medium. Incubation is carried out at cell culture conditions. After 24 hours, 500 µL of the medium is taken out and used for further studies (first and second sample solution). 500 µL fresh medium is added to the incubation medium in order to replace the sample solution. One week after starting the incubation, 500 µL of the medium is removed again (third and fourth sample solution). In total, four sample solutions are collected (24 h DMEM, 24 h DMEM with 5% FBS, 1 week DMEM and 1 week DMEM with 5% FBS).

Cells are harvested at about 70%-90% confluency. They are reseeded into 96-well plates at an approximate cell number of 16 000 fibroblastic cells per well or 30 000 osteoblastic cells per well, respectively, in 100 µL DMEM with 10% FBS. Cells are incubated at 37 °C for 24 h in order to obtain a monolayer



of cells in each well. Monolayer formation is controlled with a light microscope.

Afterwards medium is dumped off and one of the following mixtures is added to the cell monolayer:

1. **50  $\mu$ L** DMEM with 10% FBS and **50  $\mu$ L** sample solution (for sample solutions not containing FBS)
2. **50  $\mu$ L** DMEM with 5% FBS and **50  $\mu$ L** sample solution (for sample solutions containing 5% FBS)
3. **100  $\mu$ L** DMEM with 5% FBS as control

For each type of sample solution, cytotoxicity is assessed from four wells along the same column. Controls occupy the first or last column of the 96 multi-well plate. After incubation of the cells with sample solution for 24 h, a cell viability test with crystal violet is conducted (Appendix A). Absorbance is measured at 595 nm on a Multimode Microplate reader (Varioskan™ LUX, Thermo Scientific).

For cell attachment tests, materials are placed into 12 multi-well plates. Approximately 10 000 cells in 1.5 mL DMEM with 5% FBS are added into each well. Cells and coated wafers are incubated for four days. Monolayer formation after four days is confirmed with a light microscope using a transparent glass substrate as control.

MTT tests are performed according to respective protocols (Appendix A). In an additional step, coated wafers are transferred into new 12-well plates after washing of the cell monolayer with PBS (step 2). Final assay solutions, together with the coated material, are present in one well of a 12-well plate. Solution from one well is transferred to four wells of a 96-well plate and absorbance is measured at 570 nm on a Multimode Microplate reader. MTT protocol is further modified, by adjusting the amount of DMEM and MTT solution to the larger surface area. 96 multi-well plates, for which MTT protocols are usually specified, have a surface area of approximately 1.04 cm<sup>2</sup> whereas 12 well plates have a surface area of approximately 3.7 cm<sup>2</sup>. The samples themselves have a surface area of approximately 2.25 cm<sup>2</sup> which corresponds to a 2.16 fold increase in the cell surface area. In our modification of the MTT protocol the volume of the solutions is changed from 200  $\mu$ L DMEM, 20  $\mu$ L MTT and 100  $\mu$ L 0.04% HCl in isopropanol to 1500  $\mu$ L DMEM, 150  $\mu$ L MTT (7.5 fold increase) and 500  $\mu$ L 0.04% HCl in isopropanol (5 fold increase). For future tests, it is recommended to use the actual 2.15 increase in surface area for adjustments. Thereby the measured absorbance can be matched more easily with results obtained from other experiments using MTT protocol. The challenge in that case is to cover the whole thin film with MTT and 0.04% HCl solution, considering the elevation of the coated wafer from the bottom of the well.

The exact size of every coated wafer is determined by scanning the samples in a document scanner and integration of the surface area using a MatLab Script (Appendix B.2). This size correction factor (= deviation from 2.25) is introduced to eliminate contributions from small sample size differences.

Osteoblasts attached to chitosan thin films (CS<sub>T</sub>) and a glass control after three days are visualised on a Leica TCS SP5 II confocal microscope using live/dead staining assay (Appendix A). The amount of assay solution is halved to 5  $\mu$ L assay solution A, 2.5  $\mu$ L assay solution B and 2.5 mL PBS. The sample is covered with 2 ml PBS and 1 ml of the assay solution mixture. Excitation/emission wavelengths are 490/515 nm for the detection of viable cells and 535/617 nm for the detection of dead cells.

### 4.3.6 Tensile testing

Dumbbell specimens stamped out of foils are glued between two sheets of construction paper at the shoulders of the specimen with cyanoacrylate superglue. Afterwards samples are fixed between the upper and lower tensile grips of a Shimadzu AGS-X Series universal tensile testing machine (Figure 4.10). The reason behind the additional use of construction paper is that at the edge of the grips foils are frequently cut, due the fact that foils have a low thickness. Uniaxial tensile tests are performed at a loading speed of 0.5 mm/min. Elastic modulus, yield strength, ultimate tensile strength and break strain of 5 dumbbell specimen obtained from two different foils are monitored. Mechanical properties of all 6 types of foils are determined .

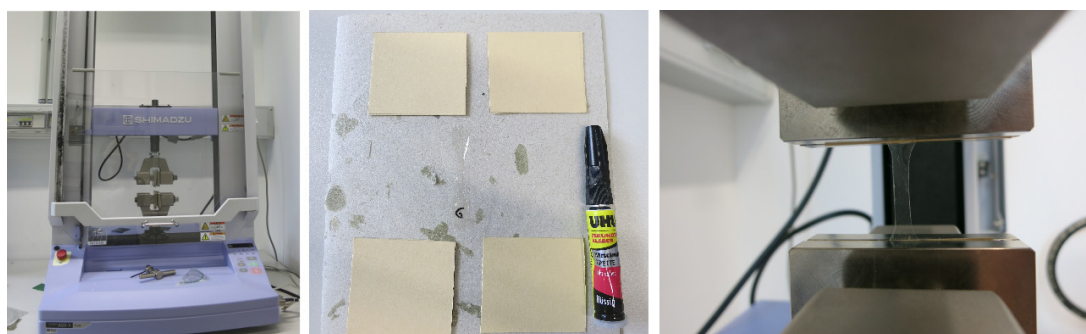


FIGURE 4.10: Tensile testing of dumbbell specimen stamped out of chitosan and chitosan hybrid foils at a electromechanical universal testing machine (AGS-X Series, Shimadzu).

### 4.3.7 Dynamic mechanical analysis (DMA)

Mechanical properties of foils at different relative humidities are investigated by means of dynamic mechanical analysis. DMA measurements are carried out at a TA Instruments Q800 DMA (Figure 4.11). Dimensions of the foil are determined and the test specimen is clamped between the ends of two parallel sample arms. To adjust humidity, a special DMA-RH accessory chamber is mounted on the DMA. Measurements are carried out at ambient temperature at a frequency of 1 Hz, an applied oscillating strain of 0.0300% and an initial static load of 0.01 N. Storage modulus ( $G'$ ) as a function of the relative humidity is monitored.

Foils from neat chitosan  $CS_M$ , chitosan foils containing 5.8% TEOS derived silica particles and chitosan foils containing 7.3% chitin nanocrystals are studied by means of DMA.

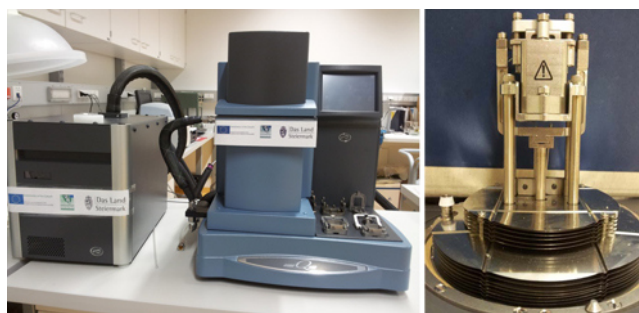


FIGURE 4.11: Dynamic Mechanical Analysis instrument (Q800, TA Instruments). Figure is taken from the homepage of the Institute for Chemistry and Technology of Materials (ICTM) [96].

# Chapter 5

## Results and Discussion

Prepared chitosan and chitosan hybrid materials (Figure 5.1) show excellent film forming capability. In addition, all prepared hybrid materials display similar characteristics in terms of their film forming capability and film stability, segregation not being observed in any case. Film formation of chitosan is facilitated by the formation of intermolecular hydrogen bonds between chitosan molecules. Inorganic constituents from the sol-gel processing of alkoxy silanes are incorporated into the chitosan matrix through covalent and hydrogen bonding interactions between hydroxyl rich silica particles and the hydroxyl groups of chitosan. The amino groups of chitosan do not form covalent bonds with the (functional) silica particles, but support network formation via hydrogen bonding [5].

Thin films on silicon wafers are macroscopically uniform, being free of streaks or holes. Films produced from spin coating of neat chitosan have a characteristic light blue colour. This blue colour is related to the specific refractive indices at the substrate/thin film and thin film/air interfaces. Therefore a change in film thickness, which can for example be achieved by ethanol dilution, will also change the observable colour. Hybrid thin films can also be deposited onto gold (for SPR measurements) and titanium substrates. Foils prepared from solution casting are transparent and have an average thickness of 20-30  $\mu\text{m}$ .

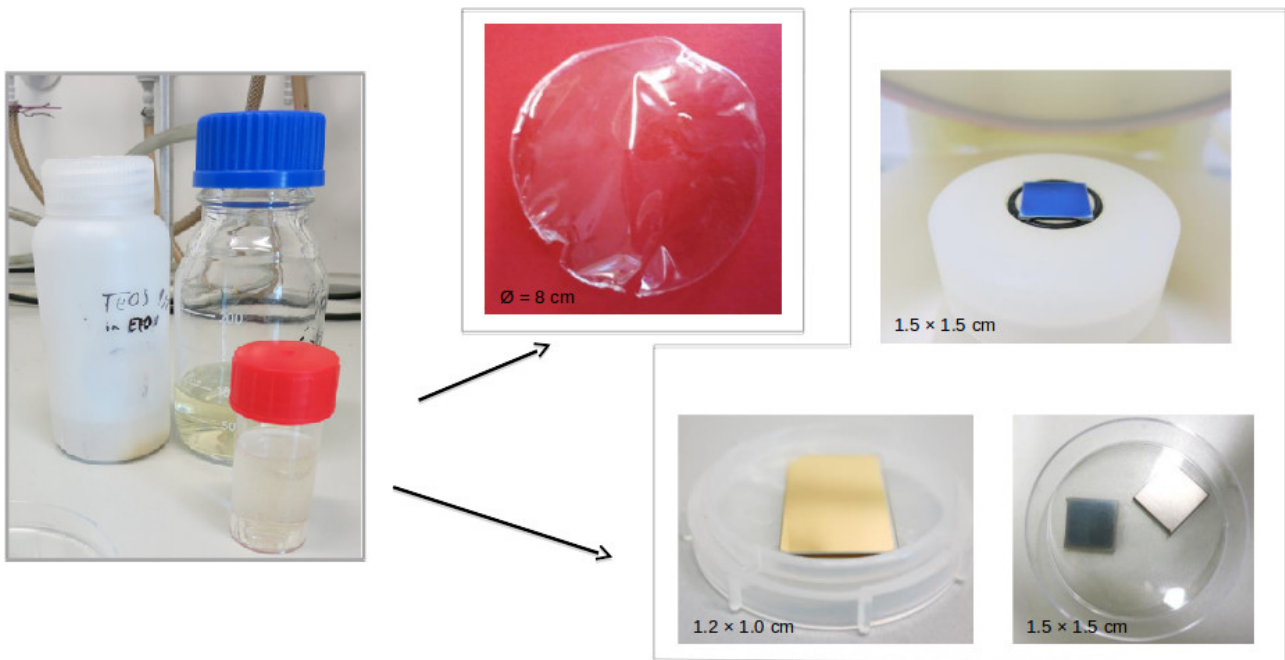


FIGURE 5.1: Chitosan hybrid materials can be processed into different forms: thin films on silicon wafers (top right), titanium (bottom right) and gold (bottom center) prepared by spin coating; foils (top center) from solution casting.

## 5.1 Film thickness

Thickness of hybrid thin films on silicon wafers produced by spin coating is determined via Diamond Stylus Profilometry. Results (Figure 5.2 and 5.3) are mean values of three measurements. All measured values can be found in Appendix C.1. The layer thickness decreases with increasing particle content. Hybrid materials with chitosan solution to particle solution ratios of 9:1 show highest thickness and materials with ratios of 2:1 display lowest thickness. Prepared thin films have a thickness in the range of 55-105 nm. Beside the particle content, the influence of chitosan with different molecular weight ( $M_w \sim 50$  kDa and 600 kDa) and the type of particle on the film thickness is studied.

Thin film preparation of chitosan hybrid materials with particles from sol-gel processing of alkoxy-silanes has been previously studied in detail by *Spirk et al.* [5]. They were able to demonstrate that the thickness of hybrid thin films, with a similar or the same composition as presented materials, can be controlled between 5 and 70 nm by ethanol dilution. This means that the observed reduced layer thickness with increasing particle content (Figure 5.2 and 5.3) is related to the higher ethanol content in the acetic acid/water/ethanol solvent mixture, since all used particles exist as dispersions in ethanol.

A small dependence of alkoxy-silane type and resulting layer thickness, which was in previous studies found by *Spirk et al.*, can also be confirmed in this work. Notably, their mixtures employed in thin film preparation were diluted with ethanol to a high degree. In the hybrid materials with the highest particle content (chitosan solution and particle solution in a ratio of 2:1), film thickness of materials containing APTES and GLYMO derived particles is higher than in materials containing silica particles from the polymerisation of TEOS and commercial silicon dioxide nanoparticles. The increase in thickness seems to be related to the higher molecular size of the organofunctional silanes compared to the silica particles, which is also reflected by a higher particle weight proportion in ethanol, i.e. 0.29% (w/w) TEOS derived silica particles and SiO<sub>2</sub> particles, 0.50% (w/w) APTES derived particles and 0.71% (w/w) GLYMO derived particles.

It was expected that hybrid materials prepared from solutions of chitosan with medium molecular weight CS<sub>M</sub>, due to its higher viscosity, will produce films with higher thickness compared to films from low molecular weight chitosan CS<sub>L</sub>. Despite the difference in molecular weight of the chitosans employed ( $M_w \sim 600$  kDa and  $\sim 50$  kDa) the thickness of the prepared films is very similar. An explanation could be that viscosity of both chitosan solutions is similar, either due to the evaporation of solvent (e.g. longer storage of CS<sub>L</sub> solutions) or incomplete dissolution of medium molecular weight chitosan CS<sub>M</sub>. Another reason could be that thin films from low molecular weight chitosan display higher swelling, thereby increasing the thickness of the films. Monitoring viscosity of the chitosan solutions and changes in the film thickness over time as well as drying of the films prior to thickness measurements could help to explain the similar thickness of the films prepared from different chitosan solutions.

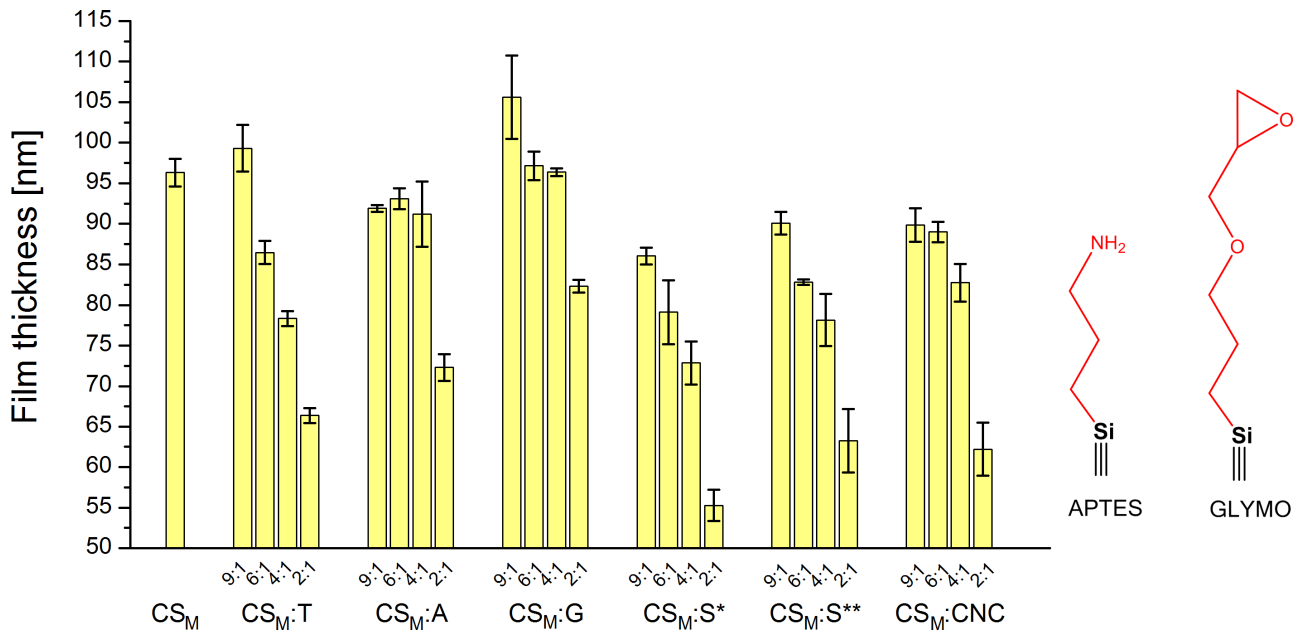


FIGURE 5.2: Thickness of thin films on silicon wafers prepared from medium molecular weight chitosan CS<sub>M</sub> and different particles by spin coating. Layer thickness is determined from three height profiles of one coating measured on a Stylus Profiler.

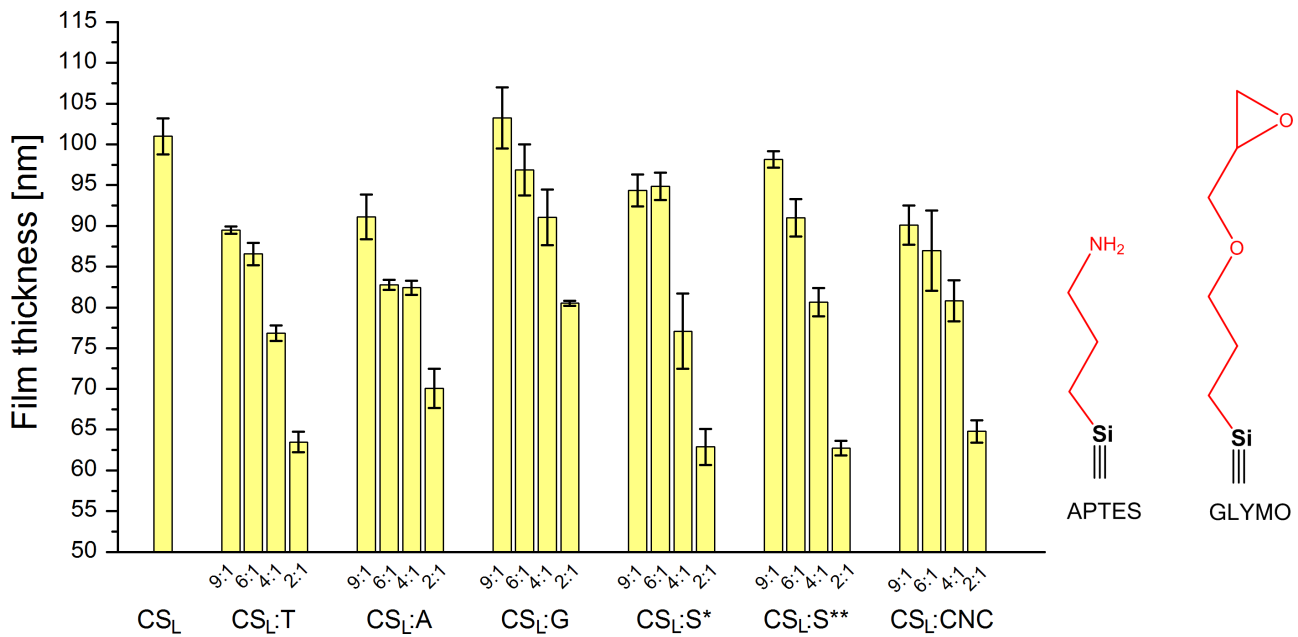


FIGURE 5.3: Thickness of thin films on silicon wafers prepared from low molecular weight chitosan CS<sub>L</sub> and different particles by spin coating. Layer thickness is determined from three height profiles of one coating measured on a Stylus Profiler.

The findings from *Spirk et al.* and the successful replication in this work show that spin coating of chitosan mixtures with particles from sol-gel processing (TEOS, APTES, GLYMO) or other nanometric particles (SiO<sub>2</sub> and CNCs) produces thin films with easily controllable thickness.

## 5.2 Contact angle

Two months after preparation contact angles of all types of prepared chitosan hybrid thin films are measured with water using the sessile drop method. Results (Figure 5.4 and 5.5) are mean values of six measurements. Measured values are summarised in Appendix C.2. In the beginning, the focus lay on the influence of increasing particle content in the hybrid material on surface wettability.

In case of low molecular weight chitosan,  $CS_L$ , as expected, both the incorporation of silica particles from sol-gel processing of TEOS and commercial silicon dioxide nanoparticles create films with lower contact angles, which corresponds to higher wettability. Both  $SiO_2$  and TEOS derived silica particles have a high density of hydroxyl groups on their surface, which can interact with water molecules, leading to the observed overall increase in hydrophilicity.

The organofunctional group of APTES is an alkyl chain with a terminal amine. On the one hand primary amines are able to form hydrogen bonds with water. Furthermore, the amino group of APTES is presumably protonated at a pH of 7.4 [97]. In turn, additional positive charges should be present in the hybrid material. On the other hand, the alkyl chain of APTES consists of three saturated hydrocarbons, which should increase hydrophobicity in the material. In literature also the former contribution is discussed [98], although in the described case APTES was not part of a composite, but rather directly used for surface modification. However in our experiments, the incorporation of APTES derived particles into low molecular weight chitosan increases contact angles, indicating that in chitosan hybrid materials the contribution from the hydrophobic alkyl chain is more prevalent with regard to surface wettability.

The organofunctional group of GLYMO consists of a propoxy chain with a terminal epoxy functionality. In acetic acid medium, an acid-catalysed opening of the epoxide will occur. Similar to APTES, the organofunctional group of GLYMO has hydrophobic and hydrophilic parts in the form of saturated hydrocarbons and terminal hydroxyl groups from the opening of the epoxy functionality, respectively. In accordance with the results of APTES, the contribution from the hydrophobic hydrocarbon chain is more prevalent with respect to surface wettability in hybrid materials with low molecular weight chitosan as matrix. In contrast to APTES, a proportional increase of hydrophobicity associated with a higher particle content is not observed. Although films with particles from GLYMO sol-gel processing have higher contact angles compared to neat chitosan when combined with low molecular weight chitosan, they display lower contact angles when combined with medium molecular weight chitosan.

It seems that in hybrid materials with medium molecular weight chitosan as matrix (Figure 5.5) the impact of all inorganic constituents on the contact angles is lower compared to low molecular weight chitosan as matrix material. Yet, contact angles on films with the composition  $CS_M$ :APTES 2:1 are higher compared to neat chitosan  $CS_M$ .

Although cellulose thin films prepared in our lab usually display contact angles in the range of 25-35° in this set of experiments no trend can be found for chitosan hybrid films containing CNCs both in low and medium molecular weight chitosan. The most likely explanation is that since prepared composites contain a maximum of just 3.3% CNCs (i.e.  $CS$ :CNC 2:1), higher CNC amounts would have been necessary to observe a reduction of the contact angle.

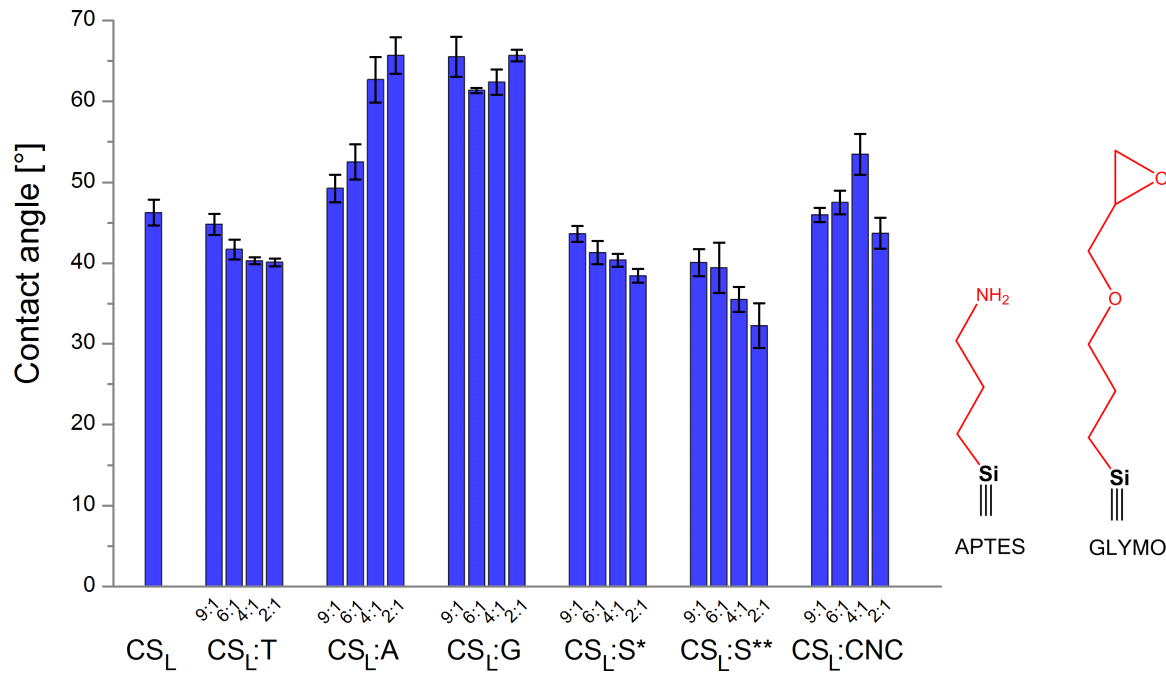


FIGURE 5.4: Static contact angles of water on films prepared from low molecular weight chitosan CS<sub>L</sub> and different particles. Six drops of 3  $\mu$ L Milli-Q water are placed on two different thin films. Measurements are carried out roughly two months after spin coating.

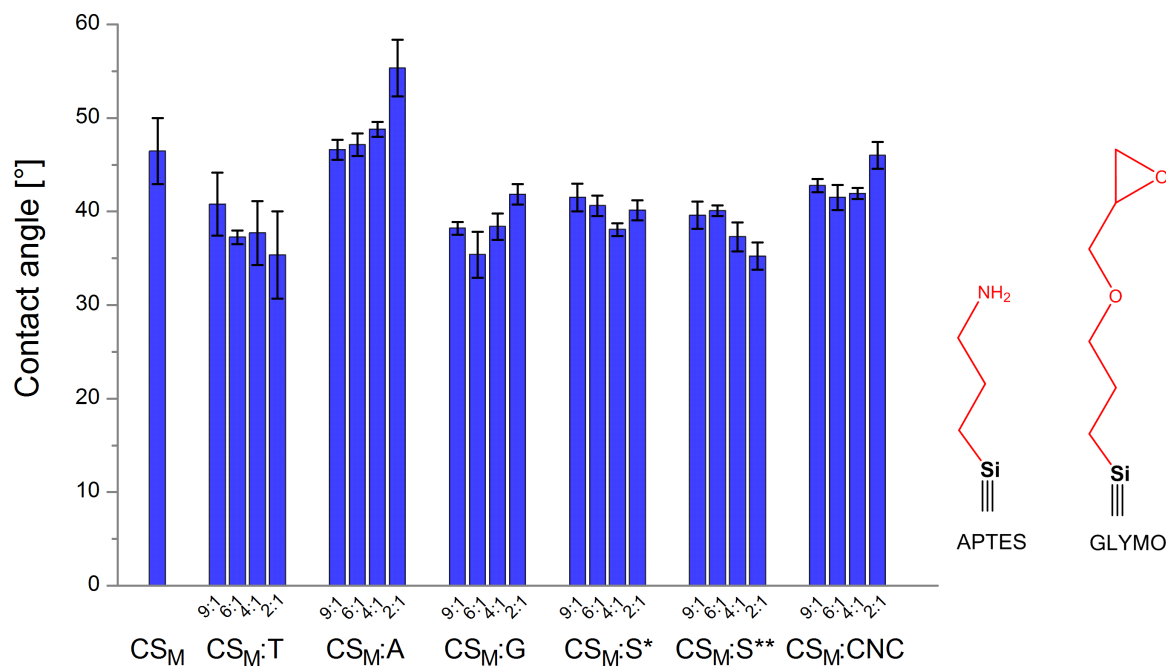


FIGURE 5.5: Static contact angles of water on films prepared from medium molecular weight chitosan CS<sub>M</sub> and different particles. Six drops of 3  $\mu$ L Milli-Q water are placed on two different thin films. Measurements are carried out roughly two months after spin coating.

Measured contact angles are compared to literature values [99, 100, 101] as well as results from unpublished previous studies. To our surprise, the observed contact angles (Figure 5.4 and 5.5) are mostly lower compared to literature values as well as values from previous studies.

New thin films of selected hybrid materials are therefore prepared and contact angles are measured once again, this time five days after preparation (Figure 5.6). The new thin films display contact angles which are in accordance to literature values for same or similar types of materials [5, 99, 100, 101].

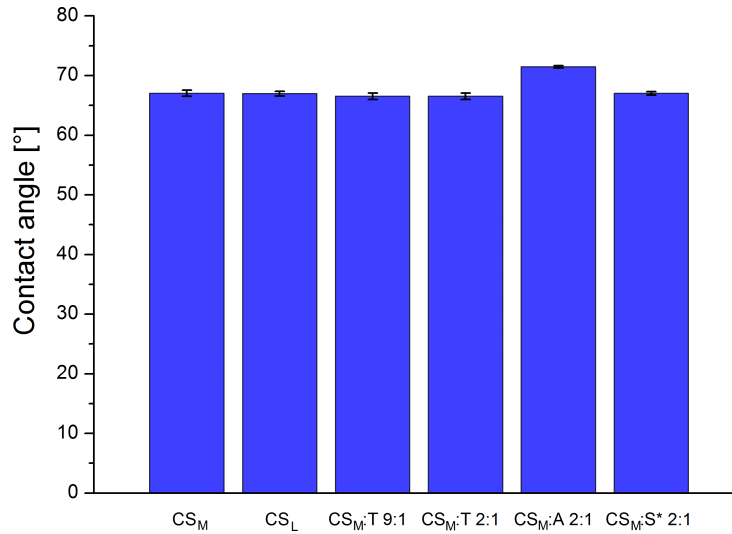


FIGURE 5.6: Static contact angles of water on chitosan and selected hybrid thin films. Three drops of 3  $\mu$ L Milli-Q water are placed on one thin film. Measurements are carried out five days after spin coating.

It is suspected that the increase in surface wettability correlates with the time between film preparation and contact angle measurements. In order to confirm this theory, thin films of neat chitosan are prepared and contact angles are measured one day, one week and two months after preparation (Figure 5.7). One day after preparation, contact angles are in the range of approx. 70°-62° and are therefore consistent with the results from Fig 5.6. After one week, no significant changes in the contact angles can be observed (approx. 73°-61°). Nevertheless, after two months surfaces exhibit contact angles in the range of approx. 51°-41°, which represents a significant increase in hydrophilicity.

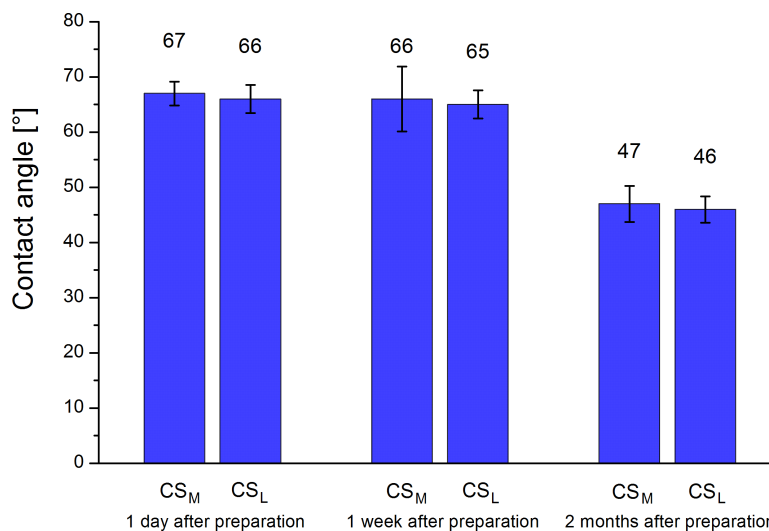


FIGURE 5.7: Static contact angles of water on neat chitosan films one day, one week and two months after preparation. 15 drops of 3  $\mu$ L Milli-Q water are placed on five different thin films.



Chitosan is hygroscopic, which also means that chitosan can easily absorb water (Chapter 2.3.2). Water molecules can induce changes in the structure of chitosan. Furthermore, water molecules adsorbed onto the surfaces can interact with water drops during contact angle measurements. Therefore a reduction of the contact angles related to water sorption and retention from air over time is reasonable. Coated wafers that have been exposed to ambient air humidity for two months, exhibiting lower contact angles, are dried in an oven for 5 minutes, 30 minutes and 60 minutes at 60 °C. Immediately after drying, contact angles are measured. In addition, water drops are placed in proximity to the newly prepared thin films for 5 minutes with subsequent measurement of the contact angle. In both cases the contact angles of the thin films do not change, indicating that reduction of contact angles over time is not caused by the adsorption of water vapour from humid air.

An increase in surface roughness over time could also explain the higher contact angle values. AFM measurements of hybrid materials with the composition  $CS_M:TEOS$  9:1 were conducted one day and approx. 2 months after spin coating. The newly prepared films exhibited surface roughnesses of 0.81 nm ( $10 \times 10 \mu m^2$ ) and 0.69 nm ( $2 \times 2 \mu m^2$ ), respectively, and older films surface roughnesses of 0.67 nm ( $10 \times 10 \mu m^2$ ) and 0.51 nm ( $2 \times 2 \mu m^2$ ). However, more detailed AFM studies are necessary to evaluate contributions of the surface roughness on the contact angle.

Another explanation for the reduction of contact angles is associated with relaxation processes within the materials. Spin coating produces films that can be thermodynamically unfavourable [102, 103]. With time, chitosan chains might adopt their equilibrium conformation thereby changing the surface chemistry and wettability.

To rule out effects from changes in the acetic acid/water to ethanol ratio in the solvent mixture, chitosan films diluted with ethanol and hence reduced layer thickness are prepared and contact angles are measured (Figure 5.8). Contact angles are not affected by ethanol dilution or layer thickness, respectively, in any case. These findings are in good agreement with previous studies [5].

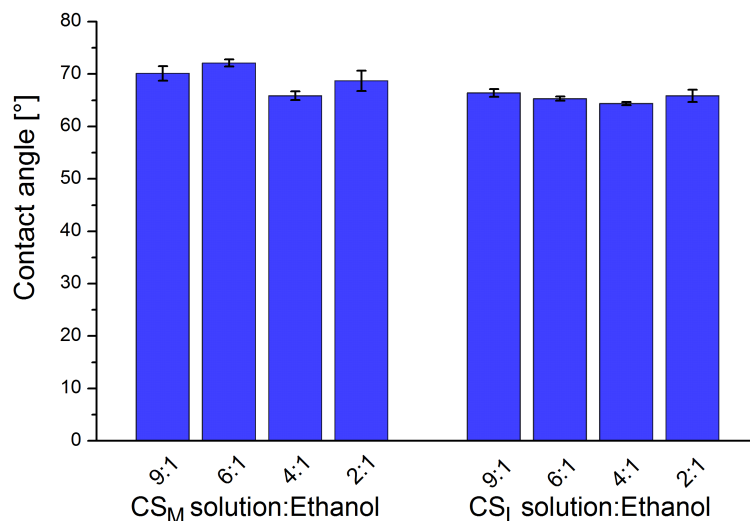


FIGURE 5.8: Static contact angles of water on thin films prepared from spin coating of mixtures with different ratios of chitosan solution and ethanol. Six drops of 3  $\mu L$  Milli-Q water are placed on two different thin films. Measurements are carried out one day after spin coating.

### 5.3 Atomic Force Microscopy (AFM)

Representative AFM images of selected chitosan hybrid thin films recorded in tapping mode on a Veeco Multimode AFM are displayed in Figure 5.9. Other recorded AFM images are depicted in Appendix B.1. The surfaces are uniform, with high similarities over a wide range of chitosan-particle combinations and layer thicknesses. With the exception of chitosan films containing silicon dioxide particles and films with the composition  $CS_M:TEOS$  2:1 ( $10 \times 10 \mu m^2$ , Appendix B.1), all films display very low surface roughness, between 0.40 nm and 0.90 nm, both in the  $25 \mu m^2$  and  $100 \mu m^2$  scan area. By way of illustration: carbon has an atomic radius of 70 pm (0.070 nm). The bright spots observable on most surfaces most likely correspond to undissolved chitosan portions. On some samples (e.g. sample  $CS_M:TEOS$  4:1, Appendix B.1) the formation of pinholes, recognisable as dark spots, is observed.

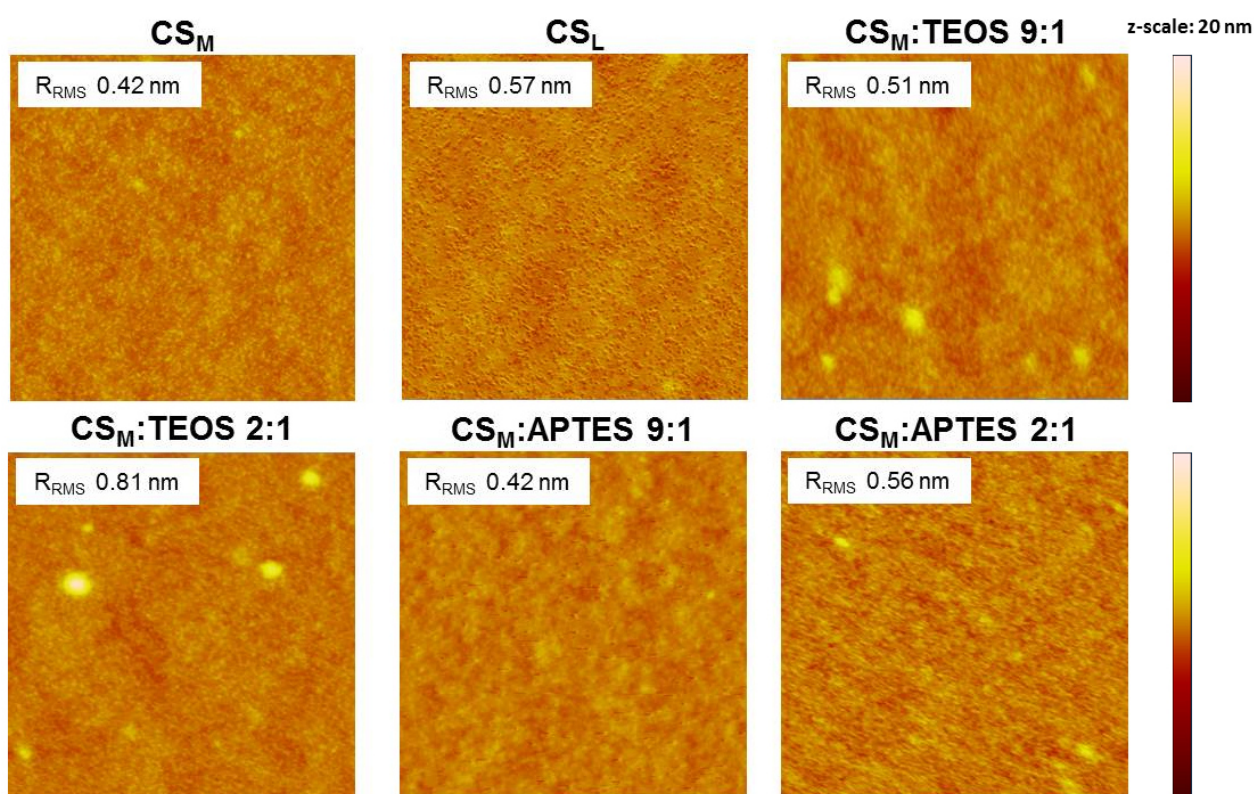


FIGURE 5.9:  $2 \times 2 \mu m^2$  AFM images of chitosan and selected chitosan hybrid thin films on silicon with a z-scale of 20 nm.  $10 \times 10 \mu m^2$  AFM images of the same materials are displayed in Figure B.1.

Altogether, surface characterisation via atomic force microscopy reveal that chitosan hybrid films, produced from spin coating, are very smooth and uniform over a broad range of compositions and possess surface roughnesses in the subnanometric range.

## 5.4 Surface Plasmon Resonance Spectroscopy (SPR)

Protein adsorption onto surfaces of chitosan and selected chitosan hybrid materials is detected by changes in the SPR angle. These shifts in the refractive index as a function of time are represented in sensograms (Figure 5.10). The onset of protein injection is accompanied by a SPR angular shift. More and more protein can adsorb to the surfaces detected by shifts of the SPR minimum to higher angles, proportional to the amount of surface adsorbed protein. During rinsing loosely bound protein is removed. The SPR angle, by the time a steady signal is achieved after rinsing, is used for the calculation of adsorbed mass per sample area. Therefore loosely bound proteins, which are immediately washed away, are not taken into account. SPR angular shifts and corresponding adsorbed protein masses for all combinations of materials and proteins are listed in Appendix C.3. A description of the experimental conditions is provided in Chapter 4.3.4.

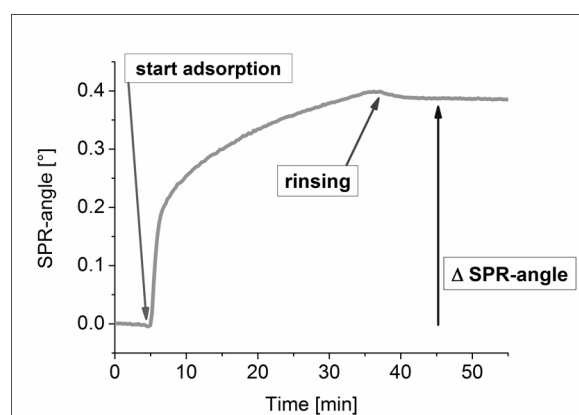


FIGURE 5.10: Typical shape of a SPR sensogram for the adsorption of proteins.

Protein adsorption is studied with bovine serum albumin and fibrinogen (Figure 5.11).

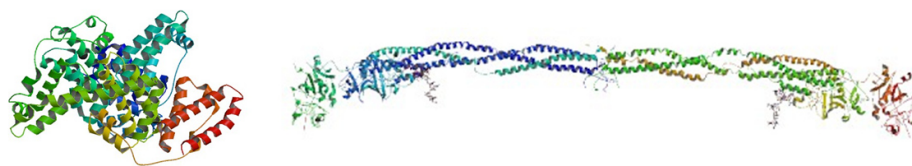


FIGURE 5.11: Crystal structure of bovine serum albumin (left) and human fibrinogen (right). Figures reprinted from [106] and [107].

Bovine serum albumin (BSA) is a widely used marker for unspecific protein adsorption and a frequently used model protein. Albumin is abundant in the body in the blood plasma where it is important for the control of osmotic pressure and the transport of fatty acids. It consists of 583 amino acids and has a molecular weight of approx. 66.5 kDa. Its isoelectric point in water is around 4.5-5.0, which means that BSA has an overall negative charge in aqueous buffer with a pH of 7.4. BSA has a globular tertiary structure. Since it displays high conformational adaptability and denaturates easily upon adsorption to a surface it is considered as "soft protein". [104]

Fibrinogen on the other hand is a large elongated protein consisting of 3410 amino acids with a molecular weight of approx. 340 kDa. It plays an important role in the blood coagulation cascade

(Chapter 2.2.2). The isoelectric point of fibrinogen in water is around 5.1-6.3 and therefore fibrinogen, just like BSA, is negatively charged in aqueous buffer with a pH of 7.4. [105]

Sensograms for the adsorption of bovine serum albumin (BSA) are depicted in Figure 5.12 and corresponding adsorbed protein masses are summarised in Figure 5.13. Protein is injected at  $t = 5$  min and surfaces are rinsed with buffer at  $t = 35$  min. Results for adsorbed protein masses are mean values of three measurements.

Notably during measurements the detection limit of the instrument is approached, which is indicated by the unsteady signal. BSA adsorption on chitosan thin films is generally low ( $0.15 \pm 0.01$  mg/m<sup>2</sup>) in comparison to other albumin adsorption experiments onto chitosan reported from literature [110, 111]. The incorporation of TEOS derived silica particles reduces protein adsorption and after washing with buffer practically no bovine serum albumin remains on the surfaces. Incorporation of aminopropyl-functionalised silica particles causes the opposite effect. In that case, more BSA adsorbs onto the surfaces compared to neat chitosan.

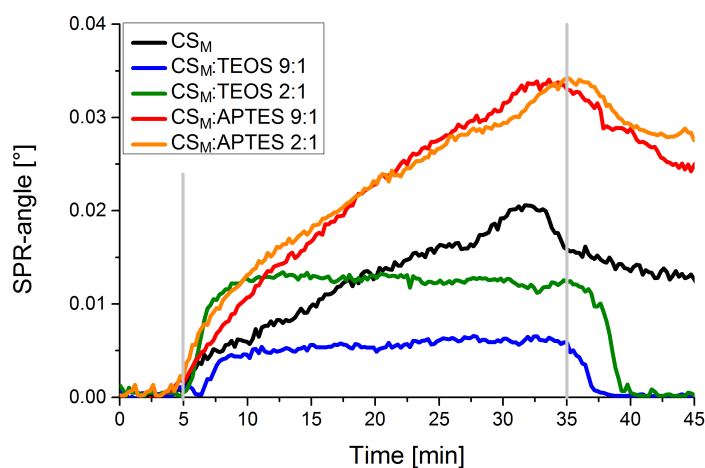


FIGURE 5.12: Overlay of SPR sensograms for the adsorption of bovine serum albumin onto chitosan and selected hybrid thin films. Protein ( $c = 1$  mg/mL in buffer) is injected at  $t = 5$  min and surfaces are rinsed with buffer (pH 7.4, 10 mM PBS + 100 mM NaCl) at  $t = 35$  min. Flow rate is set to 20  $\mu$ L/min.

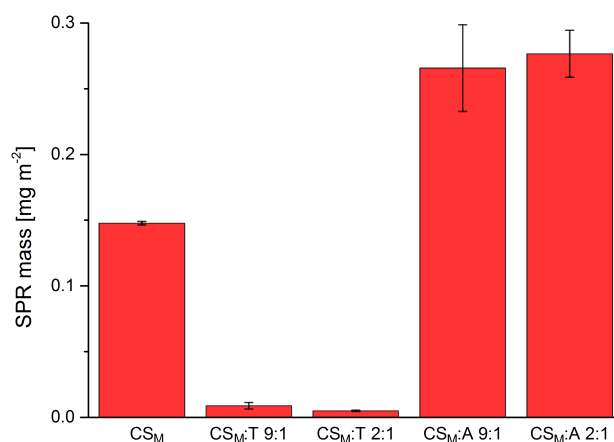


FIGURE 5.13: Bovine serum albumin mass adsorbed onto chitosan and selected hybrid thin films determined from three SPR measurements.

The results from SPR measurements of fibrinogen adsorption onto chitosan hybrid materials provides a similar picture. Sensograms for the adsorption of fibrinogen are depicted in Figure 5.14 and the corresponding adsorbed protein masses are summarised in Figure 5.15. Protein is injected at  $t = 5$  min and surfaces are rinsed with buffer at  $t = 35$  min. Results for adsorbed protein masses are mean values of three measurements.

A remarkable difference to the adsorption of BSA is that in case of fibrinogen, higher amounts of protein adsorb onto hybrid materials containing aminopropyl-functionalised silica particles (APTES). Moreover, it is observed that an increasing amount of APTES derived particles will directly enhance fibrinogen adsorption. The incorporation of TEOS derived silica-particles reduces fibrinogen adsorption onto material surfaces, compared to neat chitosan, just as it is the case for BSA. Again, the protein adsorption onto neat chitosan is low ( $0.12 \pm 0.03$  mg/m<sup>2</sup>).

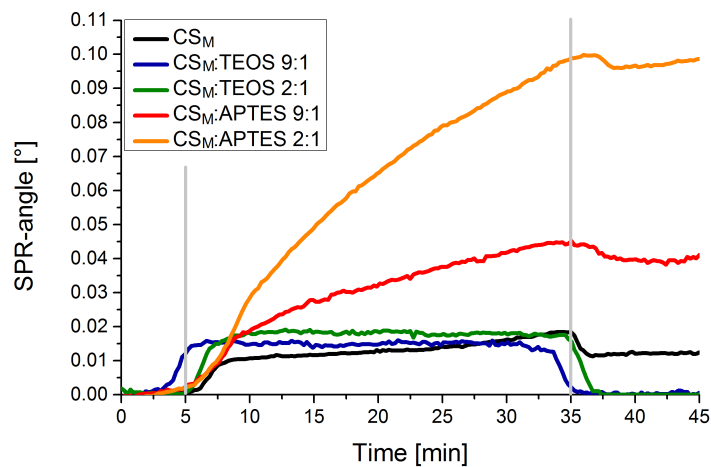


FIGURE 5.14: Overlay of SPR sensograms for the adsorption of fibrinogen onto chitosan and selected hybrid thin films. Protein ( $c = 1$  mg/mL in buffer) is injected at  $t = 5$  min and surfaces are rinsed with buffer (pH 7.4, 10 mM PBS + 100 mM NaCl) at  $t = 35$  min. Flow rate is set to 20  $\mu$ L/min.

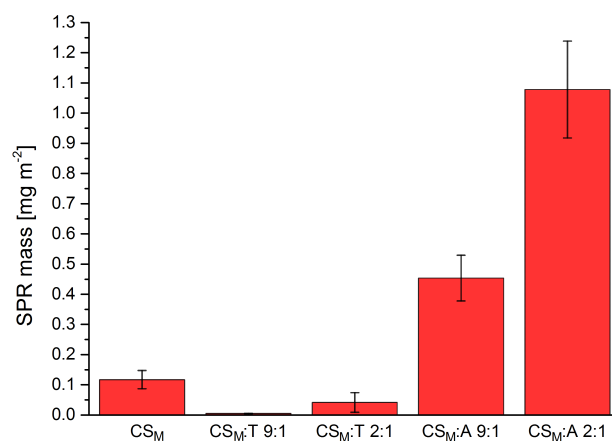


FIGURE 5.15: Fibrinogen mass adsorbed onto chitosan and selected hybrid thin films determined from three SPR measurements.

The protein adsorption experiments reveal that the use of hybrid materials incorporating sol-gel processes offer the possibility to increase and decrease protein adsorption in comparison to neat chitosan depending on the type alkoxy silane. It is hence possible to tune BSA adsorption between 0.01 mg/m<sup>2</sup>

and 0.28 mg/m<sup>2</sup> and fibrinogen adsorption between 0.01 mg/m<sup>2</sup> and 1.08 mg/m<sup>2</sup>. For a BSA monolayer in side-on configuration, which albumin usually adopts at low surface concentrations [108], the maximum theoretically adsorbed amount of albumin is about 2.3-2.6 mg/m<sup>2</sup> [109]. For the adsorption of proteins on surfaces different driving forces are important, which can also simultaneously occur, namely hydrophobic interactions, hydrogen bonding, and electrostatic interactions [110]. Therefore systematic effects of the salt concentration, protein charge, protein dipole moment, surface charge or surface hydrophobicity have been described [28]. Proteins can undergo structural rearrangements during adsorption, e.g. by exposing its hydrophobic core in the presence of a hydrophobic substrate [112].

Surfaces of chitosan-based materials containing TEOS derived silica particles are inert to protein adsorption as determined from SPR measurements. The reduced protein adsorption compared to neat chitosan could be due to the higher hydrophilicity or changes in the orientation of interfacial dipole moments and associated water at the interface, which according to *Grunze* are important parameters for inert surfaces [112].

It is suggested that the higher protein adsorption on surfaces containing APTES derived particles is related to electrostatic interactions between the negatively charged proteins and the positively charged APTES functionalities at a pH of 7.4. In the work of *Ladam et al.* [108] polyelectrolyte multilayers were prepared and their interaction with human serum albumin was studied. The multilayers were either terminated with a negatively charged polystyrenesulfonate (PSS) or with a positively charged polyallylamine (PAH). As expected, albumin, due to its negative charge, interacted more efficiently with the polyallylamine (PAH) terminated surfaces. It was pointed out that electrostatic interactions played an important role in the formation of the albumin layers on the multilayer surfaces, indicated by the high sensitivity of the adsorption process to changes in the salt concentration. Adsorption of albumin, fibrinogen, ribonuclease and lysozyme was found to be higher on quaternary-ammonium chitosan surfaces compared to unfunctionalised chitosan surfaces, as a result of a higher positive surface charge. A similar observation was made by *Mohan et al.* [113], which studied the binding of FITC-BSA to cellulose and different cationic cellulose derivatives. They were able to demonstrate that protein affinity towards cationic cellulose derivatives is higher compared to unmodified cellulose, enabling a tailoring of protein adsorption. Furthermore, in the work of *Williams et al.* [97] a high affinity of positively charged APTES molecules, which were used for the functionalisation of silicon carbide surfaces, to bovine serum albumin has been found at a pH of 7.4.

In contradiction to its polycationic character, protein adsorption onto chitosan is low in our experiments. However, higher protein adsorption has been reported in literature, for instance by *Hoven et al.* [110] (approx. 4.0 mg/m<sup>2</sup> BSA) using biochemical assays and *Benesch et al.* [111] (approx. 6.0 mg/m<sup>2</sup> HSA) using ellipsometry. Protein adsorption does not only depend on the chemical composition of the surface, but also its surface topography i.e. its roughness. The observed low protein adsorption onto chitosan, is probably related to the low surface roughness of the hybrids as revealed by atomic force microscopy. For example on chitosan thin films prepared in the work of *Benesch et al.* 6.0 mg/m<sup>2</sup> human serum albumin adsorbed onto chitosan thin film surfaces with a roughness of 5 nm, which corresponds to a ten-fold higher surface roughness compared to prepared surfaces in our laboratory.

## 5.5 Cell testing

### 5.5.1 Cytotoxicity

Cells are exposed to sample solutions and their number is compared to untreated cells (= control) in crystal violet assays. The amount of dye taken up by the cells forming a monolayer is equal to the total cell number. Crystal violet assays represent a quick and easy method to observe cytotoxic effects and are particularly useful when a first screening of a wide range of materials or substances is desired. In order to better predict the biological response towards new materials, several other assays may be used in succession (e.g. determination of reactive oxygen species [114] or cytokine profiles of monocytes/macrophages [25]).

Sample solutions correspond to medium that was in contact with the chitosan hybrid thin films, therefore containing possible release and degradation products. Results are mean values of four measurements and are summarised in Appendix C.4. A graphical representation of fibroblast viability for chitosan and selected hybrid materials is provided in Figure 5.16.

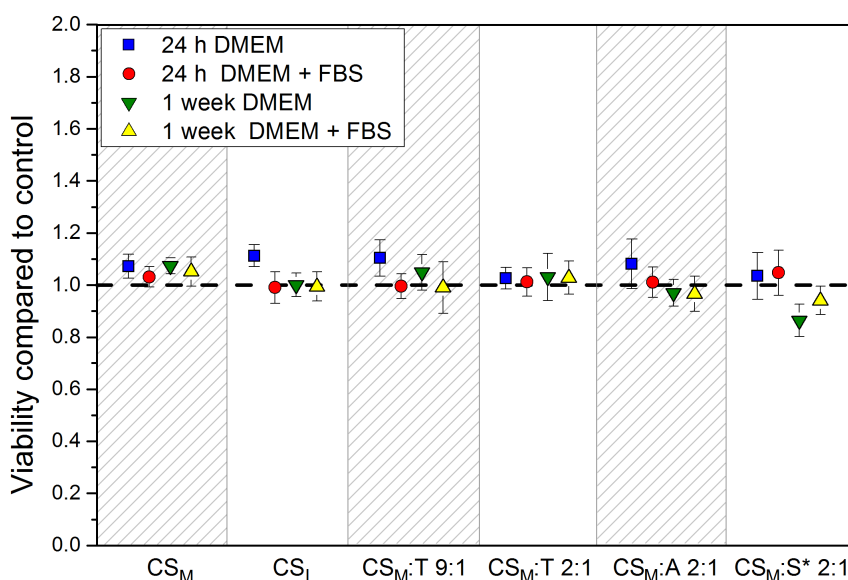


FIGURE 5.16: Fibroblast viability, compared to untreated cells, when exposed to sample solutions that were in contact with chitosan and selected hybrid thin films. Cell number is determined from four measurements using crystal violet staining. Different material incubation times (24 h, 1 week) and incubation media (with or without 5% FBS) are tested.

Toxic effects against fibroblastic cells, which would be indicated by a significant reduction in cell number compared to the control, cannot be observed for any selected hybrid material as well as neat chitosan with low molecular and medium molecular weight (Figure 5.16). Longer material incubation times for the preparation of sample solutions (24 h or 1 week), and different composition of the incubation medium containing either no or 5% FBS, do not influence cell viability.

Also in the case of osteoblasts cytotoxic effects are not observed for any tested material, different material incubation times or different composition of the incubation medium (with or without 5% FBS) (Figure 5.17). Figure 5.18 shows results from cytotoxicity assays conducted for materials containing different amounts of TEOS derived silica particles. The particle content does not influence cell viability.

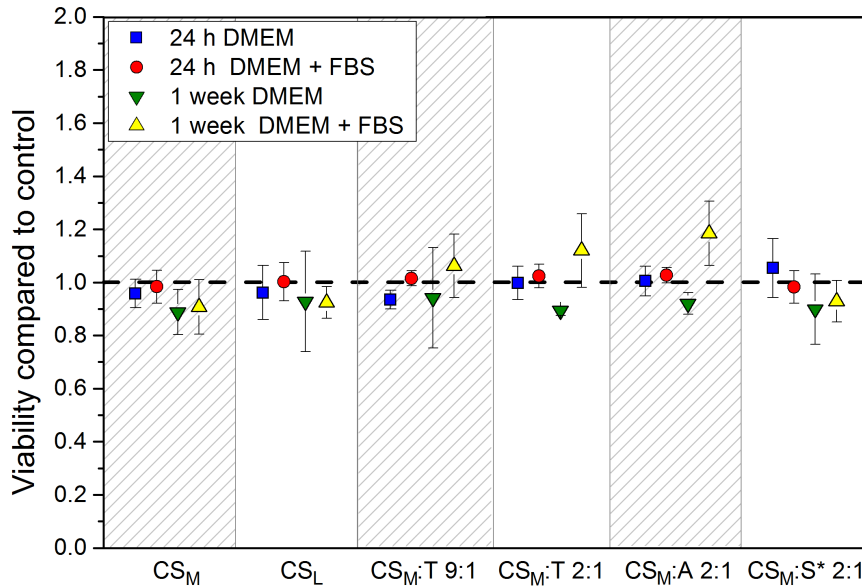


FIGURE 5.17: Osteoblast viability, compared to untreated cells, when exposed to sample solutions that were in contact with chitosan and selected hybrid thin films. Cell number is determined from four measurements using crystal violet staining. Different material incubation times (24 h, 1 week) and incubation media (with or without 5% FBS) are tested.

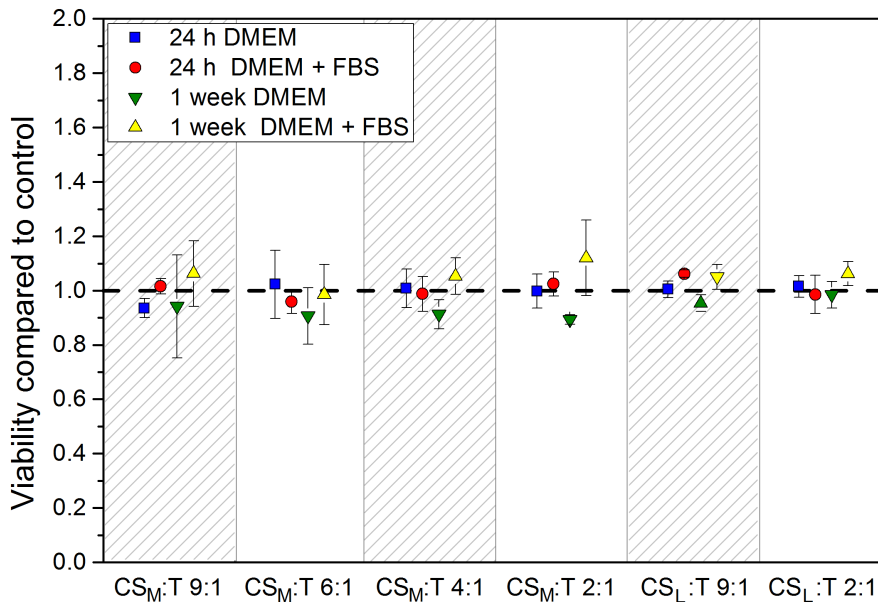


FIGURE 5.18: Osteoblast viability, compared to untreated cells, when exposed to sample solutions that were in contact with hybrid thin films containing TEOS derived silica particles. Cell number is determined from four measurements using crystal violet staining. Different material incubation times (24 h, 1 week) and incubation media (with or without 5% FBS) are tested.



Cytotoxicity assays with osteoblasts are performed with a broad set of different materials (Figure 5.19). This not only includes hybrid materials containing particles from the polycondensation of TEOS and APTES but also different types of thin films containing GLYMO sol-gel products, silicon dioxide nanoparticles and cellulose nanocrystals.

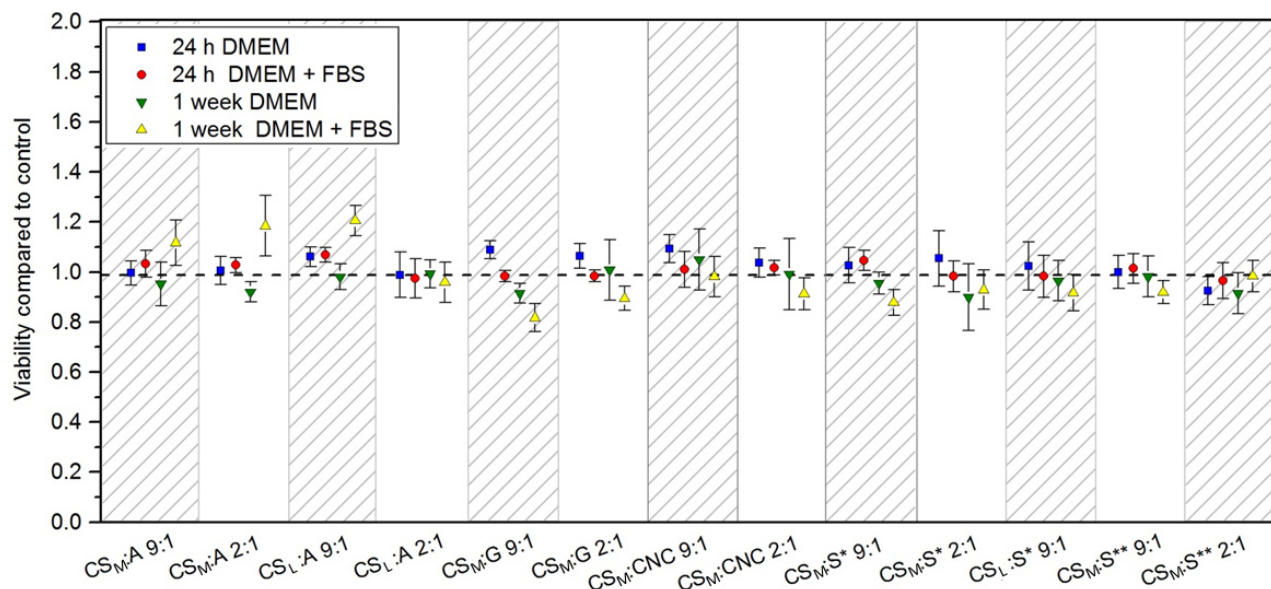


FIGURE 5.19: Osteoblast viability, compared to untreated cells, when exposed to sample solutions that were in contact with hybrid thin films containing a broad range of particles. Cell number is determined from four measurements using crystal violet staining. Different material incubation times (24 h, 1 week) and incubation media (with or without 5% FBS) are tested.

The good cytocompatibility of chitosan, for instance towards fibroblasts and osteoblasts, is described in literature [115, 116] and can also be demonstrated in this work.

Biological and physiological effects of nanosized particles can be different from microsized particles due to the larger aspect ratio and differences in cellular mechanism. The major issues in the clinical use of nanoparticles are their potential cytotoxic, genotoxic and other health related risks. [117]

In the case of silica particles, cancerogenic properties are with respect to its inhalation. Orally administered silica in water has no toxic effects even at high concentrations, clearly revealing the importance of the route of exposure. Silicon is found in the blood plasma at a concentration of 50  $\mu\text{g}/\text{dL}$  as well as in different tissues in particular bone. For instance, in chicks and rats it is known to be necessary for growth and skeletal development. [118]

Furthermore, silica has been found to decrease blood coagulation time by adsorbing and stimulating intrinsic pathway coagulation factors [119], an interesting property for wound dressing applications.

However, there is not any significant toxic effect towards fibroblasts and osteoblasts associated with the tested hybrid materials as determined from crystal violet assay. An induction of cell viability can not be observed as well. In our studies nanometric chitosan hybrid materials incorporating alkoxy silane sol-gel products (TEOS, APTES, GLYMO) or other nanometric particles ( $\text{SiO}_2$ , CNCs) display the same *in vitro* cytocompatibility as neat chitosan.

### 5.5.2 Cell attachment

Chitosan has gained considerable attention for applications as scaffolds for tissue engineering, as coatings for orthopaedic devices and as wound dressing. In this context, cell attachment and proliferation are important parameters. Therefore, it is our aim to demonstrate that chitosan hybrid thin films are suitable substrates for the growth of fibroblasts and osteoblasts. The focus lies on hybrid materials containing particles from the sol-gel processing of TEOS and APTES as well as silicon dioxide.

Cells are seeded onto coated wafers and are allowed to attach and proliferate on its surfaces. The growth of cells is monitored under a light microscope using a glass control. In order to evaluate the cell's morphology and viability, after three days osteoblasts on thin films from neat chitosan (CS<sub>L</sub>) and a glass control are stained with Live/Dead cell viability kit and imaged using confocal microscopy (Figure 5.20).

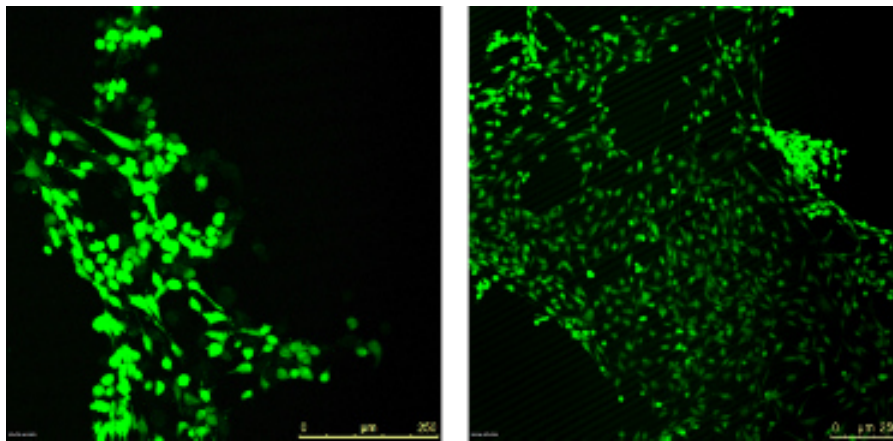


FIGURE 5.20: Fluorescence images as an overlay of two images recorded at different excitation/emission wavelengths, of osteoblastic cells on chitosan thin films (left) and a glass control (right) using a combination of Live/Dead staining assay and confocal microscopy.

Green fluorescent cells correspond to live cells, whereas red fluorescent cells would correspond to dead cells. Staining Kit contains calcein-am (acetoxymethyl ester of calcein) for the staining of live cells and propidium iodide for dead cells, respectively. Calcein-am is not fluorescent by itself, only when converted into calcein by intracellular esterases in viable cells. Propidium iodide intercalates between the bases of DNA, thereby enhancing the fluorescence signal as well as shifting its excitation and emission maxima. In viable cells, propidium iodide is membrane impermeable.

As can be discerned from the acquired images, attached osteoblasts are viable and cell death is not observed for both the chitosan thin film and the glass control. Osteoblasts are spherically shaped and show only small signs of cell spreading. In the work of *Fakhry et al.* [121] osteoblasts were seeded onto chitosan coated glass cover slips. Osteoblasts in their experiments also readily attach to the chitosan surfaces, but display high spreading already after 24 hours. Notably, in their experiments actin stress fibres were specifically stained, which could represent a better method of displaying cell spreading since actin filaments are part of the cytoskeleton of eukaryotic cells, maintaining and changing its shape.

The number of attached cells on chitosan and different hybrid thin films after four days is quantitatively determined using a modified MTT assay. Cells are counted four times at 595 nm on a Multimode Microplate Reader. In order to eliminate contributions from small differences in wafer size, a size factor is introduced accounting for deviations from the normal sample size of 1.5 cm x 1.5 cm (Appendix B.2). Absorbance of all hybrid thin films is represented in relation to the absorbance of neat chitosan thin films (=1.00). Results for the attachment and proliferation of fibroblasts are summarised in Table 5.1. Chitosan's ability to serve as a biocompatible substrate for the attachment and proliferation of fibroblasts and osteoblasts is described in literature [121, 122]. Furthermore, *Fakhry et al.* [121] found that chitosan preferentially supports the initial attachment and spreading of osteoblasts over fibroblasts.

Amount of cells on chitosan hybrid thin films compared to thin films from neat chitosan are shown in Figure 5.21. It is apparent that hybrid thin films are as capable of accelerating the attachment and proliferation of fibroblasts as thin films from neat chitosan. Attachment to the silicon wafer is higher compared to coated wafers. Lower adhesion of cells towards polymers in comparison to metals and ceramics can be related to differences in the surface energy [120].

TABLE 5.1: Summary of the MTT test results from the growth of fibroblasts on chitosan and different hybrid thin films with silicon wafers as substrates. The size factor accounts for deviations from the normal sample size. Attachment of cells on hybrid materials is expressed in relation to neat chitosan thin films (=1.00).

Material	Absorbance	Wafer size [cm <sup>2</sup> ]	Size factor	Absorbance (with size factor)	Cell attachment
CS <sub>M</sub>	0.2384 ± 0.0045	2.477	1.101	0.2165 ± 0.0041	1.000 ± 0.019
CS <sub>M</sub> :T 9:1	0.2270 ± 0.0054	2.399	1.066	0.2129 ± 0.0050	0.983 ± 0.023
CS <sub>M</sub> :T 2:1	0.2202 ± 0.0095	2.438	1.083	0.2032 ± 0.0088	0.939 ± 0.040
CS <sub>M</sub> :A 2:1	0.2461 ± 0.0079	2.381	1.058	0.2326 ± 0.0074	1.074 ± 0.034
CS <sub>M</sub> :S* 2:1	0.2517 ± 0.0020	2.329	1.035	0.2432 ± 0.0019	1.123 ± 0.009
Silicon	0.2960 ± 0.0014	2.284	1.015	0.2916 ± 0.0014	1.347 ± 0.006

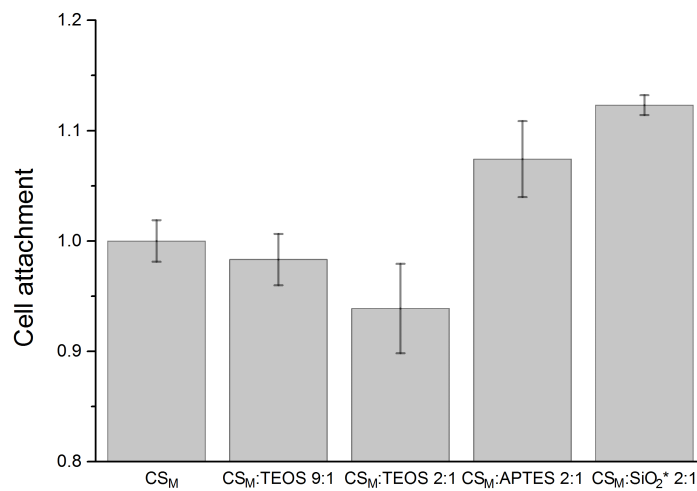


FIGURE 5.21: Fibroblast attachment and proliferation on surfaces of selected hybrid thin films in relation to neat chitosan thin films as determined by MTT assay.

As can be discerned from Figure 5.21 fibroblast attachment correlates with BSA and fibrinogen adsorption (Figure 5.13 and 5.15). In both cases attachment/adsorption to the chitosan hybrid materials containing TEOS derived particles is lower, whereas the attachment/adsorption to the material containing APTES derived particles is higher. In the previous chapter it was described how differences in the surface properties (i.e. chemistry, structure) of the hybrid materials can be used to tune protein adsorption, which in turn may also determine cell adhesion.

Results from the attachment of osteoblastic cells are listed in Table 5.2. Just as with fibroblasts, chitosan hybrid thin films are as capable of accelerating the attachment of osteoblasts as thin films from neat chitosan. In all cases, the number of attached osteoblasts on hybrid thin films is slightly higher, clearly demonstrating the hybrid material's promising properties for bone regeneration applications (e.g. facilitating osseointegration). The highest number of osteoblasts is observed on  $CS_M:SiO_2^* 2:1$ .

TABLE 5.2: Summary of the MTT test results from the growth of osteoblasts on chitosan and different hybrid thin films with silicon wafers as substrates. The size factor accounts for deviations from the normal sample size. Attachment of cells on hybrid materials is expressed in relation to neat chitosan thin films (=1.00).

Material	Absorbance	Wafer size [cm <sup>2</sup> ]	Size factor	Absorbance (with size factor)	Cell attachment
$CS_M$	$0.2428 \pm 0.0052$	2.417	1.074	$0.2287 \pm 0.0049$	$1.000 \pm 0.021$
$CS_M:T 9:1$	$0.2707 \pm 0.0073$	2.355	1.047	$0.2603 \pm 0.0070$	$1.138 \pm 0.030$
$CS_M:T 2:1$	$0.2657 \pm 0.0022$	2.337	1.039	$0.2556 \pm 0.0021$	$1.118 \pm 0.009$
$CS_M:A 2:1$	$0.2640 \pm 0.0038$	2.396	1.065	$0.2479 \pm 0.0036$	$1.084 \pm 0.016$
$CS_M:S^* 2:1$	$0.2875 \pm 0.0096$	2.369	1.053	$0.2775 \pm 0.0091$	$1.214 \pm 0.040$
Silicon	$0.3087 \pm 0.0030$	2.150	0.955	$0.3222 \pm 0.0031$	$1.409 \pm 0.014$

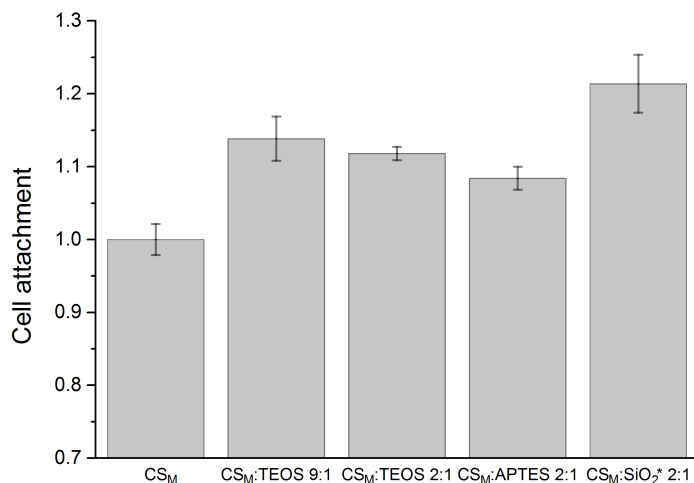


FIGURE 5.22: Osteoblast attachment and proliferation on surfaces of selected hybrid thin films in relation to neat chitosan thin films as determined by MTT assay.

In addition, silica has been reported to possess osteoinductive properties, upregulating osteogenic markers [123]. *Lee et al.* [124] found that inorganic-organic hybrid materials based on chitosan and sol-gel derived silica induce alkaline phosphatase activities in osteoblasts, which is a marker of osteoblastic differentiation, as well as enhancing the bone regeneration rate in a defect using a rat calvarial model.

## 5.6 Tensile testing

Chitosan displays poor mechanical properties in the presence of water, which also limits its application and further development [125]. Particulate-reinforced chitosan hybrid materials can present an alternative and can be prepared by sol-gel polymerisation of TEOS solutions with different concentrations. In this work foils are reinforced with 2.9%, 5.8% and 11.5% silica particles from TEOS sol-gel processing and 7.3% chitin nanocrystals. Mechanical properties, i.e. elastic modulus, yield strength at 0.2% offset, ultimate tensile strength and break strain, are measured in uniaxial tensile tests. Results are mean values of five measurements. A detailed summary of measured values is provided in Appendix C.5.

The acetic acid/water to ethanol ratio in the solvent mixture can possibly influence the structural organisation of the bulk material formed upon solvent evaporation and in turn its mechanical properties. For that reason, the acetic acid/water to ethanol ratio is set to 9:1. To rule out differences from the preparation of foils from pure chitosan solutions and preparation from chitosan solutions containing ethanol both materials are subjected to tensile tests. Results are listed in Table 5.3 and representative stress-strain curves are depicted in Figure 5.23.

TABLE 5.3: Mechanical parameters obtained from uniaxial tensile tests of chitosan foils prepared from mixtures of chitosan dissolved in acetic acid/water diluted with ethanol in a ratio of 9:1 (w/w) in comparison to neat chitosan foils. Results are mean values of five measurements.

Material	Elastic modulus [MPa]	Yield Strength [MPa]	Ultimate Tensile Strength [MPa]	Break Strain [%]
CS <sub>M</sub>	2563 ± 511	47.1 ± 2.1	70.0 ± 5.6	10.47 ± 2.79
CS <sub>M</sub> :EtOH 9:1	2939 ± 577	49.3 ± 2.6	72.9 ± 4.7	8.50 ± 0.76

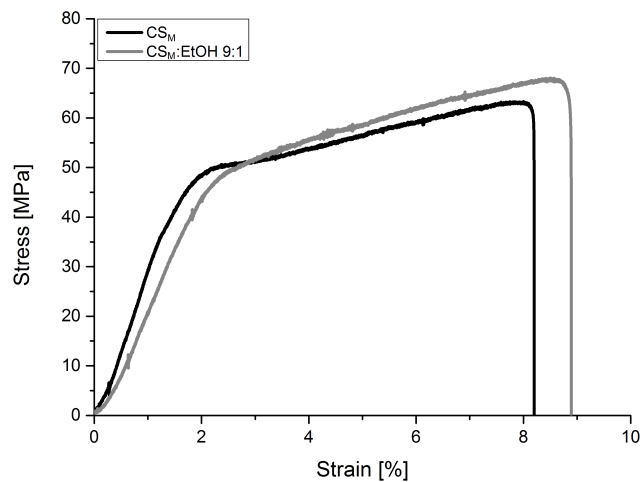


FIGURE 5.23: Representative stress-strain curves of chitosan foils prepared from mixtures of acetic acid/water and ethanol in a ratio of 9:1 (w/w) in comparison to neat chitosan foils. The loading speed is 0.5 mm/min.

Elastic modulus, yield strength and tensile strength are slightly higher for chitosan foils containing ethanol in the solvent mixture. However, differences in the mechanical properties are not significant. It should hence be possible to directly compare results from materials, reinforced with particles dispersed in ethanol, with neat chitosan.

Mechanical values of chitosan foils reinforced with TEOS derived silica-particles are listed in Table 5.4 and representative stress-strain curves are depicted in Figure 5.24. The prepared silica particles are rich in hydroxyl groups and interact with the amino and hydroxyl groups of chitosan via hydrogen and covalent bonding. Ultimate tensile strength, yield strength and elastic modulus increases, whereas break strain decreases when chitosan is reinforced with 2.9% and 5.8% TEOS derived silica particles. The changes are related to the additional strength and brittleness introduced by the inorganic constituents. However, in materials containing 11.5% silica particles strength declines.

In the work of *Huang et al.* [126] polyimide-silica nanocomposites were prepared using a commercial silica sol. Similar to our findings, reinforcement of polyimide materials with a tensile strength of 98 MPa with 10, 20 and 30% silica particles, changes the tensile strength accordingly to 112, 116 and 105 MPa. Chitosan-based hybrid materials reinforced with different amounts of sol-gel processed tetraethyl orthosilicate/vinyl triethoxysilane have been prepared in the work of *Yeh et al.* [127]. They observed an initial increases of tensile strength which declines again, when a certain concentration of the particle in the composite is exceeded.

An explanation for the deviating mechanical properties of chitosan foils containing 11.5% silica particles could be that at highest particle concentrations, silica particles aggregate, thereby giving rise to possible stress concentrators. In addition, a high particle concentration could impact film formation by interfering intermolecular interactions of chitosan chains. In this context, performance of SAXS experiments, e.g. under a simultaneous application of a tensile load, would be interesting.

TABLE 5.4: Mechanical parameters obtained from uniaxial tensile tests of chitosan foils reinforced with silica particles from the sol-gel process of TEOS in comparison to neat chitosan foils. The loading speed is 0.5 mm/min.

Material	Elastic modulus [MPa]	Yield Strength [MPa]	Ultimate Tensile Strength [MPa]	Break Strain [%]
CS <sub>M</sub>	2563 ± 511	47.1 ± 2.1	70.0 ± 5.6	10.47 ± 2.79
CS <sub>M</sub> :T (2.9%)	2845 ± 572	66.4 ± 4.1	83.1 ± 8.0	8.30 ± 3.27
CS <sub>M</sub> :T (5.8%)	4883 ± 192	80.1 ± 4.7	101.8 ± 6.5	5.32 ± 1.54
CS <sub>M</sub> :T (11.5%)	2375 ± 390	45.5 ± 6.0	83.0 ± 6.0	11.28 ± 2.68

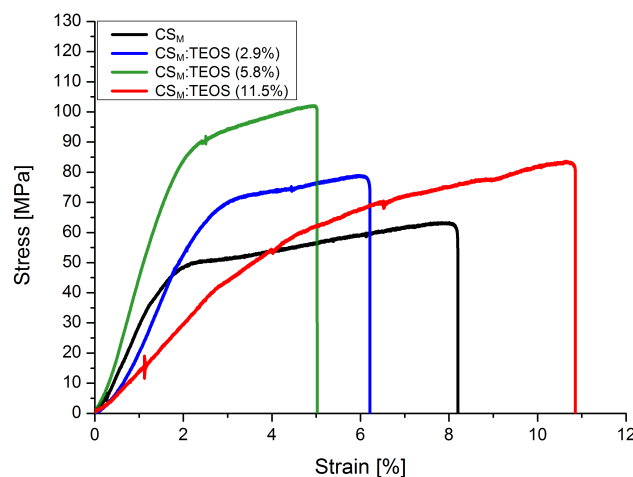


FIGURE 5.24: Representative stress-strain curves of chitosan foils reinforced with silica particles from sol-gel processing of TEOS in comparison to neat chitosan foils. Loading speed is 0.5 mm/min.

Furthermore, chitosan foils are reinforced with chitin nanocrystals. In literature materials have been reinforced both with chitin nanocrystals and chitin fibres [128, 129, 130, 131]. Chitin whiskers are highly crystalline and are prepared by acidic hydrolysis of chitin. Tensile strengths of 110.3 MPa were reached by the incorporation of 3% chitin whiskers, which presented a 2.8 fold increase compared to the non-reinforced material [128]. In another work tensile strength of reinforced films increased from 64.9 to a maximum of 83.8 MPa at a whisker content of 2.96 wt% [129]. Beyond that an increasing whisker content caused a small gradual decrease in tensile strength. Chitin nanofibres can be extracted in their natural state and usually have a thickness of approximately 10 nm and a length of 800–1000 nm [131]. They are longer and more flexible compared to chitin whiskers. Surface-deacetylated chitin nanofibres were used to reinforce chitosan films in the work of *Ifuku et al.* [130]. Tensile strength of neat chitosan films increased from 40.0 to 77.6 MPa by the incorporation of 10% nanofibres. *Mushi et al.* [131] found highest toughness in chitosan films containing 10 wt% chitin nanofibres. In several of the above mentioned works an increase in the elastic modulus and a reduction in the elongation until failure is reported for chitin nanocrystals/-fibre reinforcements.

In our materials, chitin nanocrystal reinforcement leads to an increase in yield strength, tensile strength and elastic modulus (Table 5.5, Figure 5.25). Chitin nanocrystals and nanofibres are highly compatible with the chitosan matrix, by forming a large number of hydrogen bonds as well as due to hydrophobic and electrostatic interactions [129]. Hence higher strength can be attributed to the additional rigidity from the formation of such favourable interactions, as well as the higher strength and crystallinity of the whiskers itself.

TABLE 5.5: Mechanical parameters obtained from uniaxial tensile tests of foils reinforced with 7.3% ChNCs in comparison to neat chitosan foils. Results are mean values of five measurements.

Material	Elastic modulus [MPa]	Yield Strength [MPa]	Ultimate Tensile Strength [MPa]	Break Strain [%]
CS <sub>M</sub>	2563 ± 511	47.1 ± 2.1	70.0 ± 5.6	10.47 ± 2.79
CS <sub>M</sub> :ChNC (7.3%)	3348 ± 392	53.9 ± 5.2	90.9 ± 9.3	10.58 ± 2.08

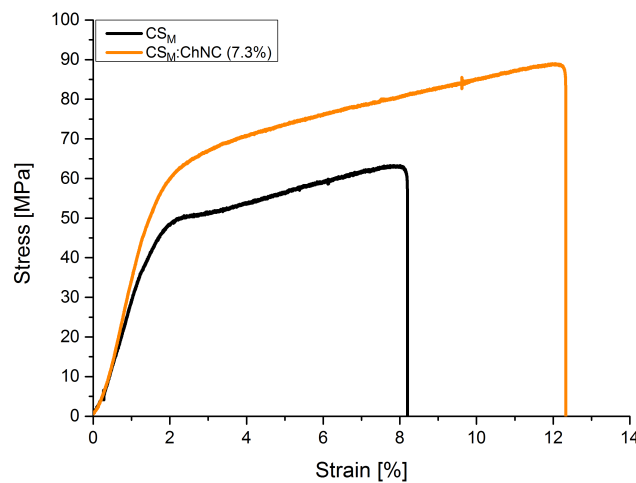


FIGURE 5.25: Representative stress-strain curves of chitosan foils reinforced with 7.3% ChNCs in comparison to neat chitosan foils. The loading speed is 0.5 mm/min.

Chitosan has different mechanical properties depending on the molecular weight and degree of deacetylation. Chitosan of higher molecular weight produces films with higher tensile strength and elongation as well as displaying increased water adsorption [132]. Chitosan with higher degrees of deacetylation possesses more crystalline regions and therefore lower moisture adsorption and swelling is observed [133]. Results from mechanical testing of chitosan films often vary greatly and can not be easily compared, due to differences in molecular weight, preparation method and environmental conditions [131]. Reports on the tensile strength of chitosan films range from 40 MPa to 100 MPa according to *Mushi et al.* [131]. Young's moduli are typically around 2.4 GPa. By way of comparison, tensile strength of common synthetic polymers is 20–30 MPa for high-density polyethylene, 8–30 MPa for low-density polyethylene, 30–40 MPa for polypropylene, 35–50 MPa for polystyrene and 50–75 MPa for polyethylene terephthalate [138]. Mechanical properties of chitosan can be improved through crosslinking, blending or the use of a reinforcing agent, for example clays and nanoparticles. The interaction between the matrix component and the reinforcing agent, the interfacial strength between the polysaccharide and the particle, greatly influences the resulting mechanical properties. Several studies have also investigated changes in mechanical properties associated with the addition of antimicrobial agents [134], plasticisers [136] or other additives (e.g. hydroxyapatite for orthopaedic applications) [137].

In summary, chitosan foils can be enhanced with silica particles from sol-gel processes, representing a significant improvement to the mechanical properties of neat chitosan (Figure 5.26).

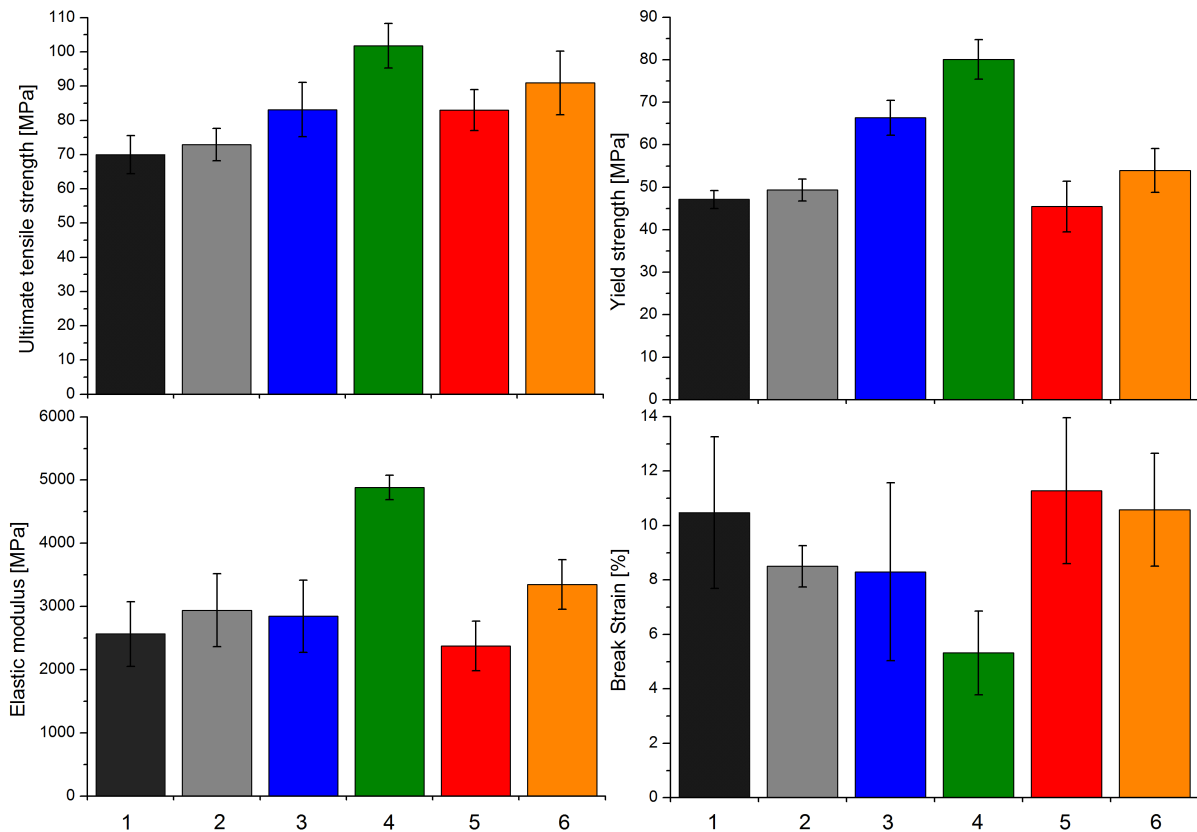


FIGURE 5.26: Summary of mechanical properties of unreinforced chitosan foils and chitosan foils reinforced with TEOS derived silica-particles and chitin nanocrystals : Ultimate tensile strength (top left), yield strength (top right), elastic modulus (bottom left) and break strain (bottom right). (1)  $CS_M$ , (2)  $CS_M:EtOH$  9:1, (3)  $CS_M:T$  (2.9%), (4)  $CS_M:T$  (5.9%), (5)  $CS_M:T$  (11.5%) and (6)  $CS_M:ChNC$  (7.3%).



## 5.7 Dynamic mechanical analysis (DMA)

The materials which displayed the best mechanical properties in stress-strain experiments are studied in more detail by means of dynamic mechanical analysis. Storage modulus of three materials, one unreinforced and two reinforced materials, as a function of relative humidity is monitored. Neat chitosan specimen have a size of 5.0700 mm x 4.4400 mm with a thickness of 35.0  $\mu\text{m}$ , silica reinforced chitosan foils a size of 6.3400 mm x 4.3400 mm with a thickness of 25.0  $\mu\text{m}$  and ChNC reinforced chitosan foils a size of 6.1700 mm x 4.3000 mm and a thickness of 28.0  $\mu\text{m}$ .

Results from neat chitosan clearly reveal that storage modulus decreases with increasing humidity (Figure 5.27), describing a concave downward function. Storage modulus represents the elastic "in-phase" component of the material, as opposed to the loss modulus representing the viscous "out-of phase" component. Furthermore, storage modulus is a measure of the stiffness of a material. Upon water uptake the material becomes more flexible due to the disruption of polymer strand interactions. Chitosan can take up large quantities of water. In the material it can persist as strongly bound non-freezing water molecules, as less tightly bound water molecules e.g. present in small capillaries or as free water molecules e.g. in large voids and large capillaries [53, 139]. The number of non-freezing bound water molecules attached to each polymer repeating unit in the amorphous region of the polymer has found to be between 3 and 8 [53]. As described in chapter 2.3.2 the water sorption isotherm of chitosan presents a sigmoidal shape, meaning that above a certain relative humidity, the water content in the material increases exponentially. Chitosan foils are porous hygroscopic materials and therefore effects from capillary condensation have to be taken into account. Capillary condensation takes place when water is confined into a capillary. At such conditions, condensation of vapour occurs below the saturation vapour pressure. According to *Rosa et al.* [52] capillary condensation in chitosan is attained at water activities of  $a_w \geq 0.80$ . In our case, above relative humidities of 70% a dramatic reduction of the storage modulus can be observed, which can be attributed to capillary condensation.

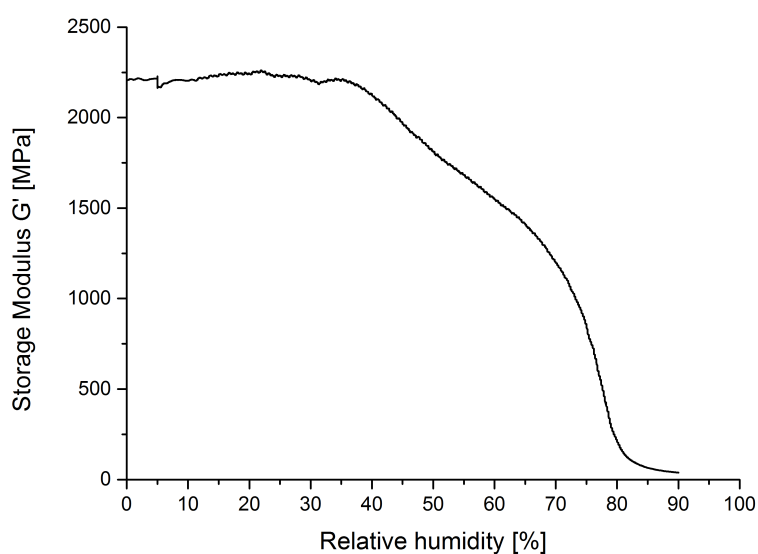


FIGURE 5.27: Storage modulus ( $G'$ ) at room temperature as a function of increasing relative humidity of neat chitosan foils. DMA measurements are performed by applying an oscillating strain of 0.0300% at a frequency of 1 Hz.

Storage moduli for hybrid materials containing 5.8% silica particles from TEOS sol-gel processes are higher over a wide range of humidities compared to neat chitosan (Figure 5.28). The same applies to chitosan foils containing 7.3% ChNCs (Figure 5.29). Silica reinforced materials display higher initial storage moduli (at RH=0). These greater storage moduli can be attributed to the higher crosslinking density in the material as well as the higher stiffness of the reinforcing agent itself (i.e. its ceramic nature). Crosslinking increases the material's rigidity by impeding free movement of polymer chains. Higher stiffness of hybrid materials based on chitosan and TEOS derived silica have also been reported by *Sagheer et al.* [140]. By the incorporation of 5, 10, 20 and 30% silica particles, storage modulus at 50 °C increased accordingly from 3.67 GPa of neat chitosan to 4.42, 4.82, 6.00 and 6.70 GPa. In their work, storage moduli of the reinforced materials were higher over a wide range of temperatures (50-210 °C) compared to neat chitosan, applying a sinusoidal strain at a frequency of 2 Hz.

Interestingly, in both of our reinforced materials storage modulus first declines and increases again after a certain humidity is reached. Maximum storage modulus, which is around 3400-3800 MPa, is hence not at zero humidity, but rather around 30% relative humidity in the case of silica reinforced materials and 45% relative humidity in the case of ChNC reinforcement. At higher humidities, materials storage modulus values describe a concave downward curve similar to the one of neat chitosan. Such a viscoelastic behaviour is unexpected. The results could be explained by the different viscoelastic behaviour of the two components, the measured curve representing an overlay of both constituents. However, in order to explain the observed viscoelastic behaviour further experiments have to be carried out, for instance detailed DMA studies involving temperature and frequency sweeps, and x-ray experiments, where it could be possible to monitor structural changes induced by water. Such additional experiments could help to explain the different behaviour of reinforced and unreinforced chitosan-based materials in dynamic mechanical analysis.

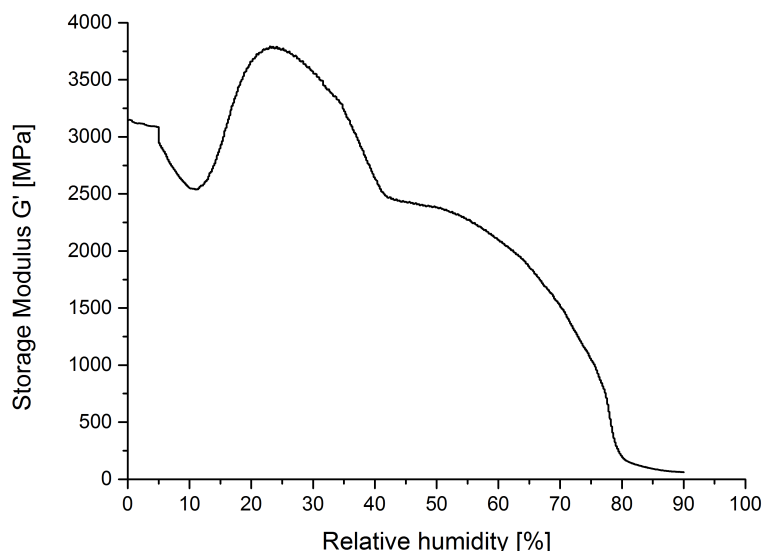


FIGURE 5.28: Storage modulus ( $G'$ ) at room temperature as a function of increasing relative humidity of chitosan foils reinforced with 5.8% silica particles from sol-gel processing of TEOS. DMA measurements are performed by applying an oscillating strain of 0.0300% at a frequency of 1 Hz.

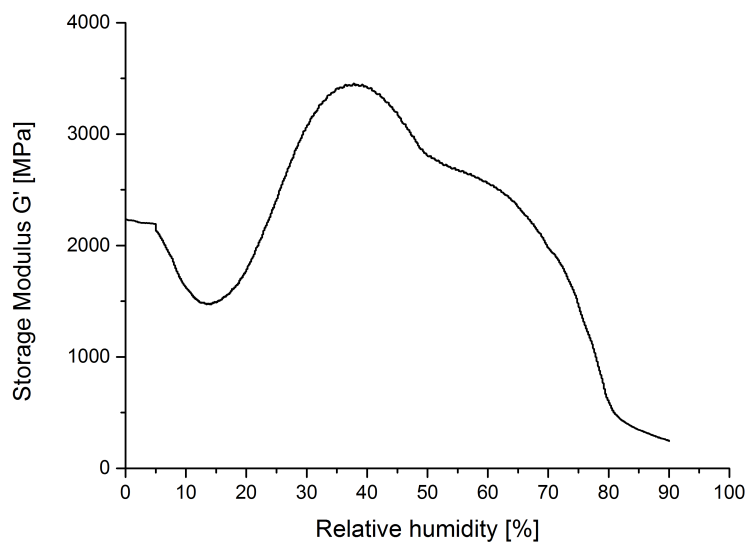


FIGURE 5.29: Storage modulus ( $G'$ ) at room temperature as a function of increasing relative humidity of chitosan foils reinforced with 7.3% ChNCs. DMA measurements are performed by applying an oscillating strain of 0.0300% at a frequency of 1 Hz.



# Summary and Conclusion

In this work, the preparation of several hybrid materials from acetic acid solutions of chitosan and prehydrolysed/-condensed alkoxysilanes is demonstrated. Materials can be processed into films with a thickness of 20-30  $\mu\text{m}$  (i.e. foils) by solution casting or into thin films with a thickness between 55 nm and 105 nm on different substrates by spin coating.

Surfaces of the thin films are highly similar over a wide range of material combinations and exhibit subnanometre roughness. The use of TEOS in the material preparation increases hydrophilicity in the product while the incorporation of APTES derived inorganic constituents lowers surface wettability. An interesting observation is related to the changes of the static contact angle over time, probably due to relaxations processes within the thin film. Significant lowering of the contact angle is observed when measurements are carried out two months after thin film preparation. As revealed by multi-parameter surface plasmon resonance spectroscopy (MP-SPR), adsorption of bovine serum albumin and fibrinogen is comparatively low on both chitosan and chitosan-based hybrid material surfaces. Incorporation of TEOS sol-gel products into the chitosan matrix provides films, for which the amount of adsorbed protein is near or below the detection limit of the SPR instrument. This observation is particularly interesting with respect to medical applications, where prevention of protein adsorption is desired. In contrast, the incorporation of APTES derived particles into the chitosan matrix increases protein adsorption. Hence protein adsorption can be tailored by varying the type and content of alkoxysilane employed in the material preparation. Hybrid materials show the same excellent cytocompatibility as neat chitosan. The combined results from cytotoxicity assays, confocal microscopy and cell attachment tests are all directing towards a high biocompatibility of chitosan hybrid thin films, capable of accelerating the attachment and proliferation of fibroblasts and osteoblasts.

The mechanical properties of chitosan can be significantly increased by the incorporation of particles from the sol-gel process. Prepared chitosan-based hybrid materials display higher mechanical strength and by the use of TEOS derived particles a 1.45 fold increase in tensile strength and a 1.91 fold increase in the elastic modulus can be achieved. In addition, stiffness of the hybrid material is higher over a wide range of humidities.

Therefore, the presented chitosan-based hybrid materials are promising candidates for applications in orthopaedic coatings, scaffolds for tissue engineering or in wound dressings, areas where chitosan is already intensively studied. Further investigations could focus on the coating of titanium, the most widely used metal in dental and orthopaedic implants, and the improvement of the material adhesion to selected substrates. In addition, further knowledge and understanding of the material's structure could help to better correlate composition with biological and mechanical characteristics of hybrid materials in the future.



# Bibliography

- [1] Jayakumar, R.; Prabakaran, M.; Sudheesh Kumar, P. T.; Nair, S. V.; Tamura, H. Biomaterials based on chitin and chitosan in wound dressing applications. *Biotechnology Advances* 2011, 29 (3), 322–337.
- [2] Dash, M.; Chiellini, F.; Ottenbrite, R. M.; Chiellini, E. Chitosan-a versatile semi-synthetic polymer in biomedical applications. *Progress in Polymer Science* 2011, 36 (8), 981–1014.
- [3] Muzzarelli, R. A. A. Chitins and chitosans for the repair of wounded skin, nerve, cartilage and bone. *Carbohydrate Polymers* 2009, 76 (2), 167–182.
- [4] Kim, I.-Y.; Seo, S.-J.; Moon, H.-S.; Yoo, M.-K.; Park, I.-Y.; Kim, B.-C.; Cho, C.-S. Chitosan and its derivatives for tissue engineering applications. *Biotechnology Advances* 2008, 26 (1), 1–21.
- [5] Spirk, S.; Findenig, G.; Doliska, A.; Reichel, V. E.; Swanson, N. L.; Kargl, R.; Ribitsch, V.; Stankleinschek, K. Chitosan-silane sol-gel hybrid thin films with controllable layer thickness and morphology. *Carbohydrate Polymers* 2013, 93 (1), 285–290.
- [6] Shirotsaki, Y.; Tsuru, K.; Hayakawa, S.; Osaka, A.; Lopes, M. A.; Santos, J. D.; Costa, M. A.; Fernandes, M. H. Physical, chemical and in vitro biological profile of chitosan hybrid membrane as a function of organosiloxane concentration. *Acta Biomaterialia* 2009, 5 (1), 346–355.
- [7] Amado, S.; Simões, M. J.; Armada da Silva, P. A. S.; Luís, A. L.; Shirotsaki, Y.; Lopes, M. A.; Santos, J. D.; Fregnan, F.; Gambarotta, G.; Raimondo, S.; et al. Use of hybrid chitosan membranes and N1E-115 cells for promoting nerve regeneration in an axonotmesis rat model. *Biomaterials* 2008, 29 (33), 4409–4419.
- [8] Kean, T.; Thanou, M. Biodegradation, biodistribution and toxicity of chitosan. *Advanced Drug Delivery Reviews* 2010, 62 (1), 3–11.
- [9] Kong, M.; Chen, X. G.; Xing, K.; Park, H. J. Antimicrobial properties of chitosan and mode of action: a state of the art review. *International Journal of Food Microbiology* 2010, 144 (1), 51–63.
- [10] Rao, S. B.; Sharma, C. P. Use of chitosan as a biomaterial: studies on its safety and hemostatic potential. *Journal of Biomedical Materials Research* 1997, 34 (1), 21–28.
- [11] Ilschner, B.; Lees, J. K.; Dhingra, A. K.; McCullough, R. L. Composite Materials. In *Ullmann's Encyclopedia of Industrial Chemistry*; Wiley-VCH Verlag GmbH & Co. KGaA, 2000.
- [12] KICKELBICK, G. *Hybrid Materials: Synthesis, Characterization, and Applications*; John Wiley & Sons, 2007.
- [13] Fiedler, B.; Gojny, F. H.; Wichmann, M. H. G.; Nolte, M. C. M.; Schulte, K. Fundamental aspects of nano-reinforced composites. *Composites Science and Technology* 2006, 66 (16), 3115–3125.
- [14] Gao, F. Clay/polymer Composites: The Story. *Materials Today* 2004, 7 (11), 50–55.
- [15] Tomas Åström, B. Chapter 2 Thermoplastic sheet forming: materials and manufacturing techniques. In *Composite Materials Series*; Elsevier, 1997.

- [16] Meyers, M. A.; Chen, P.-Y.; Lin, A. Y.-M.; Seki, Y. Biological materials: Structure and mechanical properties. *Progress in Materials Science* 2008, 53 (1), 1–206.
- [17] John, M. J.; Thomas, S. Biofibres and biocomposites. *Carbohydrate Polymers* 2008, 71 (3), 343–364.
- [18] Ramakrishna, S.; Mayer, J.; Wintermantel, E.; Leong, K. W. Biomedical applications of polymer-composite materials: a review. *Composites Science and Technology* 2001, 61 (9), 1189–1224.
- [19] Drummond, J. L. Degradation, fatigue and failure of resin dental composite materials. *Journal of Dental Research* 2008, 87 (8), 710–719.
- [20] Mano, J. F.; Sousa, R. A.; Boesel, L. F.; Neves, N. M.; Reis, R. L. Bioinert, biodegradable and injectable polymeric matrix composites for hard tissue replacement: state of the art and recent developments. *Composites Science and Technology* 2004, 64 (6), 789–817.
- [21] <https://consensus.nih.gov/1982/1982Biomaterials034html.htm> (last visit Feb 16, 2016)
- [22] Vert, M.; Doi, Y.; Hellwich, K.-H.; Hess, M.; Hodge, P.; Kubisa, P.; Rinaudo, M.; Schué, F. Terminology for biorelated polymers and applications (IUPAC Recommendations 2012). *Pure and Applied Chemistry* 2012, 84 (2), 377–410.
- [23] Williams, D. F. On the mechanisms of biocompatibility. *Biomaterials* 2008, 29 (20), 2941–2953.
- [24] Shoichet, M. S. Polymer scaffolds for biomaterials applications. *Macromolecules* 2010, 43 (2), 581–591.
- [25] Anderson, J. M.; Rodriguez, A.; Chang, D. T. Foreign body reaction to biomaterials. *Seminars in Immunology* 2008, 20 (2), 86–100.
- [26] Chen, H.; Yuan, L.; Song, W.; Wu, Z.; Li, D. Biocompatible polymer materials: Role of protein–surface interactions. *Progress in Polymer Science* 2008, 33 (11), 1059–1087.
- [27] Latour, R. A. Biomaterials: Protein–surface interactions. In *Encyclopedia of Biomaterials and Biomedical Engineering*; Taylor & Francis, 2013.
- [28] Gray, J. J. The interaction of proteins with solid surfaces. *Current Opinion in Structural Biology* 2004, 14 (1), 110–115.
- [29] Wei, Q.; Becherer, T.; Angioletti-Uberti, S.; Dzubiella, J.; Wischke, C.; Neffe, A. T.; Lendlein, A.; Ballauff, M.; Haag, R. Wechselwirkungen von Proteinen mit Polymerbeschichtungen und Biomaterialien. *Angewandte Chemie* 2014, 126 (31), 8138–8169.
- [30] Szleifer, I. Protein adsorption on surfaces with grafted polymers: A theoretical approach. *Biophysical Journal* 1997, 72, 595–612.
- [31] Boateng, J. S.; Matthews, K. H.; Stevens, H. N. E.; Eccleston, G. M. Wound healing dressings and drug delivery systems: a review. *Journal of Pharmaceutical Sciences* 2008, 97 (8), 2892–2923.



- [32] <http://chinamedevice.com/Suppliers/7072/ChitosanWoundDressing-467249.html> (last visit Feb 26, 2016)
- [33] [http://jsjl.en.alibaba.com/product/512761138-802136894/Comentless\\_Stem\\_Total\\_Hip\\_Prothesis\\_Plastic\\_Cap\\_orthopaedic\\_implant\\_.html](http://jsjl.en.alibaba.com/product/512761138-802136894/Comentless_Stem_Total_Hip_Prothesis_Plastic_Cap_orthopaedic_implant_.html) (last visit Feb 26, 2016)
- [34] Alobeid, A.; Hasan, M.; Al-Suleiman, M.; El-Bialy, T. Mechanical properties of cobalt-chromium wires compared to stainless steel and  $\beta$ -titanium wires. *Journal of Orthodontic Science* 2014, 3 (4), 137–141.
- [35] Goodman, S. B.; Yao, Z.; Keeney, M.; Yang, F. The future of biologic coatings for orthopaedic implants. *Biomaterials* 2013, 34 (13), 3174–3183.
- [36] Zhang, B. G. X.; Myers, D. E.; Wallace, G. G.; Brandt, M.; Choong, P. F. M. Bioactive coatings for orthopaedic implants-recent trends in development of implant coatings. *International Journal of Molecular Science* 2014, 15 (7), 11878–11921.
- [37] Alves, N. M.; Mano, J. F. Chitosan derivatives obtained by chemical modifications for biomedical and environmental applications. *International Journal of Biological Macromolecules* 2008, 43 (5), 401–414.
- [38] Zargar, V.; Asghari, M.; Dashti, A. A review on chitin and chitosan polymers: structure, chemistry, solubility, derivatives, and applications. *ChemBioEng Reviews* 2015, 2 (3), 204–226.
- [39] Dutta, P. K. *Chitin and Chitosan for Regenerative Medicine*; Springer, 2015.
- [40] Aranaz, I.; Mengibar, M.; Harris, R.; Panos, I.; Miralles, B.; Acosta, N.; Galed, G.; Heras, A. Functional characterization of chitin and chitosan. *Current Chemical Biology* 2009, 3 (2), 203–230.
- [41] Prashanth, K. V. H.; Tharanathan, R. N. Chitin/chitosan: modifications and their unlimited application potential— an overview. *Trends in Food Science & Technology* 2007, 18 (3), 117–131.
- [42] Rinaudo, M. Chitin and chitosan: Properties and applications. *Progress in Polymer Science* 2006, 31 (7), 603–632.
- [43] da Silva, R. M. P.; Mano, J. F.; Reis, R. L. Straightforward determination of the degree of N-acetylation of chitosan by means of first-derivative UV spectrophotometry. *Macromolecular Chemistry and Physics* 2008, 209 (14), 1463–1472.
- [44] Kumar, M. N. V. R. A review of chitin and chitosan applications. *Reactive and Functional Polymers* 2000, 46 (1), 1–27.
- [45] Dumitriu, S. *Polymeric Biomaterials*; CRC Press, 2001.
- [46] Varma, A. J.; Deshpande, S. V.; Kennedy, J. F. Metal complexation by chitosan and its derivatives: a review. *Carbohydrate Polymers* 2004, 55 (1), 77–93.
- [47] Guibal, E. Interactions of metal ions with chitosan-based sorbents: a review. *Separation and Purification Technology* 2004, 38 (1), 43–74.

- [48] Berger, J.; Reist, M.; Mayer, J. M.; Felt, O.; Peppas, N. A.; Gurny, R. Structure and interactions in covalently and ionically crosslinked chitosan hydrogels for biomedical applications. *European Journal of Pharmaceutics and Biopharmaceutics* 2004, 57 (1), 19–34.
- [49] Gartner, C.; López, B. L.; Sierra, L.; Graf, R.; Spiess, H. W.; Gaborieau, M. Interplay between structure and dynamics in chitosan films investigated with solid-state NMR, dynamic mechanical analysis, and X-ray diffraction. *Biomacromolecules* 2011, 12 (4), 1380–1386.
- [50] Madeleine-Perdrillat, C.; Karbowski, T.; Raya, J.; Gougeon, R.; Bodart, P. R.; Debeaufort, F. Water-induced local ordering of chitosan polymer chains in thin layer films. *Carbohydrate Polymers* 2015, 118, 107–114.
- [51] Leceta, I.; Arana, P.; Guerrero, P.; de la Caba, K. Structure–moisture sorption relation in chitosan thin films. *Materials Letters* 2014, 128, 125–127.
- [52] Rosa, G. S.; Moraes, M. A.; Pinto, L. A. A. Moisture sorption properties of chitosan. *LWT - Food Science and Technology* 2010, 43 (3), 415–420.
- [53] Agrawal, A. M.; Manek, R. V.; Kolling, W. M.; Neau, S. H. Water distribution studies within microcrystalline cellulose and chitosan using differential scanning calorimetry and dynamic vapor sorption analysis. *Journal of Pharmaceutical Sciences* 2004, 93 (7), 1766–1779.
- [54] Wiles, J. I.; Vergano, P. J.; Barron, F. H.; Bunn, J. M.; Testin, R. F. Water vapor transmission rates and sorption behavior of chitosan films. *Journal of Food Science* 2000, 65 (7), 1175–1179.
- [55] González-Campos, J. B.; Prokhorov, E.; Luna-Bárceñas, G.; Fonseca-García, A.; Sanchez, I. C. Dielectric relaxations of chitosan: The effect of water on the  $\alpha$ -relaxation and the glass transition temperature. *Journal of Polymer Science Part B: Polymer Physics* 2009, 47 (22), 2259–2271.
- [56] Goy, R. C.; de Britto, D.; Assis, O. B. G. A review of the antimicrobial activity of chitosan. *Polímeros* 2009, 19 (3), 241–247.
- [57] Rabea, E. I.; Badawy, M. E.-T.; Stevens, C. V.; Smagghe, G.; Steurbaut, W. Chitosan as antimicrobial agent: applications and mode of action. *Biomacromolecules* 2003, 4 (6), 1457–1465.
- [58] Tan, M. L.; Shao, P.; Friedhuber, A. M.; van Moorst, M.; Elahy, M.; Indumathy, S.; Dunstan, D. E.; Wei, Y.; Dass, C. R. The potential role of free chitosan in bone trauma and bone cancer management. *Biomaterials* 2014, 35 (27), 7828–7838.
- [59] Di Martino, A.; Sittering, M.; Risbud, M. V. Chitosan: a versatile biopolymer for orthopaedic tissue-engineering. *Biomaterials* 2005, 26 (30), 5983–5990.
- [60] Sogias, I. A.; Williams, A. C.; Khutoryanskiy, V. V. Why Is chitosan mucoadhesive? *Biomacromolecules* 2008, 9 (7), 1837–1842.
- [61] The chemical modification of chitosan films for improved hemostatic and bioadhesive properties.; ProQuest, 2007.

- [62] Sonaje, K.; Chuang, E.-Y.; Lin, K.-J.; Yen, T.-C.; Su, F.-Y.; Tseng, M. T.; Sung, H.-W. Opening of epithelial tight junctions and enhancement of paracellular permeation by chitosan: microscopic, ultrastructural, and computed-tomographic observations. *Molecular Pharmacology* 2012, 9 (5), 1271–1279.
- [63] El Hadrami, A.; Adam, L. R.; El Hadrami, I.; Daayf, F. Chitosan in plant protection. *Marine Drugs* 2010, 8 (4), 968–987.
- [64] El-Sawy, N. M.; Abd El-Rehim, H. A.; Elbarbary, A. M.; Hegazy, E.-S. A. Radiation-induced degradation of chitosan for possible use as a growth promoter in agricultural purposes. *Carbohydrate Polymers* 2010, 79 (3), 555–562.
- [65] Navard, P. *The European Polysaccharide Network of Excellence (EPNOE): Research Initiatives and Results*; Springer Science & Business Media, 2012.
- [66] No, H. K.; Meyers, S. P.; Prinyawiwatkul, W.; Xu, Z. Applications of chitosan for improvement of quality and shelf life of foods: a review. *Journal of Food Science* 2007, 72 (5), R87–R100.
- [67] Gades, M. D.; Stern, J. S. Chitosan supplementation does not affect fat absorption in healthy males fed a high-fat diet, a pilot study. *International Journal of Obesity and Related Metabolic Disorders* 2002, 26 (1), 119–122.
- [68] Jull, A. B.; Ni Mhurchu, C.; Bennett, D. A.; Dunshea-Mooij, C. A.; Rodgers, A. Chitosan for overweight or obesity. *Cochrane Database of Systematic Reviews* 2008, Issue 3, CD003892.
- [69] Zeng, D.; Wu, J.; Kennedy, J. F. Application of a chitosan flocculant to water treatment. *Carbohydrate Polymers* 2008, 71 (1), 135–139.
- [70] Dai, T.; Tanaka, M.; Huang, Y.-Y.; Hamblin, M. R. Chitosan preparations for wounds and burns: antimicrobial and wound-healing effects. *Expert Review of Anti-infective Therapy* 2011, 9 (7), 857–879.
- [71] Khor, E.; Lim, L. Y. Implantable applications of chitin and chitosan. *Biomaterials* 2003, 24 (13), 2339–2349.
- [72] Bhattarai, N.; Gunn, J.; Zhang, M. Chitosan-based hydrogels for controlled, localized drug delivery. *Advanced Drug Delivery Reviews* 2010, 62 (1), 83–99.
- [73] Hench, L. L.; West, J. K. The sol-gel process. *Chemical Reviews* 1990, 90 (1), 33–72.
- [74] Petoral Jr, R. M.; Yazdi, G. R.; Spetz, A. L.; Yakimova, R.; Uvdal, K. Organosilane-functionalized wide band gap semiconductor surfaces. *Applied Physics Letters* 2007, 90 (22), 223904.
- [75] Acres, R. G.; Ellis, A. V.; Alvino, J.; Lenahan, C. E.; Khodakov, D. A.; Metha, G. F.; Andersson, G. G. Molecular structure of 3-aminopropyltriethoxysilane layers formed on silanol-terminated silicon surfaces. *The Journal of Physical Chemistry C* 2012, 116 (10), 6289–6297.
- [76] Schubert, U.; Huesing, N.; Lorenz, A. Hybrid inorganic-organic materials by sol-gel processing of organofunctional metal alkoxides. *Chemistry of Materials* 1995, 7 (11), 2010–2027.

- [77] Sakka, S. Handbook of sol-gel science and technology. 1. Sol-gel processing; Springer Science & Business Media, 2005.
- [78] Shchipunov, Y. A.; Karpenko, T. Y. Hybrid polysaccharide-silica nanocomposites prepared by the sol-gel technique. *Langmuir* 2004, 20 (10), 3882–3887.
- [79] Silva, S. S.; Ferreira, R. A. S.; Fu, L.; Carlos, L. D.; Mano, J. F.; Reis, R. L.; Rocha, J. Functional nanostructured chitosan–siloxane hybrids. *Journal of Materials Chemistry* 2005, 15 (35-36), 3952–3961.
- [80] Liu, Y.-L.; Su, Y.-H.; Lai, J.-Y. In situ crosslinking of chitosan and formation of chitosan–silica hybrid membranes with using  $\gamma$ -glycidoxypropyltrimethoxysilane as a crosslinking agent. *Polymer* 2004, 45 (20), 6831–6837.
- [81] Fuentes, S.; Retuert, P. J.; Ubilla, A.; Fernandez, J.; Gonzalez, G. Relationship between composition and structure in chitosan-based hybrid films. *Biomacromolecules* 2000, 1 (2), 239–243.
- [82] Chen, J. H.; Liu, Q. L.; Zhang, X. H.; Zhang, Q. G. Pervaporation and characterization of chitosan membranes cross-linked by 3-aminopropyltriethoxysilane. *Journal of Membrane Science* 2007, 292 (1–2), 125–132.
- [83] Yan, E.; Ding, Y.; Chen, C.; Li, R.; Hu, Y.; Jiang, X. Polymer / silica hybrid hollow nanospheres with pH-sensitive drug release in physiological and intracellular environments. *Chemical Communications* 2009, 19, 2718–2720.
- [84] Molvinger, K.; Quignard, F.; Brunel, D.; Boissière, M.; Devoisselle, J.-M. Porous chitosan-silica hybrid microspheres as a potential catalyst. *Chemistry of Materials* 2004, 16 (17), 3367–3372.
- [85] da Costa Neto, B. P.; da Mata, A. L. M. L.; Lopes, M. V.; Rossi-Bergmann, B.; Ré, M. I. Preparation and evaluation of chitosan–hydrophobic silica composite microspheres: Role of hydrophobic silica in modifying their properties. *Powder Technology* 2014, 255, 109–119.
- [86] O’Shea, D. C. *Diffraction optics: design, fabrication, and test*; SPIE Press, 2004.
- [87] Green, R. J.; Frazier, R. A.; Shakesheff, K. M.; Davies, M. C.; Roberts, C. J.; Tendler, S. J. Surface plasmon resonance analysis of dynamic biological interactions with biomaterials. *Biomaterials* 2000, 21 (18), 1823–1835.
- [88] <http://www.kla-tencor.com/surface-profilometry-and-metrology.html> (last visit Feb 26, 2016)
- [89] Bowen, W. R.; Hilal, N. *Atomic Force Microscopy in Process Engineering: An Introduction to AFM for Improved Processes and Products*; Butterworth-Heinemann, 2009.
- [90] Haugstad, G. *Atomic Force Microscopy: Understanding Basic Modes and Advanced Applications*; John Wiley & Sons, 2012.
- [91] Gstraunthaler, G.; Lindl, T. *Zell- und Gewebekultur*; Springer, 2013.

- [92] Fotakis, G.; Timbrell, J. A. In vitro cytotoxicity assays: Comparison of LDH, neutral red, MTT and protein assay in hepatoma cell lines following exposure to cadmium chloride. *Toxicology Letters* 2006, 160 (2), 171–177.
- [93] Berridge, M. V.; Herst, P. M.; Tan, A. S. Tetrazolium dyes as tools in cell biology: new insights into their cellular reduction. *Biotechnology Annual Review* 2005; 11, pp 127–152.
- [94] Zankel, A.; Poelt, P.; Gahleitner, M.; Ingolic, E.; Grein, C. Tensile tests of polymers at low temperatures in the environmental scanning electron microscope: an improved cooling platform. *Scanning* 2007, 29 (6), 261–269.
- [95] Menard, K. P. *Dynamic mechanical analysis: a practical introduction*; CRC Press, 2008.
- [96] <http://ictm.tugraz.at> (last visit Feb 16, 2016)
- [97] Williams, E. H.; Davydov, A. V.; Motayed, A.; Sundaresan, S. G.; Bocchini, P.; Richter, L. J.; Stan, G.; Steffens, K.; Zangmeister, R.; Schreifels, J. A.; et al. Immobilization of streptavidin on 4H–SiC for biosensor development. *Applied Surface Science* 2012, 258 (16), 6056–6063.
- [98] Stewart, A.; Schlosser, B.; Douglas, E. P. Surface modification of cured cement pastes by silane coupling agents. *ACS Applied Materials & Interfaces* 2013, 5 (4), 1218–1225.
- [99] Enescu, D.; Hamciuc, V.; Ardeleanu, R.; Cristea, M.; Ioanid, A.; Harabagiu, V.; Simionescu, B. C. Polydimethylsiloxane modified chitosan. Part III: Preparation and characterization of hybrid membranes. *Carbohydrate Polymers* 2009, 76 (2), 268–278.
- [100] Chu, E.; Sidorenko, A. Surface reconstruction by a "grafting through" approach: polyacrylamide grafted onto chitosan film. *Langmuir* 2013, 29 (40), 12585–12592.
- [101] Rutnakornpituk, M.; Ngamdee, P.; Phinyocheep, P. reparation and properties of polydimethylsiloxane-modified chitosan. *Carbohydrate Polymers* 2006, 63 (2), 229–237.
- [102] Tsui, O. K. C.; Wang, Y. J.; Lee, F. K.; Lam, C.-H.; Yang, Z. Equilibrium pathway of spin-coated polymer films. *Macromolecules* 2008, 41 (4), 1465–1468.
- [103] Müller-Buschbaum, P. Influence of surface cleaning on dewetting of thin polystyrene films. *The European Physical Journal E* 2004, 12 (3), 443–448.
- [104] Puleo, D. A.; Bizios, R. *Biological interactions on materials surfaces: understanding and controlling protein, cell, and tissue responses*; Springer Science & Business Media, 2009.
- [105] Fibrinogen native protein | MyBioSource [http://www.mybiosource.com/prods/Native-Protein/Fibrinogen/datasheet.php?products\\_id=318356](http://www.mybiosource.com/prods/Native-Protein/Fibrinogen/datasheet.php?products_id=318356) (accessed Feb 27, 2016).
- [106] <http://www.rcsb.org/pdb/explore.do?structureId=3V03> (last visit Feb 27, 2016)
- [107] <http://www.rcsb.org/pdb/explore.do?structureId=3ghg> (last visit Feb 27, 2016)

- [108] Ladam, G.; Gergely, C.; Senger, B.; Decher, G.; Voegel, J.-C.; Schaaf, P.; Cuisinier, F. J. G. Protein interactions with polyelectrolyte multilayers: interactions between human serum albumin and polystyrene sulfonate/polyallylamine multilayers. *Biomacromolecules* 2000, 1 (4), 674–687.
- [109] Wang, X.; Herting, G.; Odnevall Wallinder, I.; Blomberg, E. Adsorption of bovine serum albumin on silver surfaces enhances the release of silver at pH neutral conditions. *Physical Chemistry Chemical Physics* 2015, 17 (28), 18524–18534.
- [110] Hoven, V. P.; Tangpasuthadol, V.; Angkitpaiboon, Y.; Vallapa, N.; Kiatkamjornwong, S. Surface-charged chitosan: Preparation and protein adsorption. *Carbohydrate Polymers* 2007, 68 (1), 44–53.
- [111] Benesch, J.; Tengvall, P. Blood protein adsorption onto chitosan. *Biomaterials* 2002, 23 (12), 2561–2568.
- [112] Ostuni, E.; Grzybowski, B. A.; Mrksich, M.; Roberts, C. S.; Whitesides, G. M. Adsorption of proteins to hydrophobic sites on mixed self-assembled monolayers. *Langmuir* 2003, 19 (5), 1861–1872.
- [113] Mohan, T.; Niegelhell, K.; Zarth, C. S. P.; Kargl, R.; Köstler, S.; Ribitsch, V.; Heinze, T.; Spirk, S.; Stana-Kleinschek, K. Triggering protein adsorption on tailored cationic cellulose surfaces. *Biomacromolecules* 2014, 15 (11), 3931–3941.
- [114] Liu, W. F.; Ma, M.; Bratlie, K. M.; Dang, T. T.; Langer, R.; Anderson, D. G. Real-time in vivo detection of biomaterial-induced reactive oxygen species. *Biomaterials* 2011, 32 (7), 1796–1801.
- [115] Chatelet, C.; Damour, O.; Domard, A. Influence of the degree of acetylation on some biological properties of chitosan films. *Biomaterials* 2001, 22 (3), 261–268.
- [116] Campos, M. G. N.; Mei, L. H. I.; Jr, S.; Rodrigues, A.; Campos, M. G. N.; Mei, L. H. I.; Jr, S.; Rodrigues, A. Sorbitol-plasticized and neutralized chitosan membranes as skin substitutes. *Materials Research* 2015, 18 (4), 781–790.
- [117] Elsaesser, A.; Howard, C. V. Toxicology of nanoparticles. *Advanced Drug Delivery Reviews* 2012, 64 (2), 129–137.
- [118] Martin, K. R. The chemistry of silica and its potential health benefits. *The Journal of Nutrition Health and Aging* 2007, 11 (2), 94–97.
- [119] Gryshchuk, V.; Galagan, N. Silica nanoparticles effects on blood coagulation proteins and platelets. *Biochemistry Research International* 2016, e2959414.
- [120] Hallab, N. J.; Bundy, K. J.; O'Connor, K.; Moses, R. L.; Jacobs, J. J. Evaluation of metallic and polymeric biomaterial surface energy and surface roughness characteristics for directed cell adhesion. *Tissue Engineering* 2001, 7 (1), 55–71.
- [121] Fakhry, A.; Schneider, G. B.; Zaharias, R.; Senel, S. Chitosan supports the initial attachment and spreading of osteoblasts preferentially over fibroblasts. *Biomaterials* 2004, 25 (11), 2075–2079.

- [122] Hamilton, V.; Yuan, Y.; Rigney, D. A.; Puckett, A. D.; Ong, J. L.; Yang, Y.; Elder, S. H.; Bumgardner, J. D. Characterization of chitosan films and effects on fibroblast cell attachment and proliferation. *Journal of Materials Science: Materials in Medicine* 2006, 17 (12), 1373–1381.
- [123] Mieszawska, A. J.; Fourligas, N.; Georgakoudi, I.; Ouhib, N. M.; Belton, D. J.; Perry, C. C.; Kaplan, D. L. Osteoinductive silk-silica composite biomaterials for bone regeneration. *Biomaterials* 2010, 31 (34), 8902–8910.
- [124] Lee, E.-J.; Shin, D.-S.; Kim, H.-E.; Kim, H.-W.; Koh, Y.-H.; Jang, J.-H. Membrane of hybrid chitosan-silica xerogel for guided bone regeneration. *Biomaterials* 2009, 30 (5), 743–750.
- [125] Kim, K. M.; Son, J. H.; Kim, S.-K.; Weller, C. L.; Hanna, M. A. Properties of chitosan films as a function of pH and solvent type. *Journal of Food Science* 2006, 71 (3), E119–E124.
- [126] Huang, J.-W.; Wen, Y.-L.; Kang, C.-C.; Yeh, M.-Y. Preparation of polyimide-silica nanocomposites from nanoscale colloidal silica. *Polymer Journal* 2007, 39 (7), 654–658.
- [127] Yeh, J.-T.; Chen, C.-L.; Huang, K.-S. Synthesis and properties of chitosan/SiO<sub>2</sub> hybrid materials. *Materials Letters* 2007, 61 (6), 1292–1295.
- [128] Ma, B.; Qin, A.; Li, X.; Zhao, X.; He, C. Structure and properties of chitin whisker reinforced chitosan membranes. *International Journal of Biological Macromolecules* 2014, 64, 341–346.
- [129] Sriupayo, J.; Supaphol, P.; Blackwell, J.; Rujiravanit, R. Preparation and characterization of  $\alpha$ -chitin whisker-reinforced chitosan nanocomposite films with or without heat treatment. *Carbohydrate Polymers* 2005, 62 (2), 130–136.
- [130] Ifuku, S.; Ikuta, A.; Egusa, M.; Kaminaka, H.; Izawa, H.; Morimoto, M.; Saimoto, H. Preparation of high-strength transparent chitosan film reinforced with surface-deacetylated chitin nanofibers. *Carbohydrate Polymers* 2013, 98 (1), 1198–1202.
- [131] Mushi, N. E.; Utsel, S.; Berglund, L. A. Nanostructured biocomposite films of high toughness based on native chitin nanofibers and chitosan. *Frontiers in chemistry* 2014, 2, 99.
- [132] Park, S. y.; Marsh, K. s.; Rhim, J. w. Characteristics of different molecular weight chitosan films affected by the type of organic solvents. *Journal of Food Science* 2002, 67 (1), 194–197.
- [133] Wenling, C.; Duohui, J.; Jiamou, L.; Yandao, G.; Nanming, Z.; Xiufang, Z. Effects of the degree of deacetylation on the physicochemical properties and Schwann cell affinity of chitosan films. *Journal of Biomaterials Applications* 2005, 20 (2), 157–177.
- [134] Thakhiew, W.; Devahastin, S.; Soponronnarit, S. Physical and mechanical properties of chitosan films as affected by drying methods and addition of antimicrobial agent. *Journal of Food Engineering* 2013, 119 (1), 140–149.
- [135] Khan, A.; Khan, R. A.; Salmieri, S.; Le Tien, C.; Riedl, B.; Bouchard, J.; Chauve, G.; Tan, V.; Kamal, M. R.; Lacroix, M. Mechanical and barrier properties of nanocrystalline cellulose reinforced chitosan based nanocomposite films. *Carbohydrate Polymers* 2012, 90 (4), 1601–1608.

- [136] Suyatma, N. E.; Tighzert, L.; Copinet, A.; Coma, V. Effects of hydrophilic plasticizers on mechanical, thermal, and surface properties of chitosan films. *Journal of Agricultural and Food Chemistry* 2005, 53 (10), 3950–3957.
- [137] Correlo, V. M.; Boesel, L. F.; Bhattacharya, M.; Mano, J. F.; Neves, N. M.; Reis, R. L. Hydroxyapatite reinforced chitosan and polyester blends for biomedical applications. *Macromolecular Materials and Engineering* 2005, 290 (12), 1157–1165.
- [138] plastic | chemical compound <http://www.britannica.com/science/plastic> (accessed Mar 6, 2016).
- [139] Andrae P., R. D.; Lemus M., R.; Pérez C., C. E. Models of sorption isotherms for food: uses and limitations. *Vitae* 2011, 18 (3), 325–334.
- [140] Al-Sagheer, F.; Muslim, S. Thermal and mechanical properties of chitosan/SiO<sub>2</sub> hybrid composites. *Journal of Nanomaterials* 2010, e490679.



# Appendix A

## Protocols

### Basic protocol for cell trypsinization and seeding

1. Flasks (25 cm<sup>2</sup>) with cells forming monolayer.
2. Discard medium and wash cells with 2 mL trypsin + EDTA.
3. Add 1 mL trypsin + EDTA and incubate at 37 °C till the cells are detached (check with light microscope).
4. Add 9 mL of fresh culture medium into the flask, resuspend cells and transfer into sterile centrifuge tube.
5. Centrifuge (800 rpm, 5 min, 22 °C) and pour away medium.
6. Add 2-8 mL of fresh medium with 5% serum (FBS) and resuspend cells.
7. Count the cells.
8. Put back 1/5 of the cells for new cell culture.

### Mitochondrial activity (MTT assay)

1. Dump off the medium into a sink.
2. Wash the cell monolayer once with PBS.
3. Add into each well 200 µL of DMEM advance without phenol red and antibiotics, supplemented with L-glutamine only.
4. Add into each well 20 µL of MTT solution (5 mg/mL in 1 x PBS).  
MTT [= (3-(4,-dimethylthiazolyl)-2, 5-diphenyltetrazolium bromide)]: yellow solution  
stock: 100 mg/10 mL of 1 x PBS in fridge
5. Place plate on shaking table for 5 minutes to mix MTT into the medium.
6. Incubate at 37 °C and 5% CO<sub>2</sub> for 1-5 hours.
7. Dump off the medium and dry on paper towels.
8. Add 10 µL of 0.04% HCl in isopropanol into each well to solubalize formazin (MTT metabolic product).
9. Place the plate on a shaking table for 5 minutes to let it mix well.
10. Incubate for 15-20 minutes.
11. Measure absorbance at 570 nm.

### Cell Viability (Crystal violet assay)

1. Dump off the medium from the plate into a sink and tap it on paper towel.
2. Add 100  $\mu$ L of 0.1% crystal violet into each well with monolayer.
3. Incubate for 2 minutes at room temperature and wash with tap water.
4. Dry on paper towels (over night or at 55 °C).
5. Add 100  $\mu$ L of 10% acetic acid into each well.
6. Place the plate on a shaking table for an hour to let it mix well.
7. Measure absorbance at 595 nm.

Preparation of 0.1% crystal violet: dissolve crystal violet (powder) in 20% ethanol to get 1% final solution. Final solution contains 0.1% crystal violet and 2% ethanol.

### Live/Dead Staining

1. Add 10  $\mu$ L solution A (calcein-am) and 5  $\mu$ L solution B (propidium iodide) to 5 mL PBS to prepare assay solution.
2. Wash cells with PBS.
3. Prepare a cell suspension with PBS in which the cell density is  $1 \times 10^5$  to  $1 \times 10^6$ .
4. Add 100  $\mu$ L of assay solution and incubate cells with the mixture at 37 °C for 15 min.
5. Detect fluorescence using 490 nm excitation for simultaneous monitoring of viable and dead cells. With 545 nm excitation only dead cells are observed.

# Appendix B

## Figures

### B.1 Atomic Force Microscopy Images

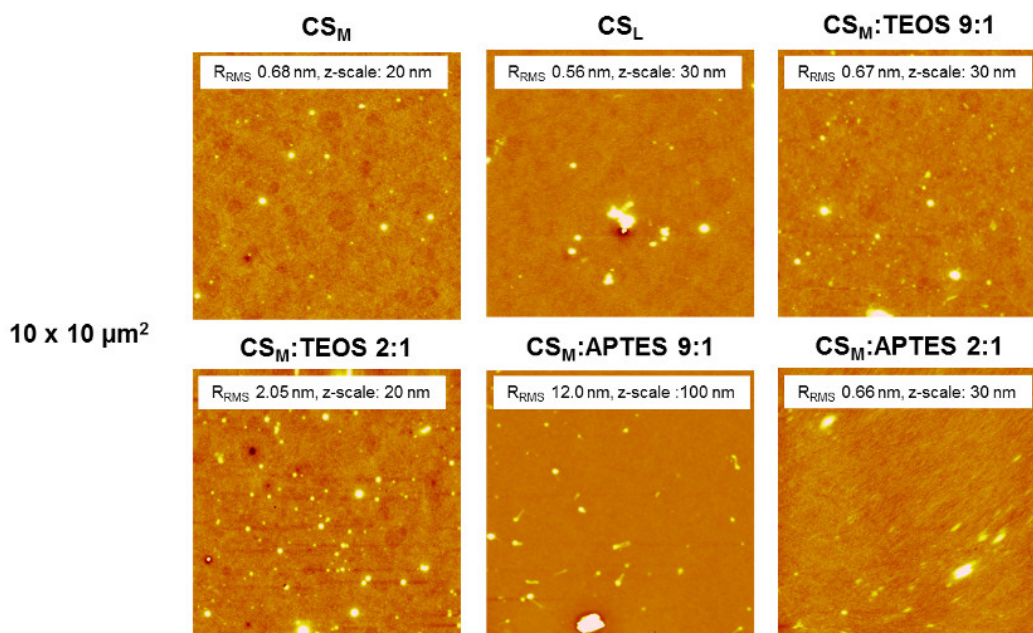


FIGURE B.1:  $10 \times 10 \mu m^2$  AFM images of chitosan and selected hybrid thin films on silicon.  $2 \times 2 \mu m^2$  AFM images of the same materials are displayed in Figure 5.9.

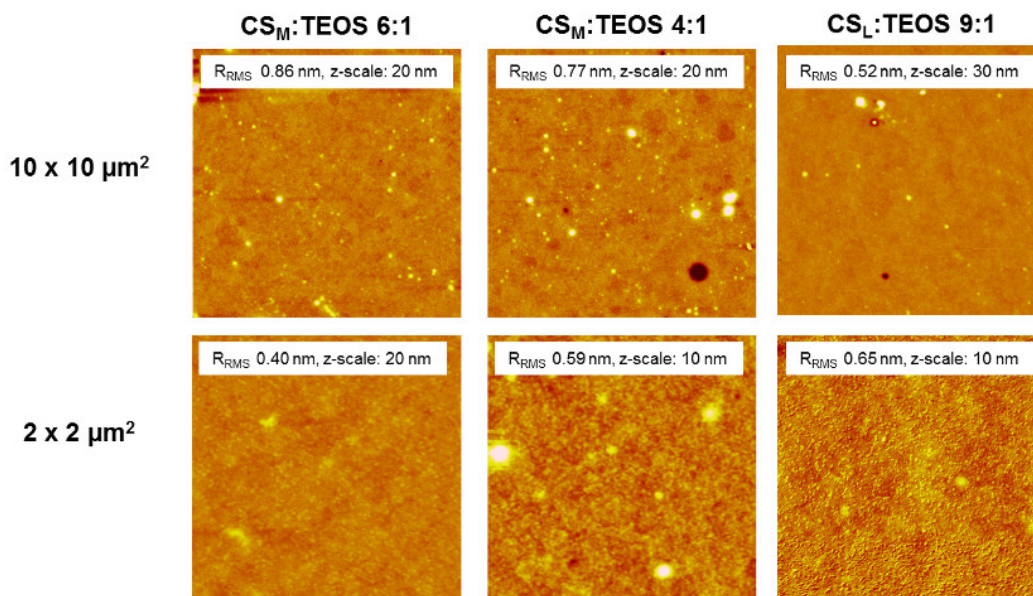


FIGURE B.2:  $10 \times 10 \mu m^2$  and  $2 \times 2 \mu m^2$  images of chitosan hybrid thin films containing particles from sol-gel processing of TEOS.

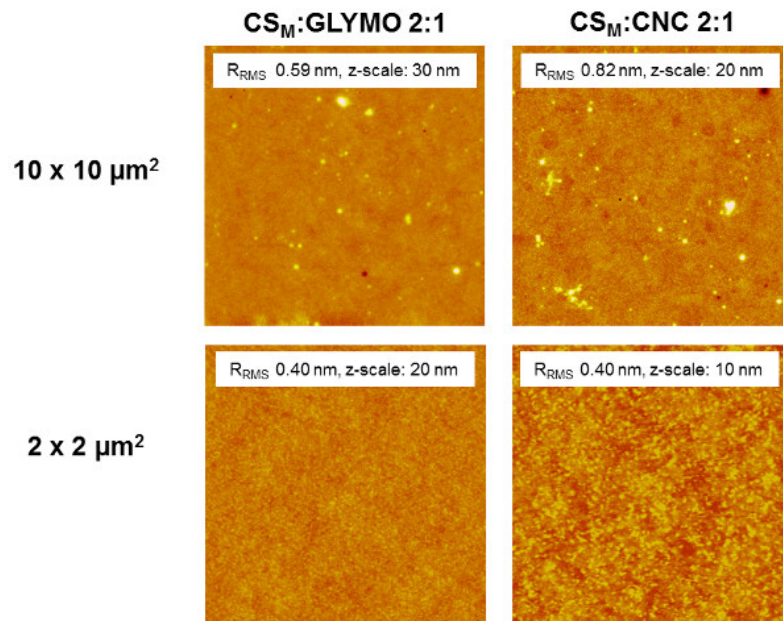


FIGURE B.3:  $10 \times 10 \mu\text{m}^2$  and  $2 \times 2 \mu\text{m}^2$  images of chitosan hybrid thin films containing particles from sol-gel processing of GLYMO as well as cellulose nanocrystals.

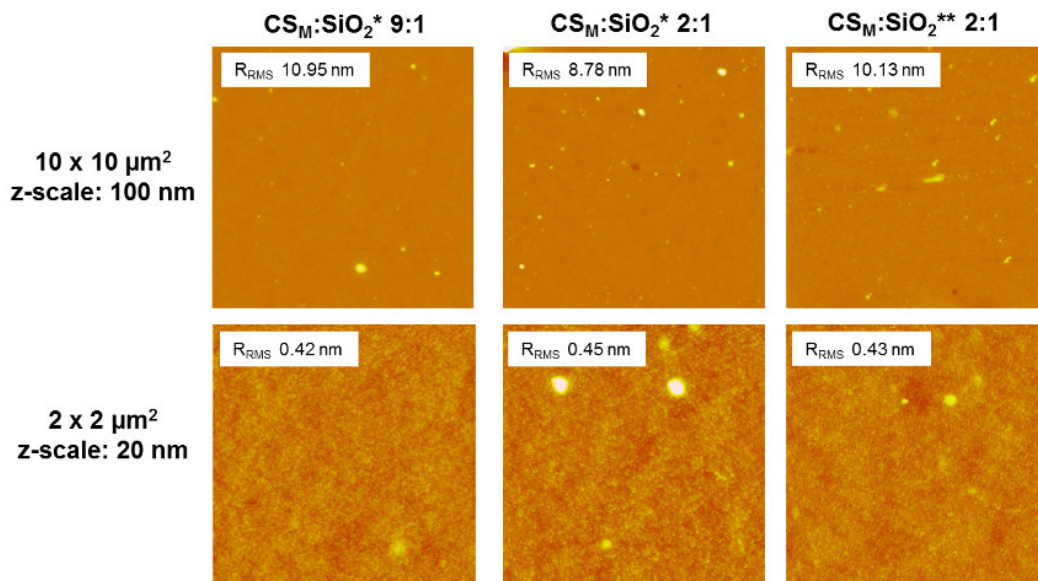


FIGURE B.4:  $10 \times 10 \mu\text{m}^2$  and  $2 \times 2 \mu\text{m}^2$  images of chitosan hybrid thin films containing silicon dioxide nanoparticles with an average BET diameter of 10 nm ( $\text{SiO}_2^*$ ) and 15 nm ( $\text{SiO}_2^{**}$ ).

## B.2 Wafer size for cell attachment tests

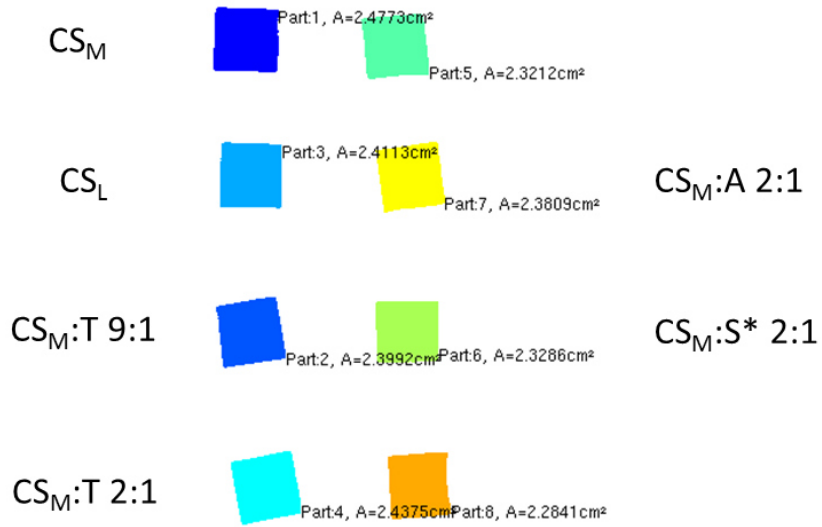


FIGURE B.5: Size of the coated wafers which have been used for fibroblast attachment tests as determined by surface integration using a MatLab script. Coloured areas correspond to different samples.

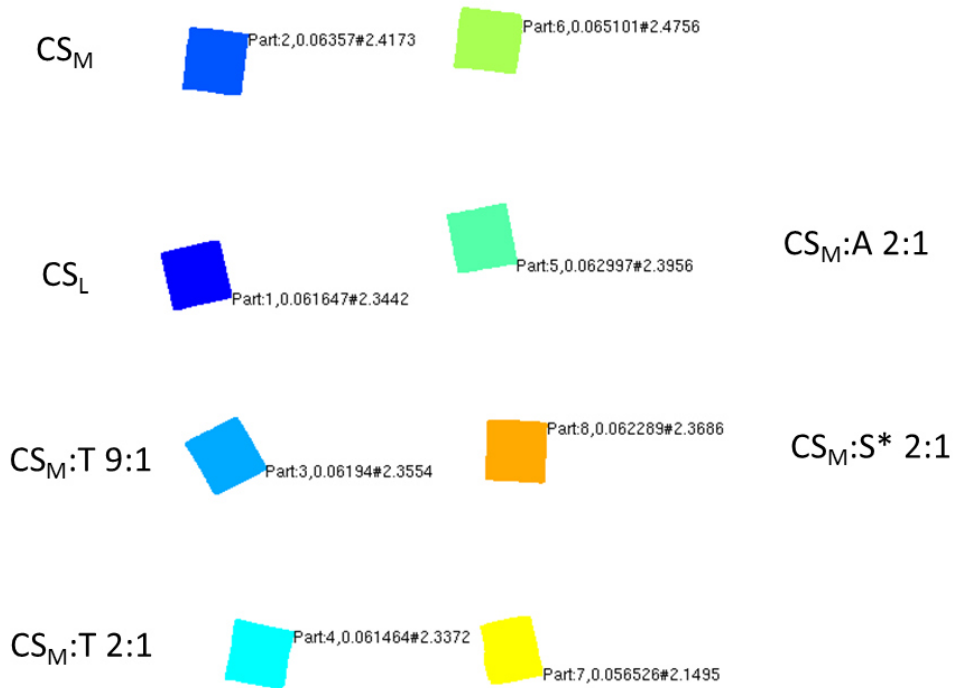


FIGURE B.6: Size of the coated wafers which have been used for osteoblast attachment tests as determined by surface integration using a MatLab script. Coloured areas correspond to different samples.



# Appendix C

## Tables

### C.1 Layer thickness

TABLE C.1: Layer thickness of thin films from neat chitosan.

Material	Thickness [nm]			Mean value $\pm$ sd
CS <sub>M</sub>	94	99	96	96 $\pm$ 2
CS <sub>M</sub>	100	99	104	101 $\pm$ 2

TABLE C.2: Layer thickness of chitosan hybrid thin films containing particles from TEOS sol-gel processing.

Material	Thickness [nm]			Mean value $\pm$ sd
CS <sub>M</sub> :T 9:1	95	102	101	99 $\pm$ 3
CS <sub>M</sub> :T 6:1	84	87	88	86 $\pm$ 1
CS <sub>M</sub> :T 4:1	79	77	79	78 $\pm$ 1
CS <sub>M</sub> :T 2:1	68	66	65	66 $\pm$ 1
CS <sub>L</sub> :T 9:1	89	89	90	89 $\pm$ 1
CS <sub>L</sub> :T 6:1	85	87	88	87 $\pm$ 1
CS <sub>L</sub> :T 4:1	77	78	76	77 $\pm$ 1
CS <sub>L</sub> :T 2:1	64	62	65	63 $\pm$ 1

TABLE C.3: Layer thickness of chitosan hybrid thin films containing particles from APTES sol-gel processing.

Material	Thickness [nm]			Mean value $\pm$ sd
CS <sub>M</sub> :A 9:1	92	92	91	92 $\pm$ 1
CS <sub>M</sub> :A 6:1	92	95	92	93 $\pm$ 1
CS <sub>M</sub> :A 4:1	86	93	95	91 $\pm$ 4
CS <sub>M</sub> :A 2:1	71	72	75	72 $\pm$ 2
CS <sub>L</sub> :A 9:1	88	91	95	91 $\pm$ 3
CS <sub>L</sub> :A 6:1	84	83	82	83 $\pm$ 1
CS <sub>L</sub> :A 4:1	82	83	81	82 $\pm$ 1
CS <sub>L</sub> :A 2:1	68	73	69	70 $\pm$ 2

TABLE C.4: Layer thickness of chitosan hybrid thin films containing particles from GLYMO sol-gel processing.

Material	Thickness [nm]			Mean value $\pm$ sd
CS <sub>M</sub> :G 9:1	99	106	112	106 $\pm$ 5
CS <sub>M</sub> :G 6:1	95	104	99	99 $\pm$ 3
CS <sub>M</sub> :G 4:1	96	96	97	96 $\pm$ 1
CS <sub>M</sub> :G 2:1	81	83	82	82 $\pm$ 1
CS <sub>L</sub> :G 9:1	100	107	99	102 $\pm$ 3
CS <sub>L</sub> :G 6:1	97	100	94	97 $\pm$ 3
CS <sub>L</sub> :G 4:1	87	90	96	91 $\pm$ 3
CS <sub>L</sub> :G 2:1	81	80	80	81 $\pm$ 1

TABLE C.5: Layer thickness of chitosan hybrid thin films containing silicon dioxide nanoparticles with an average BET diameter of 10 nm (S\*).

Material	Thickness [nm]			Mean value $\pm$ sd
CS <sub>M</sub> :S* 9:1	87	85	85	86 $\pm$ 1
CS <sub>M</sub> :S* 6:1	76	85	77	79 $\pm$ 4
CS <sub>M</sub> :S* 4:1	75	69	75	73 $\pm$ 3
CS <sub>M</sub> :S* 2:1	53	55	58	55 $\pm$ 2
CS <sub>L</sub> :S* 9:1	92	95	96	94 $\pm$ 2
CS <sub>L</sub> :S* 6:1	96	96	92	95 $\pm$ 2
CS <sub>L</sub> :S* 4:1	75	84	73	77 $\pm$ 5
CS <sub>L</sub> :S* 2:1	62	61	66	63 $\pm$ 2

TABLE C.6: Layer thickness of chitosan hybrid thin films containing silicon dioxide nanoparticles with an average BET diameter of 15 nm (S\*\*).

Material	Thickness [nm]			Mean value $\pm$ sd
CS <sub>M</sub> :S** 9:1	88	91	91	90 $\pm$ 1
CS <sub>M</sub> :S** 6:1	82	83	83	83 $\pm$ 1
CS <sub>M</sub> :S** 4:1	79	82	74	78 $\pm$ 3
CS <sub>M</sub> :S** 2:1	58	67	65	63 $\pm$ 4
CS <sub>L</sub> :S** 9:1	97	101	99	99 $\pm$ 2
CS <sub>L</sub> :S** 6:1	94	91	88	91 $\pm$ 2
CS <sub>L</sub> :S** 4:1	80	79	83	81 $\pm$ 2
CS <sub>L</sub> :S** 2:1	63	64	62	63 $\pm$ 1

TABLE C.7: Layer thickness of chitosan hybrid thin films containing cellulose nanocrystals (CNCs).

Material	Thickness [nm]			Mean value $\pm$ sd
CS <sub>M</sub> :CNC 9:1	87	92	90	90 $\pm$ 2
CS <sub>M</sub> :CNC 6:1	87	90	90	89 $\pm$ 1
CS <sub>M</sub> :CNC 4:1	81	82	86	83 $\pm$ 2
CS <sub>M</sub> :CNC 2:1	67	61	59	62 $\pm$ 3
CS <sub>L</sub> :CNC 9:1	94	88	89	90 $\pm$ 2
CS <sub>L</sub> :CNC 6:1	89	91	80	87 $\pm$ 5
CS <sub>L</sub> :CNC 4:1	83	82	77	81 $\pm$ 3
CS <sub>L</sub> :CNC 2:1	63	66	65	65 $\pm$ 1



## C.2 Contact angle measurements

TABLE C.8: Static water contact angles on thin films from neat chitosan.

Material	Contact angle [°]						Mean value $\pm$ sd
CS <sub>M</sub>	51	48	50	46	41	43	47 $\pm$ 4
CS <sub>L</sub>	47	47	49	45	45	44	46 $\pm$ 2

TABLE C.9: Static water contact angles on chitosan hybrid thin films containing particles from TEOS sol-gel processing.

Material	Contact angle [°]						Mean value $\pm$ sd
CS <sub>M</sub> :T 9:1	38	37	38	45	43	44	41 $\pm$ 3
CS <sub>M</sub> :T 6:1	37	37	37	38	38	37	37 $\pm$ 1
CS <sub>M</sub> :T 4:1	34	34	35	42	39	43	38 $\pm$ 3
CS <sub>M</sub> :T 2:1	33	33	33	43	-	-	35 $\pm$ 5
CS <sub>L</sub> :T 9:1	44	43	44	46	46	46	45 $\pm$ 1
CS <sub>L</sub> :T 6:1	44	43	41	42	41	40	42 $\pm$ 1
CS <sub>L</sub> :T 4:1	40	40	41	41	40	41	40 $\pm$ 1
CS <sub>L</sub> :T 2:1	40	40	41	40	41	40	40 $\pm$ 1

TABLE C.10: Static water contact angles on chitosan hybrid thin films containing particles from APTES sol-gel processing.

Material	Contact angle [°]						Mean value $\pm$ sd
CS <sub>M</sub> :A 9:1	46	45	47	48	47	48	47 $\pm$ 1
CS <sub>M</sub> :A 6:1	45	47	47	49	48	48	47 $\pm$ 1
CS <sub>M</sub> :A 4:1	48	47	49	50	49	49	49 $\pm$ 1
CS <sub>M</sub> :A 2:1	60	58	56	51	53	55	55 $\pm$ 3
CS <sub>L</sub> :A 9:1	47	49	49	48	49	53	49 $\pm$ 2
CS <sub>L</sub> :A 6:1	55	49	51	55	54	52	53 $\pm$ 2
CS <sub>L</sub> :A 4:1	64	57	61	65	64	65	63 $\pm$ 3
CS <sub>L</sub> :A 2:1	66	61	65	68	67	67	66 $\pm$ 2

TABLE C.11: Static water contact angles on chitosan hybrid thin films containing particles from GLYMO sol-gel processing.

Material	Contact angle [°]						Mean value $\pm$ sd
CS <sub>M</sub> :G 9:1	39	39	37	38	38	38	38 $\pm$ 1
CS <sub>M</sub> :G 6:1	40	34	36	36	34	32	35 $\pm$ 2
CS <sub>M</sub> :G 4:1	36	37	40	39	39	40	38 $\pm$ 1
CS <sub>M</sub> :G 2:1	41	44	42	41	41	42	42 $\pm$ 1
CS <sub>L</sub> :G 9:1	70	66	62	67	64	64	66 $\pm$ 2
CS <sub>L</sub> :G 6:1	62	61	62	62	61	61	61 $\pm$ 1
CS <sub>L</sub> :G 4:1	65	64	63	61	62	61	62 $\pm$ 2
CS <sub>L</sub> :G 2:1	66	65	67	66	65	65	66 $\pm$ 1

TABLE C.12: Static water contact angles on chitosan hybrid thin films containing silicon dioxide nanoparticles with an average BET diameter of 10 nm (S\*).

Material	Contact angle [°]						Mean value $\pm$ sd
CS <sub>M</sub> :S* 9:1	42	43	43	42	40	39	42 $\pm$ 1
CS <sub>M</sub> :S* 6:1	42	42	41	41	39	39	41 $\pm$ 1
CS <sub>M</sub> :S* 4:1	39	39	39	38	38	37	38 $\pm$ 1
CS <sub>M</sub> :S* 2:1	42	40	39	-	-	-	40 $\pm$ 1
CS <sub>L</sub> :S* 9:1	43	43	43	46	43	43	44 $\pm$ 1
CS <sub>L</sub> :S* 6:1	43	42	43	41	41	39	41 $\pm$ 1
CS <sub>L</sub> :S* 4:1	41	41	41	40	40	39	40 $\pm$ 1
CS <sub>L</sub> :S* 2:1	39	37	39	39	39	37	38 $\pm$ 1

TABLE C.13: Static water contact angles on chitosan hybrid thin films containing silicon dioxide nanoparticles with an average BET diameter of 15 nm (S\*\*).

Material	Contact angle [°]						Mean value $\pm$ sd
CS <sub>M</sub> :S** 9:1	41	41	41	39	38	38	40 $\pm$ 1
CS <sub>M</sub> :S** 6:1	40	40	41	39	40	40	40 $\pm$ 1
CS <sub>M</sub> :S** 4:1	39	38	39	36	37	35	37 $\pm$ 2
CS <sub>M</sub> :S** 2:1	37	36	36	36	35	32	35 $\pm$ 1
CS <sub>L</sub> :S** 9:1	42	42	41	38	40	38	40 $\pm$ 2
CS <sub>L</sub> :S** 6:1	43	42	43	37	37	36	39 $\pm$ 3
CS <sub>L</sub> :S** 4:1	38	37	37	34	34	34	36 $\pm$ 2
CS <sub>L</sub> :S** 2:1	35	34	35	32	28	29	32 $\pm$ 3

TABLE C.14: Static water contact angles on chitosan hybrid thin films containing cellulose nanocrystals (CNCs).

Material	Contact angle [°]						Mean value $\pm$ sd
CS <sub>M</sub> :CNC 9:1	42	42	43	44	42	43	43 $\pm$ 1
CS <sub>M</sub> :CNC 6:1	42	42	39	43	42	41	42 $\pm$ 1
CS <sub>M</sub> :CNC 4:1	43	41	42	42	42	42	42 $\pm$ 1
CS <sub>M</sub> :CNC 2:1	45	48	48	46	45	44	46 $\pm$ 1
CS <sub>L</sub> :CNC 9:1	46	47	45	46	47	45	46 $\pm$ 1
CS <sub>L</sub> :CNC 6:1	47	46	46	50	49	48	48 $\pm$ 1
CS <sub>L</sub> :CNC 4:1	56	51	53	57	50	54	53 $\pm$ 3
CS <sub>L</sub> :CNC 2:1	46	43	40	44	45	44	44 $\pm$ 2

TABLE C.15: Static water contact angles on selected chitosan hybrid thin films five days after preparation.

Material	Contact angle [°]			Mean value
CS <sub>M</sub>	66	68	67	67 $\pm$ 1
CS <sub>L</sub>	67	66	67	67 $\pm$ 1
CS <sub>M</sub> :T 9:1	67	67	66	67 $\pm$ 1
CS <sub>M</sub> :T 2:1	67	67	66	67 $\pm$ 1
CS <sub>M</sub> :A 2:1	72	72	71	72 $\pm$ 1
CS <sub>M</sub> :S* 2:1	67	67	67	67 $\pm$ 1

TABLE C.16: Static water contact angles on chitosan hybrid thin films prepared from different dilutions with ethanol.

Material	Contact angle [°]						Mean value $\pm$ sd
CS <sub>M</sub> :EtOH 9:1	72	70	72	69	69	69	70 $\pm$ 1
CS <sub>M</sub> :EtOH 6:1	72	73	72	71	72	73	72 $\pm$ 1
CS <sub>M</sub> :EtOH 4:1	66	65	66	66	67	66	66 $\pm$ 1
CS <sub>M</sub> :EtOH 2:1	71	70	71	67	67	67	69 $\pm$ 2
CS <sub>L</sub> :EtOH 9:1	66	65	66	67	66	68	66 $\pm$ 1
CS <sub>L</sub> :EtOH 6:1	66	65	66	66	65	65	65 $\pm$ 1
CS <sub>L</sub> :EtOH 4:1	64	64	64	64	65	65	64 $\pm$ 1
CS <sub>L</sub> :EtOH 2:1	65	64	65	68	67	67	66 $\pm$ 1

### C.3 Surface Plasmon Resonance Spectroscopy measurements

TABLE C.17: SPR angular shifts and corresponding protein masses for the adsorption onto neat chitosan surfaces after rinsing with buffer.

Protein	Measurement	SPR angle [°]	Protein mass per area [mg m <sup>-2</sup> ]
BSA	1	0.0141	0.148
	2	0.0139	0.146
	3	0.0142	0.149
	<b>Mean value <math>\pm</math> sd</b>	0.0141 $\pm$ 0.0001	0.148 $\pm$ 0.001
Fibrinogen	1	0.0103	0.108
	2	0.0150	0.158
	3	0.0081	0.085
	<b>Mean value <math>\pm</math> sd</b>	0.0111 $\pm$ 0.0029	0.117 $\pm$ 0.030

TABLE C.18: SPR angular shifts and corresponding protein masses for the adsorption onto surfaces with the composition CS<sub>M</sub>:TEOS 9:1 after rinsing with buffer.

Protein	Measurement	SPR angle [°]	Protein mass per area [mg m <sup>-2</sup> ]
BSA	1	0.0010	0.011
	2	0.0005	0.005
	3	0.0010	0.011
	<b>Mean value <math>\pm</math> sd</b>	0.0008 $\pm$ 0.0002	0.009 $\pm$ 0.002
Fibrinogen	1	0.0005	0.005
	2	0.0005	0.005
	3	0.0004	0.004
	<b>Mean value <math>\pm</math> sd</b>	0.0005 $\pm$ 0.0000	0.005 $\pm$ 0.001

TABLE C.19: SPR angular shifts and corresponding protein masses for the adsorption onto surfaces with the composition CS<sub>M</sub>:TEOS 2:1 after rinsing with buffer.

Protein	Measurement	SPR angle [°]	Protein mass per area [mg m <sup>-2</sup> ]
BSA	1	0.0005	0.005
	2	0.0005	0.005
	3	0.0004	0.004
	<b>Mean value ± sd</b>	<b>0.0005 ± 0.0001</b>	<b>0.005 ± 0.001</b>
Fibrinogen	1	0.0020	0.021
	2	0.0083	0.087
	3	0.0015	0.016
	<b>Mean value ± sd</b>	<b>0.0039 ± 0.0031</b>	<b>0.041 ± 0.032</b>

TABLE C.20: SPR angular shifts and corresponding protein masses for the adsorption onto surfaces with the composition CS<sub>M</sub>:APTES 9:1 after rinsing with buffer.

Protein	Measurement	SPR angle [°]	Protein mass per area [mg m <sup>-2</sup> ]
BSA	1	0.0280	0.294
	2	0.0270	0.284
	3	0.0209	0.219
	<b>Mean value ± sd</b>	<b>0.0253 ± 0.0031</b>	<b>0.266 ± 0.033</b>
Fibrinogen	1	0.0405	0.425
	2	0.0360	0.378
	3	0.0530	0.557
	<b>Mean value ± sd</b>	<b>0.0432 ± 0.0072</b>	<b>0.453 ± 0.076</b>

TABLE C.21: SPR angular shifts and corresponding protein masses for the adsorption onto surfaces with the composition CS<sub>M</sub>:APTES 2:1 after rinsing with buffer.

Protein	Measurement	SPR angle [°]	Protein mass per area [mg m <sup>-2</sup> ]
BSA	1	0.0240	0.252
	2	0.0270	0.284
	3	0.0280	0.294
	<b>Mean value ± sd</b>	<b>0.0263 ± 0.0017</b>	<b>0.277 ± 0.018</b>
Fibrinogen	1	0.0950	0.998
	2	0.0890	0.935
	3	0.1240	1.302
	<b>Mean value ± sd</b>	<b>0.1027 ± 0.0153</b>	<b>1.078 ± 0.160</b>

## C.4 Cytotoxicity tests

TABLE C.22: Fibroblast viability, compared to untreated cells, when exposed to sample solutions that were in contact with chitosan and selected hybrid thin films as determined by crystal violet staining.

Material	24 h DMEM	24 h DMEM + FBS	1 week DMEM	1 week DMEM + FBS
CS <sub>M</sub>	1.072 ± 0.046	1.031 ± 0.039	1.074 ± 0.031	1.052 ± 0.056
CS <sub>L</sub>	1.113 ± 0.042	0.991 ± 0.060	1.001 ± 0.045	0.995 ± 0.056
CS <sub>M</sub> :T 9:1	1.104 ± 0.070	0.996 ± 0.048	1.049 ± 0.068	0.991 ± 0.099
CS <sub>M</sub> :T 2:1	1.026 ± 0.041	1.012 ± 0.054	1.031 ± 0.091	1.028 ± 0.064
CS <sub>M</sub> :A 2:1	1.081 ± 0.095	1.011 ± 0.058	0.970 ± 0.052	0.967 ± 0.068
CS <sub>M</sub> :S* 2:1	1.035 ± 0.090	1.047 ± 0.086	0.864 ± 0.062	0.941 ± 0.054

TABLE C.23: Osteoblast viability, compared to untreated cells, when exposed to sample solutions that were in contact with chitosan and selected hybrid thin films as determined by crystal violet staining.

Material	24 h DMEM	24 h DMEM + FBS	1 week DMEM	1 week DMEM + FBS
CS <sub>M</sub>	0.959 ± 0.053	0.984 ± 0.062	0.888 ± 0.085	0.907 ± 0.103
CS <sub>L</sub>	0.962 ± 0.102	1.003 ± 0.072	0.928 ± 0.190	0.925 ± 0.060
CS <sub>M</sub> :T 9:1	0.936 ± 0.035	1.016 ± 0.029	0.942 ± 0.189	1.063 ± 0.120
CS <sub>M</sub> :T 2:1	0.998 ± 0.063	1.025 ± 0.044	0.894 ± 0.017	1.120 ± 0.139
CS <sub>M</sub> :A 2:1	1.006 ± 0.056	1.027 ± 0.030	0.921 ± 0.041	1.185 ± 0.121
CS <sub>M</sub> :S* 2:1	1.054 ± 0.111	0.983 ± 0.062	0.899 ± 0.133	0.930 ± 0.078

TABLE C.24: Osteoblast viability, compared to untreated cells, when exposed to sample solutions that were in contact with hybrid thin films containing TEOS derived silica particles as determined by crystal violet staining.

Material	24 h DMEM	24 h DMEM + FBS	1 week DMEM	1 week DMEM + FBS
CS <sub>M</sub> :T 9:1	0.936 ± 0.035	1.016 ± 0.029	0.942 ± 0.189	1.063 ± 0.120
CS <sub>M</sub> :T 6:1	1.023 ± 0.125	0.960 ± 0.044	0.907 ± 0.103	0.985 ± 0.110
CS <sub>M</sub> :T 4:1	1.008 ± 0.071	0.988 ± 0.064	0.913 ± 0.054	1.053 ± 0.067
CS <sub>M</sub> :T 2:1	0.998 ± 0.063	1.025 ± 0.044	0.894 ± 0.017	1.120 ± 0.139
CS <sub>L</sub> :T 9:1	1.005 ± 0.031	1.062 ± 0.014	0.954 ± 0.031	1.051 ± 0.046
CS <sub>L</sub> :T 2:1	1.016 ± 0.040	0.986 ± 0.070	0.985 ± 0.049	1.062 ± 0.044

TABLE C.25: Osteoblast viability, compared to untreated cells, when exposed to sample solutions that were in contact with hybrid thin films containing a wide range of different particles as determined by crystal violet staining.

Material	24 h DMEM	24 h DMEM + FBS	1 week DMEM	1 week DMEM + FBS
CS <sub>M</sub> :A 9:1	0.996 ± 0.049	1.033 ± 0.054	0.953 ± 0.087	1.222 ± 0.223
CS <sub>M</sub> :A 6:1	1.006 ± 0.056	1.027 ± 0.030	0.921 ± 0.041	1.264 ± 0.186
CS <sub>L</sub> :A 4:1	1.061 ± 0.039	1.069 ± 0.029	0.981 ± 0.051	1.280 ± 0.155
CS <sub>L</sub> :A 2:1	0.989 ± 0.090	0.975 ± 0.078	0.993 ± 0.056	0.960 ± 0.080
CS <sub>M</sub> :G 9:1	1.089 ± 0.036	0.984 ± 0.023	0.915 ± 0.039	0.817 ± 0.056
CS <sub>M</sub> :G 2:1	1.064 ± 0.049	0.984 ± 0.024	1.009 ± 0.121	0.895 ± 0.049
CS <sub>M</sub> :CNC 9:1	1.094 ± 0.055	1.011 ± 0.072	1.050 ± 0.122	0.982 ± 0.081
CS <sub>M</sub> :CNC 2:1	1.037 ± 0.058	1.016 ± 0.029	0.992 ± 0.142	0.913 ± 0.064
CS <sub>M</sub> :S* 9:1	1.027 ± 0.070	1.047 ± 0.040	0.956 ± 0.045	0.879 ± 0.051
CS <sub>M</sub> :S* 2:1	1.054 ± 0.111	0.983 ± 0.062	0.899 ± 0.133	0.930 ± 0.078
CS <sub>L</sub> :S* 9:1	1.024 ± 0.097	0.983 ± 0.084	0.966 ± 0.081	0.917 ± 0.073
CS <sub>M</sub> :S** 9:1	1.000 ± 0.066	1.014 ± 0.059	0.982 ± 0.083	0.920 ± 0.046
CS <sub>M</sub> :S** 2:1	0.925 ± 0.056	0.966 ± 0.072	0.915 ± 0.082	0.984 ± 0.063

## C.5 Tensile tests

TABLE C.26: Mechanical parameters obtained from uniaxial tensile tests of neat chitosan foils.

Measurement	Thickness [μm]	Elastic Modulus [MPa]	Yield Strength [MPa]	Ultimate Tensile Strength [MPa]	Break Strain [%]
1	25.6	2901	46.3	63.3	8.37
2	28.6	1634	46.2	73.4	12.58
3	23.0	2441	49.1	66.0	8.49
4	31.3	2746	44.1	79.0	14.94
5	25.0	3092	49.9	68.3	7.97
<b>Mean ± sd</b>	26.9	2563 ± 511	47.1 ± 2.1	70.0 ± 5.6	10.47 ± 2.79

TABLE C.27: Mechanical parameters obtained from uniaxial tensile tests of chitosan foils containing ethanol in a ratio of CS<sub>M</sub>:EtOH 9:1.

Measurement	Thickness [μm]	Elastic Modulus [MPa]	Yield Strength [MPa]	Ultimate Tensile Strength [MPa]	Break Strain [%]
1	23.3	2514	45.7	68.0	8.95
2	22.3	3002	48.7	73.2	8.85
3	22.0	3643	52.3	81.6	9.44
4	18.3	3446	47.6	71.7	7.95
5	28.3	2087	52.4	70.0	7.31
<b>Mean ± sd</b>	22.8	2939 ± 577	49.3 ± 2.6	72.9 ± 4.7	8.50 ± 0.76

TABLE C.28: Mechanical parameters obtained from uniaxial tensile tests of chitosan foils containing 2.9% silica particles from sol-gel processing of TEOS.

Measurement	Thickness [μm]	Elastic Modulus [MPa]	Yield Strength [MPa]	Ultimate Tensile Strength [MPa]	Break Strain [%]
1	30.6	2086	58.6	81.2	11.13
2	31.0	2951	68.6	98.8	13.18
3	17.6	3841	69.6	80.0	5.13
4	28.0	2689	65.6	76.8	5.65
5	22.6	2659	69.3	79.0	6.42
<b>Mean ± sd</b>	26.0	2845 ± 572	66.4 ± 4.1	83.1 ± 8.0	8.30 ± 3.27

TABLE C.29: Mechanical parameters obtained from uniaxial tensile tests of chitosan foils containing 5.8% silica particles from sol-gel processing of TEOS.

Measurement	Thickness [μm]	Elastic Modulus [MPa]	Yield Strength [MPa]	Ultimate Tensile Strength [MPa]	Break Strain [%]
1	24.3	4676	85.4	100.1	4.15
2	25.6	4926	84.1	102.1	5.08
3	29.6	4650	80.3	113.6	8.14
4	25.0	5141	78.3	93.9	3.78
5	24.6	5021	72.3	99.3	5.45
<b>Mean ± sd</b>	25.8	4883 ± 192	80.1 ± 4.6	101.8 ± 6.5	5.32 ± 1.54

TABLE C.30: Mechanical parameters obtained from uniaxial tensile tests of chitosan foils containing 11.5% silica particles from sol-gel processing of TEOS.

Measurement	Thickness [μm]	Elastic Modulus [MPa]	Yield Strength [MPa]	Ultimate Tensile Strength [MPa]	Break Strain [%]
1	24.6	2475	38.8	86.3	15.02
2	26.0	2300	56.5	76.4	7.35
3	20.3	2769	42.9	92.1	13.26
4	24.0	2668	43.6	76.6	9.74
5	21.0	1664	45.5	83.6	11.01
<b>Mean ± sd</b>	23.2	2375 ± 390	45.5 ± 6.0	83.0 ± 6.0	11.28 ± 2.68

TABLE C.31: Mechanical parameters obtained from uniaxial tensile tests of chitosan foils containing 7.3% chitin nanocrystals (ChNCs).

Measurement	Thickness [μm]	Elastic Modulus [MPa]	Yield Strength [MPa]	Ultimate Tensile Strength [MPa]	Break Strain [%]
1	32.0	3653	44.9	93.8	11.83
2	28.0	3210	54.2	86.8	7.67
3	26.0	3520	53.3	106.7	12.38
4	29.6	2645	60.5	78.4	8.47
5	32.6	3713	56.8	89.0	12.54
<b>Mean ± sd</b>	29.6	3348 ± 392	53.9 ± 5.2	90.9 ± 9.3	10.58 ± 2.08